75N13792

NASA TECHNICAL NOTE

NASA TN D-7778

NASA TN D-7778

WIND-TUNNEL INVESTIGATION OF A TWIN-ENGINE STRAIGHT-WING UPPER-SURFACE BLOWN JET-FLAP CONFIGURATION

by Arthur E. Phelps III

Langley Directorate
U.S. Army Air Mobility R&D Laboratory
Hampton, Va. 23665

NATIONAL AERONAUTICS AND SPACE ADMINISTRATION • WASHINGTON, D. C. • JANUARY 1975

1. Report No. NASA TN D-7778	2. Government Accession No.	3. Recipient's Catalog No.

4. Title and Subtitle WIND-TUNNEL INVESTIGATION OF A TWIN-ENGINE STRAIGHT-WING UPPER-SURFACE BLOWN JET-FLAP CONFIGURATION	5. Report Date January 1975
	6. Performing Organization Code
7. Author(s) Arthur E. Phelps III, Langley Directorate, U.S. Army Air Mobility R&D Laboratory	8. Performing Organization Report No. L-9758
9. Performing Organization Name and Address NASA Langley Research Center Hampton, Va. 23665	10. Work Unit No. 760-61-02-01
	11. Contract or Grant No.
	13. Type of Report and Period Covered Technical Note
12. Sponsoring Agency Name and Address National Aeronautics and Space Administration Washington, D.C. 20546	14. Sponsoring Agency Code

15. Supplementary Notes

16. Abstract

An investigation has been conducted in the Langley full-scale tunnel to determine the performance and aerodynamic characteristics of a twin-engine straight-wing upper-surface blown jet-flap configuration. The model had two simulated high-bypass-ratio turbofan engines with rectangular nozzles exhausting onto the upper surface of the wing at the 35-percent-chord station. The model was tested with an aspect-ratio-8.2 wing and with the wingtips removed to give an aspect ratio of 6.0.

17. Key Words (Suggested by Author(s)) Powered lift Upper-surface blowing Jet-augmented flap	18. Distribution Statement Unclassified – Unlimited STAR Category 01

19. Security Classif. (of this report) Unclassified	20. Security Classif. (of this page) Unclassified	21. No. of Pages 78	22. Price* $4.75

*For sale by the National Technical Information Service, Springfield, Virginia 22151

WIND-TUNNEL INVESTIGATION OF A TWIN-ENGINE STRAIGHT-WING UPPER-SURFACE BLOWN JET-FLAP CONFIGURATION

By Arthur E. Phelps III
Langley Directorate, U.S. Army Air Mobility R&D Laboratory

SUMMARY

An investigation has been conducted in the Langley full-scale tunnel to determine the performance and aerodynamic characteristics of a twin-engine straight-wing upper-surface blown jet-flap configuration. The model had two simulated high-bypass-ratio turbofan engines with rectangular nozzles exhausting onto the upper surface of the wing at the 35-percent-chord station. The model was tested with an aspect-ratio-8.2 wing and with the wingtips removed to give an aspect ratio of 6.0.

The results of the investigation showed that the configuration, as tested, could provide the high lift coefficients necessary for powered-lift operation and that the performance was generally similar to that of other externally blown high-lift configurations in which the exhaust flow was fairly well localized inboard on the wing. Flow surveys in the region of a high horizontal tail indicated fairly conventional downwash characteristics. An analysis based on the flow surveys indicated that a high horizontal tail could provide both stability and trim over the entire angle-of-attack range for the test thrust coefficients. The tail-on directional stability was positive and increased rapidly with increasing power as a result of favorable sidewash on the vertical tail. The tail-on effective dihedral was positive at all angles of attack and was relatively low due to the lack of wing sweep. The use of blowing boundary-layer control on the leading edge and aileron of the failed-engine wing was an effective means of trimming the engine-out rolling moments.

INTRODUCTION

The upper-surface blown (USB) jet-flap concept has been shown to be an effective means of providing good powered-lift performance for short-field operation of transport-type aircraft (refs. 1 and 2), and acoustic studies of aircraft utilizing this concept have indicated that substantial reductions in the ground-level noise might reasonably be expected (ref. 2). Results of earlier research have encouraged continued research into some of the fundamental problems associated with the successful application of the USB concept to operational aircraft. The present investigation was part of a general research program aimed at providing fundamental research information on the USB jet-flap concept and consisted of static and dynamic force tests of a small-scale free-flight model of a twin-engine straight-wing configuration. A large-scale model equipped with two JT15D-1 turbofan engines was used to provide information regarding the effects of hot-engine exhaust on the overall aerodynamic performance of the USB concept, noise measurements for an operational type of engine installation, and an indication of the type of problems to be expected from temperature and local acoustic loadings on the airframe.

The present model had a straight wing with a leading-edge Krueger flap, leading-edge blowing boundary-layer control (BLC), partial-span double-slotted trailing-edge flaps, partial-span drooped ailerons with BLC, and smooth continuously curved flaps inboard behind the engines. Power for the model was provided by two single-stage tip-turbine turbofan simulators driven by compressed air. Static tests were performed for two flap deflections with four horizontal-tail and vertical-tail configurations over a range of angle of attack, angle of sideslip, and thrust coefficient. A few roll and yaw forced-oscillation tests were performed for the landing flap configuration for use in theoretical stability and control studies and for interpretation of flight-test results.

SYMBOLS

The longitudinal data are referred to the stability-axis system and the lateral data are referred to the body-axis system. (See fig. 1.) The origin of the axes for the static force tests was located to correspond to a center-of-gravity position of 0.40 mean aerodynamic chord of the aspect-ratio-8.2 wing as shown in figure 2. The center-of-gravity position for the forced-oscillation tests was at 0.20 mean aerodynamic chord of the aspect-ratio-8.2 wing. Unless otherwise indicated, all coefficients are based on the aspect-ratio-8.2 wing geometry.

Measurements and calculations were made in U.S. Customary Units and are presented in both the International System of Units (SI) and U.S. Customary Units. Equivalent dimensions were determined by using the conversion factors given in reference 3.

b	wing span, m (ft)
C_D	drag coefficient, $\frac{F_D}{qS}$
C_L	lift coefficient, $\frac{F_L}{qS}$
C_l	rolling-moment coefficient, $\frac{M_X}{qSb}$

C_m	pitching-moment coefficient, $\frac{M_Y}{qS\bar{c}}$
C_n	yawing-moment coefficient, $\frac{M_Z}{qSb}$
C_Y	side-force coefficient, $\frac{F_Y}{qS}$
C_μ	engine total gross-thrust coefficient, $\frac{T}{qS}$
$C_{\mu,a}$	aileron blowing jet momentum coefficient, $\frac{F_R}{qS}$
$C_{\mu,le}$	wing leading-edge blowing jet momentum coefficient, $\frac{F_R}{qS}$
c	local chord, m (ft)
$\bar{c}$	mean aerodynamic chord, m (ft)
F_A	axial force, N (lb)
F_D	drag force, N (lb)
F_L	lift force, N (lb)
F_N	normal force, N (lb)
F_R	resultant force, N (lb)
F_Y	side force, N (lb)
f	frequency of oscillation, Hz (cps)
i_t	horizontal-tail incidence angle, positive when leading edge is up, deg
k	reduced-frequency parameter, $\frac{\omega b}{2V}$

l_t	tail arm (horizontal distance between model center of gravity and horizontal-tail aerodynamic center), m (ft)
M_X	rolling moment, m-N (ft-lb)
M_Y	pitching moment, m-N (ft-lb)
M_Z	yawing moment, m-N (ft-lb)
p,r	body-axis rolling and yawing velocities, rad/sec
q	free-stream dynamic pressure, $\frac{\rho V^2}{2}$, Pa (lb/ft^2)
S	wing area, m^2 (ft^2)
S_t	horizontal-tail area, m^2 (ft^2)
T	static thrust, N (lb)
V	free-stream velocity, m/sec (ft/sec)
X,Y,Z	body reference axes
X_s,Y_s,Z_s	stability reference axes
x,y,z	rectangular Cartesian coordinates, m (ft)
α	angle of attack, deg
β	angle of sideslip, deg
$\dot{\beta}$	rate of change of angle of sideslip, rad/sec
δ_a	aileron deflection, positive when trailing edge is down, deg

δ_e	elevator deflection, positive when trailing edge is down, deg
δ_f	total flap deflection, deg (see fig. 3(a))
δ_j	jet deflection, positive downward, deg
δ_r	rudder deflection, positive when trailing edge is left, deg
δ_s	spoiler deflection, positive when trailing edge is up, deg
δ_v	vane deflection, deg
ϵ	downwash angle measured with respect to free stream, deg
ρ	air density, kg/m3 (slugs/ft3)
ω	angular velocity, $2\pi f$, rad/sec

$$C_{l_\beta} = \frac{\partial C_l}{\partial \beta}, \text{ per deg} \qquad C_{l_p} = \frac{\partial C_l}{\partial \frac{pb}{2V}} \qquad C_{l_r} = \frac{\partial C_l}{\partial \frac{rb}{2V}}$$

$$C_{n_\beta} = \frac{\partial C_n}{\partial \beta}, \text{ per deg} \qquad C_{n_p} = \frac{\partial C_n}{\partial \frac{pb}{2V}} \qquad C_{n_r} = \frac{\partial C_n}{\partial \frac{rb}{2V}}$$

$$C_{Y_\beta} = \frac{\partial C_Y}{\partial \beta}, \text{ per deg} \qquad C_{Y_p} = \frac{\partial C_Y}{\partial \frac{pb}{2V}} \qquad C_{Y_r} = \frac{\partial C_Y}{\partial \frac{rb}{2V}}$$

$$C_{l_{\dot\beta}} = \frac{\partial C_l}{\partial \frac{\dot\beta b}{2V}} \qquad C_{n_{\dot\beta}} = \frac{\partial C_n}{\partial \frac{\dot\beta b}{2V}} \qquad C_{Y_{\dot\beta}} = \frac{\partial C_Y}{\partial \frac{\dot\beta b}{2V}}$$

Subscripts:

a	aileron
e	elevator
f	flap
L	left
l	lower
R	right
t	horizontal tail
u	upper
v	vane
w	wing

Abbreviations:

BLC	boundary-layer control
FRP	fuselage reference plane
G	gap
I.D.	inside diameter
L.E.	leading edge
O	overlap
W.L.	water line

MODEL AND APPARATUS

Tests were conducted on the twin-engine high-wing upper-surface blown jet-flap model shown in figure 2. The wing had an aspect ratio of 8.2 and was equipped with removable tips which reduced the aspect ratio to 6.0. The principal dimensional characteristics of the model are presented in table I.

Power for the model was provided by two single-stage tip-turbine turbofan simulators driven by compressed air. The exhaust nozzle of the engine nacelle was contoured so that the exhaust center line was directed downward toward the upper surface of the wing ahead of the knee of the trailing-edge flap as shown in figure 2(b). Additional jet deflection was provided by the use of the short flat-plate deflector also shown in figure 2(b). The model was tested only with the deflectors on. Some wind-off tests were conducted with the flow fence shown in figure 2(c).

Details of positions and deflections of the leading-edge and trailing-edge flaps are presented in figure 3(a); figure 3(b) illustrates the essential features of leading-edge and aileron BLC installations. The wing leading edge was fitted with a Krueger flap extending from the side of the nacelle to the wingtip and was provided with a slot for supplying blowing BLC. Wing trailing-edge high-lift devices consisted of a partial-span double-slotted flap and a blown drooped aileron. The upper surface of the double-slotted flaps directly behind the engines was covered with a thin metal plate forming a smooth continuously curved surface, or Coanda flap, for turning the exhaust flow as shown in figure 2. The wing was equipped with spoilers extending from the outboard edge of the Coanda flap to the wingtip. Coordinates for the double-slotted trailing-edge flap are given in table II and coordinates for the leading-edge Krueger flap are presented in table III.

The four different horizontal-tail and vertical-tail configurations tested are shown in figure 4. The center vertical tails were equipped with a rudder which could be deflected 40° to either side of the model plane of symmetry for yaw trim; the tip-mounted vertical fins were flat plates having no rudder surfaces. Each of the two horizontal tails was equipped with a leading-edge slat and a single-slotted elevator. Details of the tail slat and elevator are shown in figure 5.

Tests were performed in the 9- by 18-m (30- by 60-ft) open-throat test section of the Langley full-scale tunnel with the model mounted about 3 m (10 ft) above the ground board. All the tests were made with a six-component internal strain-gage balance. The model installed for conventional (static) wind-tunnel tests is shown in figure 6. Dynamic force tests were made on the forced-oscillation equipment illustrated in reference 4 and described in detail in reference 5.

TESTS AND PROCEDURES

In preparation for the tests calibrations were made to determine the installed static thrust of each engine as a function of engine rotational speed. The engine calibrations were performed with the engines and nacelles installed on top of the wing but with the trailing-edge flaps removed. The static thrust was then computed to be the resultant of the measured normal and axial forces $\left(T = \sqrt{F_N^2 + F_A^2}\right)$. Power-on tests were run by setting the engine speed to provide the desired level of static thrust and holding this speed constant through the angle-of-attack range. At the speeds used in investigations of this type, experience has shown that the effect of forward velocity on the gross thrust of the engine simulators is negligible, and it is gross thrust which is used in defining C_μ.

Tests were first made at zero airspeed to determine jet-turning angles and thrust-recovery efficiencies. Both the wind-off and wind-on tests were performed for trailing-edge flap deflections of 20° (takeoff flap) and 60° (landing flap). Most of the tests were made with the aspect-ratio-8.2 wing. A few tests were performed with the aspect-ratio-6.0 wing to provide data for correlating with results from the investigation of the large-scale version of this model. Wind-on tests were made over an angle-of-attack range from -4° to 36° for a thrust coefficient range from 0 to 3.6. In order to investigate the effects of asymmetric thrust and the attendant uneven flow fields on longitudinal and lateral trim characteristics of the model, tests were made over a range of angle of attack and thrust coefficient for sideslip angles of 5° and -5°. Some of the engine-out tests were performed with the Coanda flap behind the inoperative engine removed to provide slotted flaps inboard to the side of the fuselage. Tests were made with and without the horizontal and vertical tails to obtain longitudinal and lateral data. Also, tests were conducted with the four different horizontal-tail and vertical-tail configurations described earlier. The free-stream dynamic pressure for the tests was 105 Pa (2.2 lb/ft^2) for an airspeed of 13.1 m/sec (42.9 ft/sec) and a Reynolds number of 2.88×10^5 based on the mean aerodynamic chord of the aspect-ratio-8.2 wing.

In addition to the static force tests, a few roll and yaw forced-oscillation tests were performed at angles of attack of 0° and 10° for the 60° flap configuration with and without the T-tail. The tests were made at oscillation frequencies of 1.0 and 0.5 Hz (cps), which correspond to values of the reduced-frequency parameter k of 0.64 and 0.32, respectively. The free-stream conditions for the oscillation tests were the same as those for the static force tests.

No wind-tunnel wall corrections were considered necessary since the model was very small relative to the test-section size.

RESULTS AND DISCUSSION

Static Turning

Static turning tests were made to evaluate the effectiveness of the Coanda flap in turning the engine exhaust flow. The results of these tests are presented in figure 7. Although the data show relatively poor static turning $\left(\delta_j = 44^\circ \text{ for the } 60^\circ \text{ flap}\right)$, tuft and smoke-flow studies revealed well attached flow over the full length and width of the Coanda flap. The flow visualization studies also showed that the exhaust was spreading an appreciable distance to either side of the nozzle exit, and a large portion of the jet exhaust was flowing aft along the top of the fuselage and provided no powered-lift benefit.

In order to restrict the inboard spreading of the jet exhaust, a chordwise flow fence extending from the exhaust nozzle aft to the trailing edge of the Coanda flap was placed along the inboard side of the nacelle, as shown in figure 2(c). The data in figure 7 show that the static turning performance was improved with respect to both turning angle and thrust recovery efficiency after the addition of the fence, and tuft studies indicated that the fence was extremely effective in containing the inboard spreading of the exhaust jet. In a subsequent section of the report, however, the model performance in the forward flight condition is shown to be as good without the fences as with them and, therefore, most of the tests were run with the fences off.

The flow visualization tests conducted prior to the wind-on investigation also showed that the exhaust flow was attaching to the fuselage side and turning down underneath the model, although no data were recorded with the model in this configuration. A pair of small triangular strakes was attached to the fuselage side at the trailing edge of the Coanda flap as shown in figure 2(a) to trip the jet and separate it from the fuselage side. All data were recorded with these strakes installed.

Longitudinal Aerodynamic Characteristics

The tail-off longitudinal aerodynamic characteristics of the model with the aspect-ratio-8.2 wing are shown in figures 8 and 9 for flap deflections of 60° and 20°, respectively. The data show the characteristic increase in maximum lift coefficient, in stall angle of attack, and in negative pitching-moment coefficient with increasing thrust coefficient. A maximum untrimmed lift coefficient of 9.2 was achieved for the model with 60° flap deflection and with BLC on both the leading and trailing edges of the wing. The large pitching-moment coefficients accompanying the high lift coefficients are characteristic of externally blown powered-lift configurations but are somewhat more severe than those obtained from sweptwing models of previous investigations (for example, ref. 1) and are due primarily to the aft center of pressure resulting from the unswept planform.

The results of tests to define the tail-off longitudinal aerodynamic characteristics of the aspect-ratio-6.0 wing are shown in figure 10. These data were obtained for use in correlating the results from small-scale and large-scale model tests and are presented here to give an indication of the effects of wing aspect ratio on the longitudinal characteristics of such a configuration. All the remaining data in this report are based on the aspect-ratio-8.2 wing configuration.

Figure 11 presents the lift and drag characteristics of the model with and without the chordwise flow fences discussed in the section entitled "Static Turning." The data indicate that there was virtually no difference in lift or drag performance with fences or without fences. The flow control observed in the static case with the fences installed was not required for the wind-on case, evidently because forward speed prevented the jet-exhaust flow from spreading as wide as it did in the zero-speed condition. The tests were therefore made with no fences.

The tail-on longitudinal aerodynamic characteristics of the model with the 60° flap configuration (landing flaps) are presented in figures 12, 13, and 14 for the T-tail, the high T-tail, and the low tail, respectively. Data for the 20° flap configuration (takeoff flaps) with the T-tail are presented in figure 15. The data show that none of the tail arrangements tested on the model were effective in providing stability and trim for the power-on conditions or at very high angles of attack.

In order to provide some fundamental information for use in analyzing the nature of the tail-on stability and trim problems, downwash surveys were performed in the plane of each horizontal tail. Figure 16 presents the variation of the downwash across the span of the horizontal tail for two thrust coefficients and two angles of attack. The data of figure 16 are summarized in figure 17 in terms of average downwash factor $1 - \frac{\partial\epsilon}{\partial\alpha}$ for each tail as a function of thrust coefficient. The downwash factors in figure 17 indicate extremely low effectiveness for the low tail, as expected. The T-tails, however, were in a position where the downwash characteristics were more favorable and should therefore have provided some stability. The fact that the T-tail horizontal tail, as tested, did not provide any stability at the high thrust settings suggests that the tail was stalled, and a few tail-alone tests were made to determine the horizontal-tail characteristics.

Figure 18 presents tail-alone data for three different horizontal-tail configurations: the tail arrangement as tested on the model, or "design" tail $(\delta_e = 40^{\circ})$; the "clean" tail with no high-lift devices as a reference $(\delta_e = 0^{\circ})$; and a modified tail having more powerful high-lift devices. An examination of the tail-alone data shows that the maximum lift coefficient of the design tail was only about 2.0, and an analysis of the tail-off data of figure 8(b) indicates that this value of tail lift coefficient is too low to provide trim at the higher test thrust coefficients. In order to provide trim capability, the design tail was modified by replacing the 15-percent-chord leading-edge slat with a 20-percent-chord Krueger flap and by tailoring the elevator slot to provide attached flow for a 60° elevator deflection. These modifications increased the maximum lift coefficient from 2.0 to 2.6 and provided a substantial increase in the tail lift-curve slope.

Figure 19 presents the results of an analysis performed to determine the requirements of the horizontal tail for providing longitudinal stability and trim. The results of the analysis indicate that the modified horizontal tail can provide longitudinal trim up to the stall for the highest power setting in any of the three vertical positions tested, but the tail must be placed in the high T-tail position before stability can be maintained throughout the angle-of-attack range.

Lateral Characteristics

Symmetric power.- The tail-off and tail-on static lateral stability derivatives are shown in figure 20 for the landing flap configuration, and the tail-on characteristics for the takeoff flap configuration are shown in figure 21. Tail-on data of figures 20(b) and 21 show that the model had positive effective dihedral $\left(\text{negative } C_{l_\beta}\right)$ with power and had very high directional stability $\left(\text{positive } C_{n_\beta}\right)$ up to the stall. The large stabilizing effect of power on the directional stability is evidently due to the effects of the exhaust flow on the vertical tail since C_{n_β} for the model with tail off is relatively unaffected by the application of power (fig. 20(a)). The relatively small values of C_{l_β} in figure 20(b) appear to be due primarily to the lack of wing sweep and are only moderately affected by power.

Asymmetric power.- The lateral asymmetries of the model with the left engine inoperative are shown in figures 22 and 23 for landing and takeoff flap deflections, respectively. Under conditions of asymmetric power, the lateral asymmetries are usually of primary importance because of their large magnitude. The loss of thrust from one engine, however, also has a direct effect on lift; this is especially true for a two-engine configuration where the loss of one engine reduces the direct thrust component by one-half. The lateral characteristics are therefore presented along with the corresponding longitudinal characteristics for the various configurations tested. The data of figures 22 and 23 show the anticipated large rolling and yawing asymmetries attendant with the loss of an engine. These engine-out moments are comparable with those shown in an earlier study with a two-engine configuration although the model of the present investigation produced somewhat higher lift coefficients with an engine out than the model of reference 1.

As shown in reference 6, one effective means of trimming the lateral asymmetries in engine-out operation is the use of differential BLC along the leading and trailing edges of the wing. This method relies, in principle, upon the capability of BLC on the unpowered wing to restore the induced circulation lift lost when the engine contribution is removed. The results of applying this technique to the present model are shown in figures 24 and 25 for the landing $\left(\delta_f = 60^{\circ}\right)$ and takeoff $\left(\delta_f = 20^{\circ}\right)$ flap configurations, respectively. At the highest power $\left(C_{\mu} = 1.8\right)$ and at high angles of attack, the rolling moments for the landing flap were still negative, although significantly reduced.

Figure 26 presents the results of tests to determine the effect of spoiler deflection on the lateral and longitudinal aerodynamic characteristics of the model. As expected, the spoilers provided large increments in rolling-moment coefficient with increasing power and produced a moderate amount of favorable yaw.

Figure 27 is a summary plot using the data from figures 24 and 26 and shows the estimated rolling-moment and yawing-moment coefficients obtained when spoilers and differential BLC are used together to provide engine-out lateral trim. Data were not obtained for incremental spoiler deflections and are therefore presented for a full 45° spoiler deflection. Figure 27 clearly indicates that only a part of the total deflection was required for trim although the data do not permit a determination of the precise amount required. Spoilers, therefore, appear to be effective for providing additional engine-out trim although it is recognized that some lift penalty will be associated with their use.

Another suggested means of reducing the engine-out rolling moments is to open the slots of the double-slotted flap behind the failed engine and to allow this area of the wing to operate in a conventional unpowered high-lift mode. This approach was used in a few tests made with the landing flap configuration. The results of these tests are presented in figures 28 and 29 and are summarized in figure 30. The data from the summary plot of figure 30 indicate that the open slots of the double-slotted flap provided a relatively small reduction in engine-out rolling moments.

The rudder power available for yaw trim is shown in figure 31 for the model with symmetric power. The data show that the rudder effectiveness was substantially increased with the addition of engine power. A comparison of the data of figure 31 with the engine-out trim data of figure 24, which include the contribution of a -30° rudder deflection, reveals that the rudder power was too low for yaw trim, as expected for an unblown rudder. A high-lift rudder is therefore required to provide yaw trim for the engine-out condition.

The flow surveys discussed previously in connection with the downwash characteristics included measurements of the sidewash characteristics across the span of the horizontal tail and, as a result, revealed an interesting pattern of sidewash variation. It was found that during single-engine operation the engine exhaust wake entrained large amounts of the free-stream flow on either side of the wake; this caused a fairly powerful flow across the model center line toward the exhaust wake. For example, the sketch in figure 32(a) shows that with the right engine operating, the vertical tail is in a cross flow which will produce an adverse yawing moment (nose left). If the vertical tail were located outboard of the exhaust-wake center line, however, the engine-induced cross flow would result in a favorable vertical-tail yawing moment (nose right).

The data of figure 32 show the vertical-tail contribution to the engine-out problem of three different tail configurations. Moving the horizontal tail from a high to a low position resulted in a significant reduction in the adverse yawing moments, evidently because of reduced vertical-tail effectiveness resulting from the removal of the end-plate contribution of the high tail. An additional modest increase in favorable yawing moment was obtained by changing from a center vertical tail to a pair of vertical fins mounted outboard on the tip of the horizontal tail.

Dynamic Stability Derivatives

Rolling.- The variations of the dynamic stability derivatives due to rolling with angle of attack are presented in figure 33 for values of reduced-frequency parameter k of 0.32 and 0.64. The data show that the model had positive damping in roll $\left(\text{negative values of } C_{l_p} + C_{l_{\dot{\beta}}} \sin \alpha\right)$ for angles of attack up to the stall. For angles of attack below the stall, power had little effect on the damping in roll except at zero angle of attack where there was a modest reduction in damping with increasing power. The yawing moment due to rolling derivative $C_{n_p} + C_{n_{\dot{\beta}}} \sin \alpha$ became consistently more negative with increasing angle of attack and increasing power. A comparison of figures 33(a) and 33(b) shows that a change in the reduced-frequency parameter has little effect on the dynamic stability derivatives due to rolling.

Yawing.- The variations of the dynamic stability derivatives due to yawing with angle of attack are shown in figure 34 for values of reduced-frequency parameter of 0.32 and 0.64. The model had positive damping in yaw $\left(\text{negative values of } C_{n_r} - C_{n_{\dot{\beta}}} \cos \alpha\right)$ which was generally unaffected by changes in either the reduced-frequency parameter or thrust coefficient throughout the test angle-of-attack range.

SUMMARY OF RESULTS

From force tests of a straight-wing twin-engine upper-surface blown jet-flap configuration, the following results were obtained:

1. The high lift coefficients necessary for powered-lift operation could be achieved with the test configuration, and the performance was generally comparable with that of

other externally blown powered-lift configurations in which the exhaust flow was fairly well localized inboard on the wing.

2. Flow surveys in the region of the high horizontal tail indicated conventional downwash characteristics. An analysis based on flow surveys indicated that a high horizontal tail could provide both stability and trim over the entire angle-of-attack range for the test thrust coefficients.

3. The tail-on directional stability was positive and increased rapidly with increasing power as a result of favorable sidewash on the vertical tail.

4. The tail-on effective dihedral was positive at all angles of attack and was relatively low due to the lack of wing sweep.

5. The engine-out rolling moments were large and of about the same order of magnitude as those of other externally blown high-lift concepts.

6. The use of blowing boundary-layer control on the leading edge and drooped aileron of the failed-engine wing and a spoiler on the operating-engine wing was an effective means of reducing the engine-out rolling moments.

Langley Research Center,
National Aeronautics and Space Administration,
Hampton, Va., October 30, 1974.

REFERENCES

1. Phelps, Arthur E., III; and Smith, Charles C., Jr.: Wind-Tunnel Investigation of an Upper Surface Blown Jet-Flap Powered-Lift Configuration. NASA TN D-7399, 1973.

2. Smith, Charles C., Jr.; Phelps, Arthur E., III; and Copeland, W. Latham: Wind-Tunnel Investigation of a Large-Scale Semispan Model With an Unswept Wing and an Upper-Surface Blown Jet Flap. NASA TN D-7526, 1974.

3. Mechtly, E. A.: The International System of Units – Physical Constants and Conversion Factors (Second Revision). NASA SP-7012, 1973.

4. Grafton, Sue B.; Parlett, Lysle P.; and Smith, Charles C., Jr.: Dynamic Stability Derivatives of a Jet Transport Configuration With High Thrust-Weight Ratio and an Externally Blown Jet Flap. NASA TN D-6440, 1971.

5. Chambers, Joseph R.; and Grafton, Sue B.: Static and Dynamic Longitudinal Stability Derivatives of a Powered 1/9-Scale Model of a Tilt-Wing V/STOL Transport. NASA TN D-3591, 1966.

6. Parlett, Lysle P.: Free-Flight Wind-Tunnel Investigation of a Four-Engine Swept-wing Upper-Surface Blown Transport Configuration. NASA TM X-71932, 1974.

TABLE I.- DIMENSIONS OF MODEL

Wing (aspect ratio of 8.2):	
Area, m^2 (ft^2)	0.91 (9.74)
Span, cm (in.)	269.24 (106.00)
Mean aerodynamic chord, cm (in.)	36.63 (14.42)
Root chord, cm (in.)	50.80 (20.00)
Tip chord, cm (in.)	16.76 (6.60)
Sweep of quarter-chord line, deg	-3.5
Dihedral, deg	5
Incidence of root chord, deg	3
Airfoil sections:	
Root	NACA 23012
Tip	NACA 23012
Trailing-edge high-lift devices:	
Vane:	
Span, cm (in.)	65.53 (25.80)
Root chord at side of fuselage, cm (in.)	8.64 (3.40)
Tip chord, cm (in.)	5.97 (2.35)
Flap:	
Span, cm (in.)	65.53 (25.80)
Root chord at side of fuselage, cm (in.)	8.36 (3.29)
Tip chord, cm (in.)	5.84 (2.30)
Aileron:	
Span, cm (in.)	56.89 (22.40)
Root chord, cm (in.)	6.35 (2.50)
Tip chord, cm (in.)	3.56 (1.40)
Engines:	
Spanwise station, cm (in.)	22.81 (8.98)
Chordwise position of nozzle exit, percent wing chord	35.0
Nozzle exit aspect ratio, Width/Height	4.0
Horizontal tails:	
T-tail:	
Span, cm (in.)	121.92 (48.00)
Area, m^2 (ft^2)	0.27 (2.93)
Ratio of tail length to wing mean aerodynamic chord	3.0
Ratio of tail area to wing area	0.30
Aspect ratio	5.46
Low tail:	
Span, cm (in.)	102.87 (40.50)
Area, m^2 (ft^2)	0.20 (2.16)
Ratio of tail length to wing mean aerodynamic chord	3.0
Ratio of tail area to wing area	0.22
Aspect ratio	5.27
Vertical tails:	
T-tail:	
Span, cm (in.)	48.77 (19.20)
Area, m^2 (ft^2)	0.173 (1.86)
Aspect ratio	1.38
High T-tail:	
Span, cm (in.)	64.01 (25.20)
Area, m^2 (ft^2)	0.214 (2.30)
Aspect ratio	1.92
Low tail:	
Span, cm (in.)	48.51 (19.10)
Area, m^2 (ft^2)	0.132 (1.42)
Aspect ratio	1.78

TABLE II.- COORDINATES OF DOUBLE-SLOTTED TRAILING-EDGE FLAPS

(a) Vane

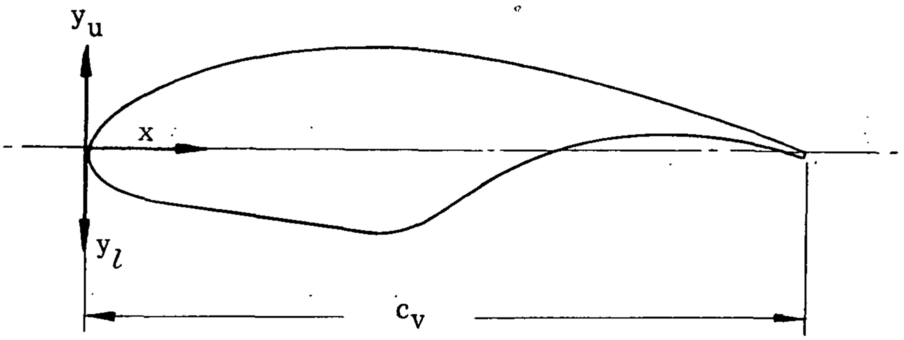

x, percent c_v	y_u, percent c_v	y_l, percent c_v
0	0	0
1.25	3.392	-2.167
2.50	4.715	-2.883
5.00	6.852	-3.739
7.25	8.412	-4.308
10.00	9.950	-4.761
20.00	12.925	-5.868
30.00	14.416	-6.852
40.00	14.743	-7.801
45.00	14.697	-5.664
50.00	14.298	-1.797
60.00	12.814	2.374
70.00	10.488	3.934
80.00	7.264	3.694
90.00	3.709	2.103
100.00	.203	0
$c_v = 0.18c_w$		

TABLE II.- COORDINATES OF DOUBLE-SLOTTED TRAILING-EDGE FLAPS – Concluded

(b) Flap

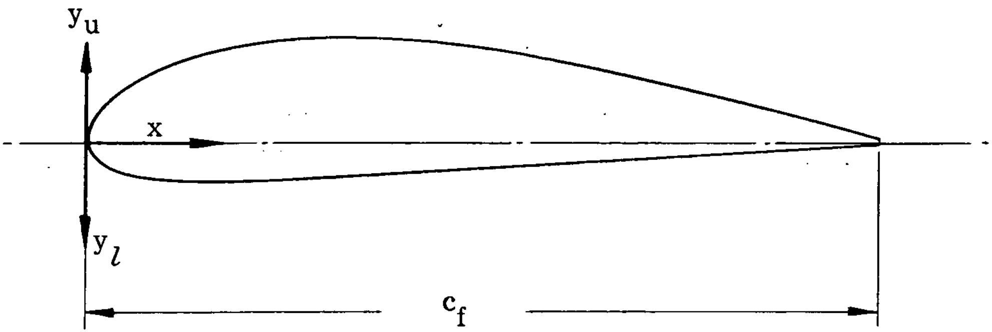

x, percent c_f	y_u, percent c_f	y_l, percent c_f
0	0	0
.0125	.02366	-.01670
.025	.03444	-.02226
.05	.05156	-.02783
.0725	.06491	-.02922
.10	.07849	-.02957
.20	.10925	.02841
.30	.12070	.02676
.40	.12348	.02500
.45	.12175	.02370
.50	.11862	.02276
.60	.10475	.02087
.70	.08077	.01782
.80	.05446	.01465
.90	.02844	.00976
1.00	.001734	.00173
$c_f = 0.175c_w$		

TABLE III.- AIRFOIL COORDINATES FOR LEADING-EDGE KRUEGER FLAP

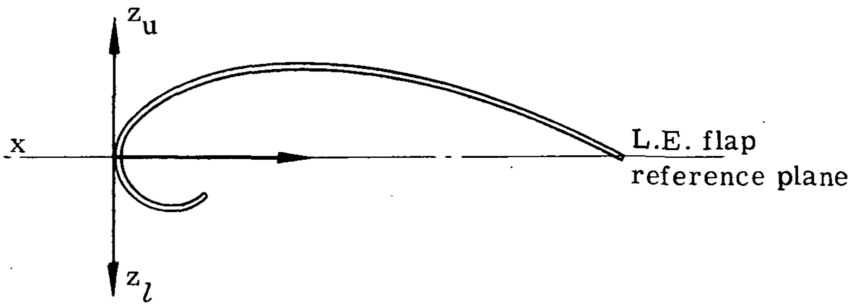

x, percent c_w	z, percent c_w	z_l, percent c_w
0	0	-----
.5	1.118	-1.450
1.0	1.723	-1.825
2.0	2.415	-1.980
3.0	2.910	-1.695
4.0	3.320	-----
6.0	3.825	-----
8.0	3.995	-----
10.0	4.005	-----
12.0	3.730	-----
14.0	3.250	-----
16.0	2.530	-----
18.0	1.472	-----
20.0	0	-----

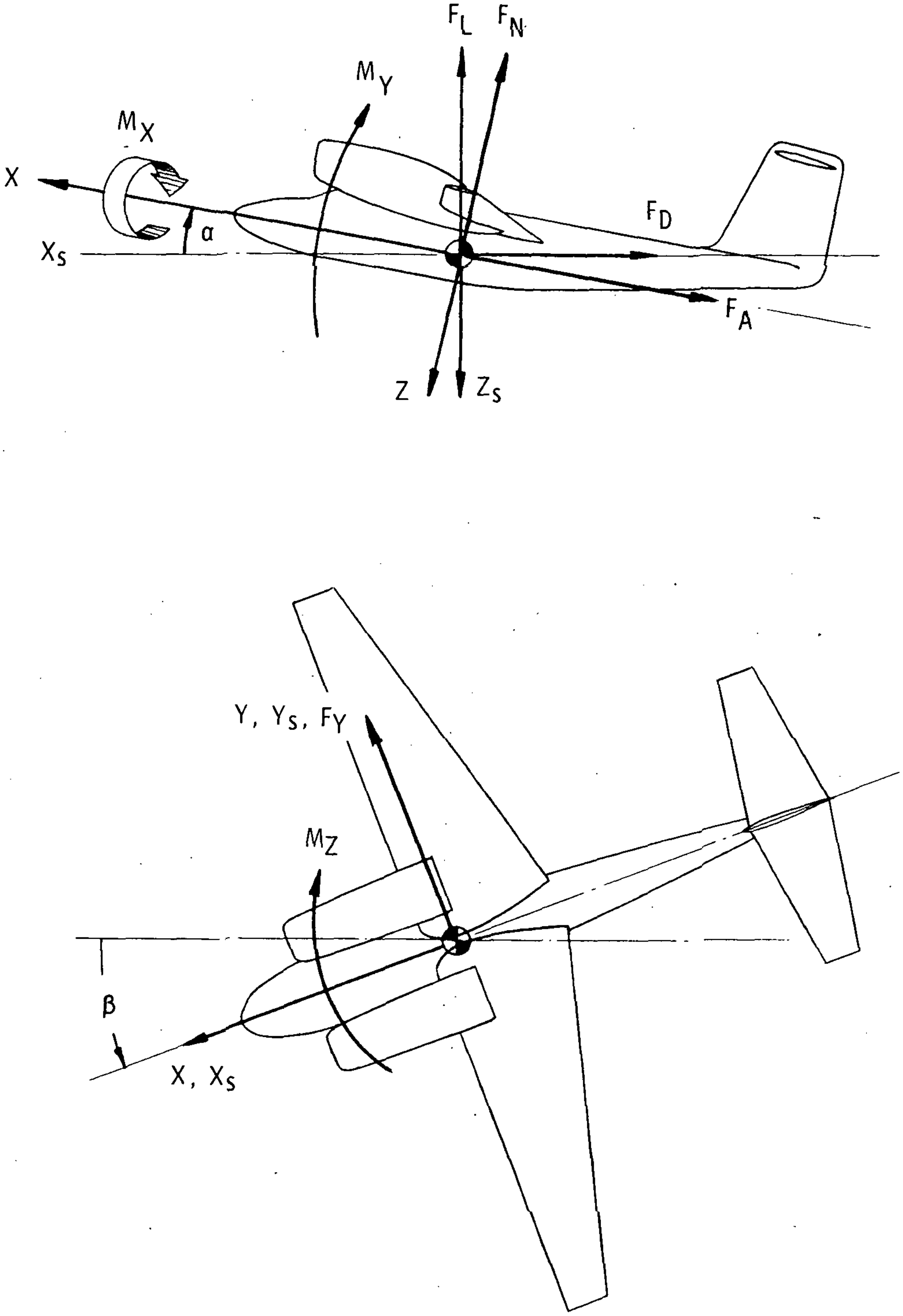

Figure 1.- Axis systems used in presentation of data. Arrows indicate positive direction of forces, moments, axes, and angles.

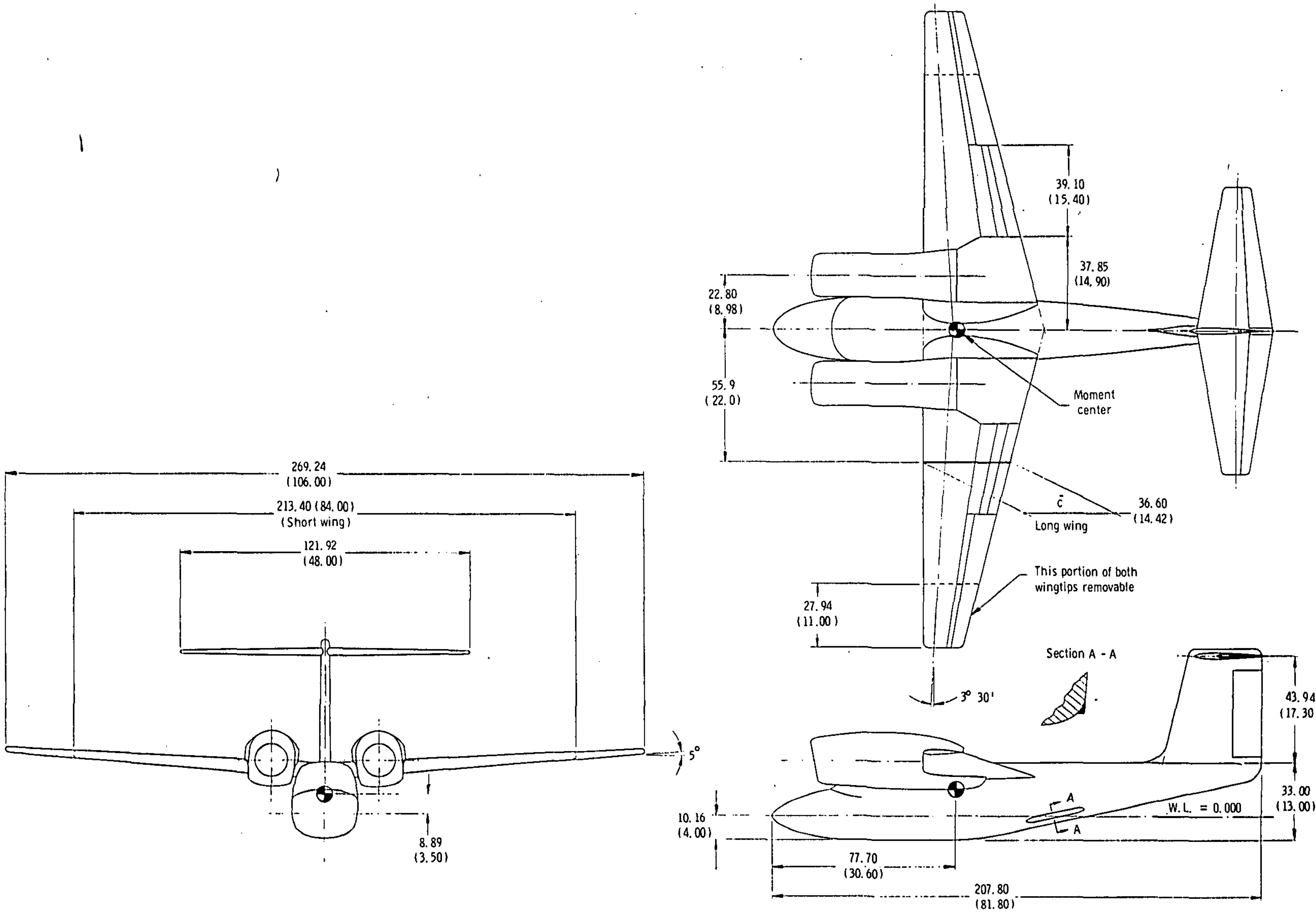

(a) Three-view drawing of model.

Figure 2.- Drawings of model used in investigation. All linear dimensions are in centimeters (inches).

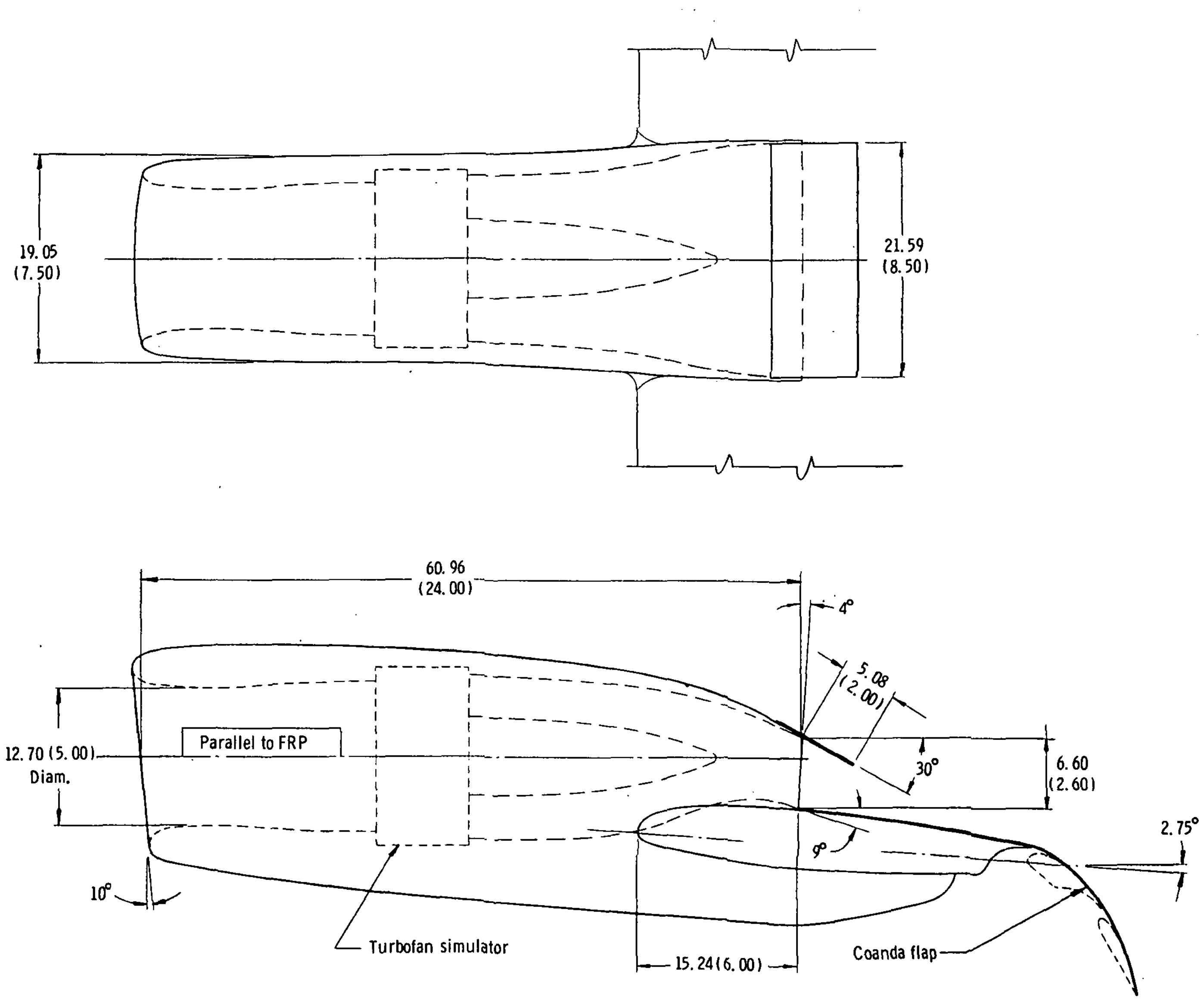

(b) Drawing of nacelle installation on wing.

Figure 2.- Continued.

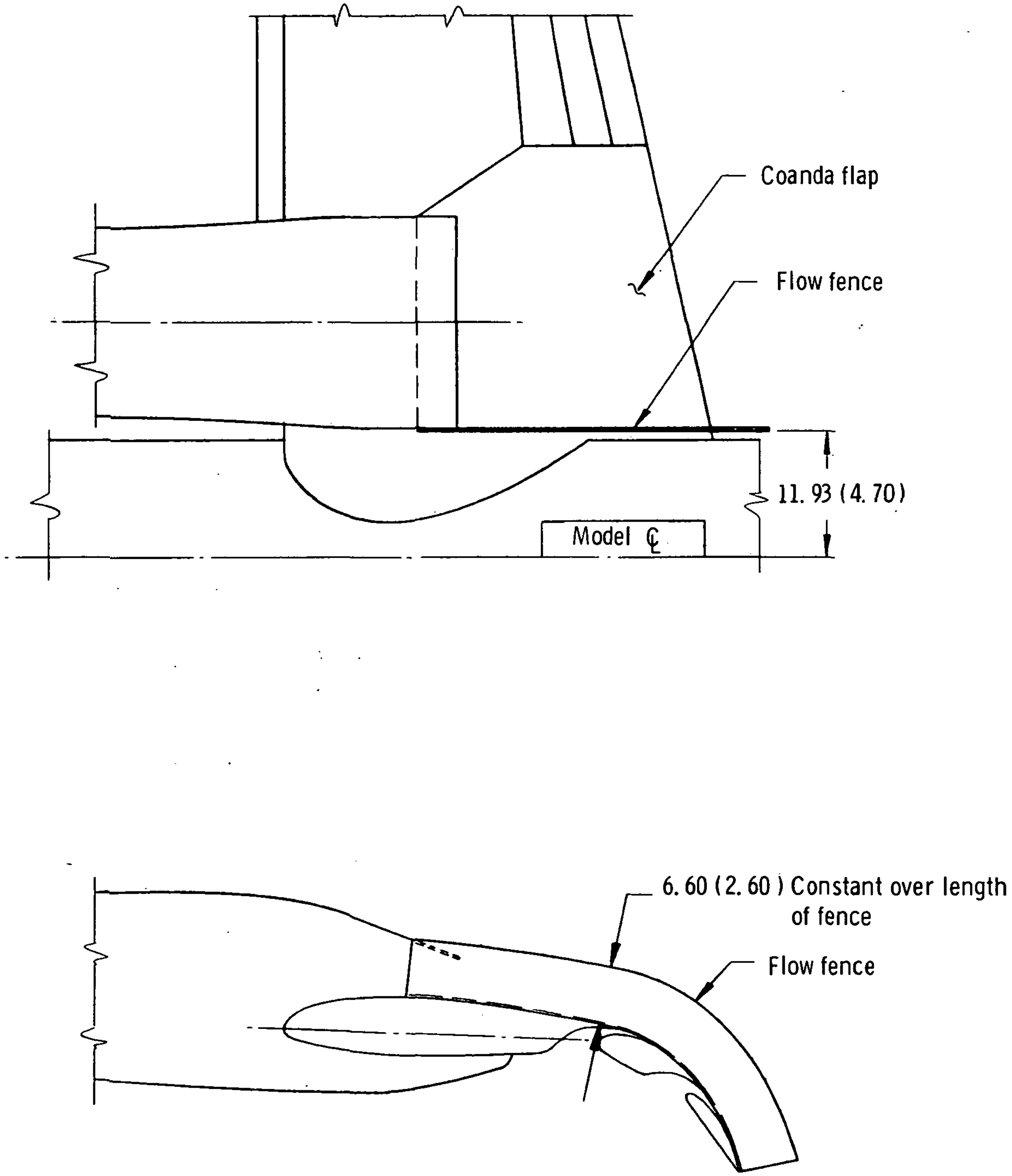

(c) Details of flow fence used for some wind-off tests.

Figure 2.- Concluded.

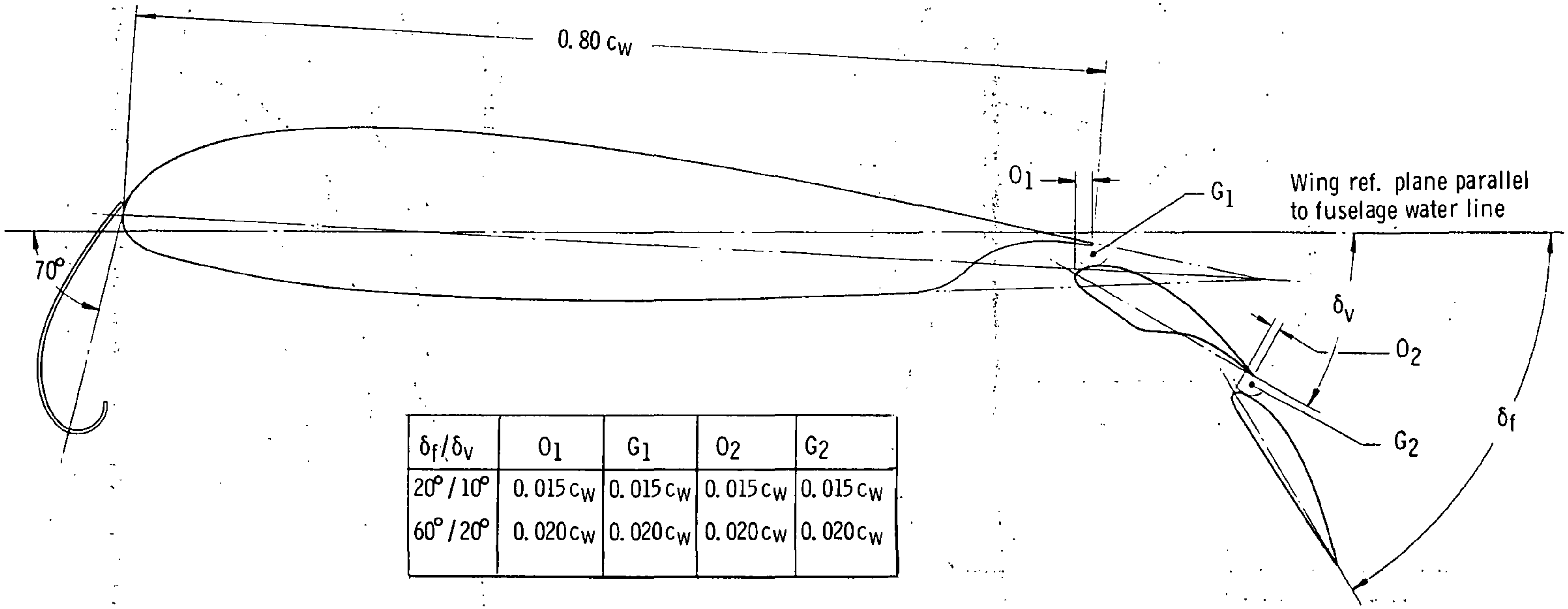

δ_f/δ_v	O_1	G_1	O_2	G_2
20°/10°	0.015 c_W	0.015 c_W	0.015 c_W	0.015 c_W
60°/20°	0.020 c_W	0.020 c_W	0.020 c_W	0.020 c_W

(a) Double-slotted trailing-edge flap and leading-edge Krueger flap.

Figure 3.- Details of wing leading-edge and trailing-edge flaps.

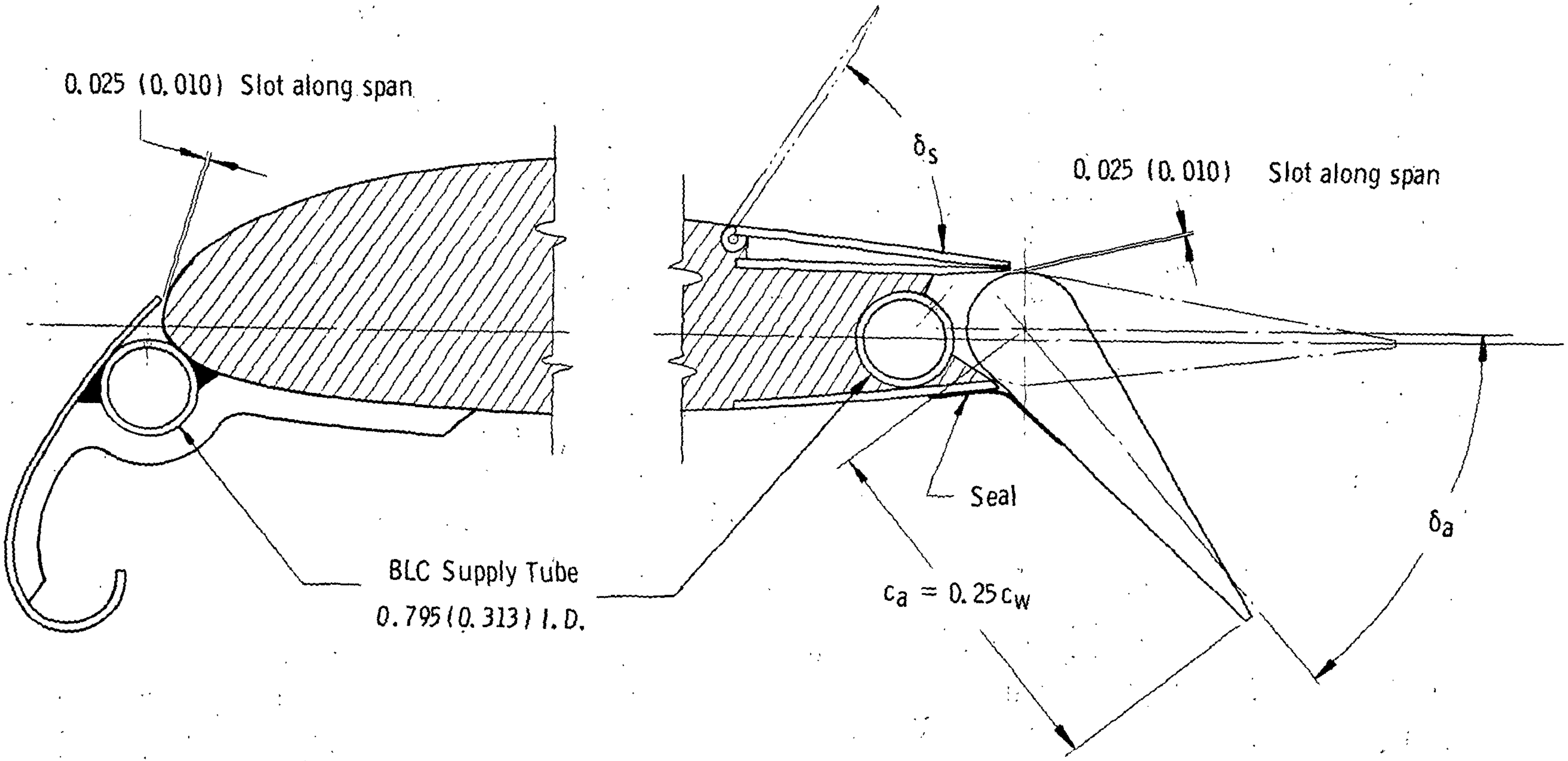

(b) Details of wing leading-edge and aileron BLC installation. Dimensions are in centimeters (inches).

Figure 3.- Concluded.

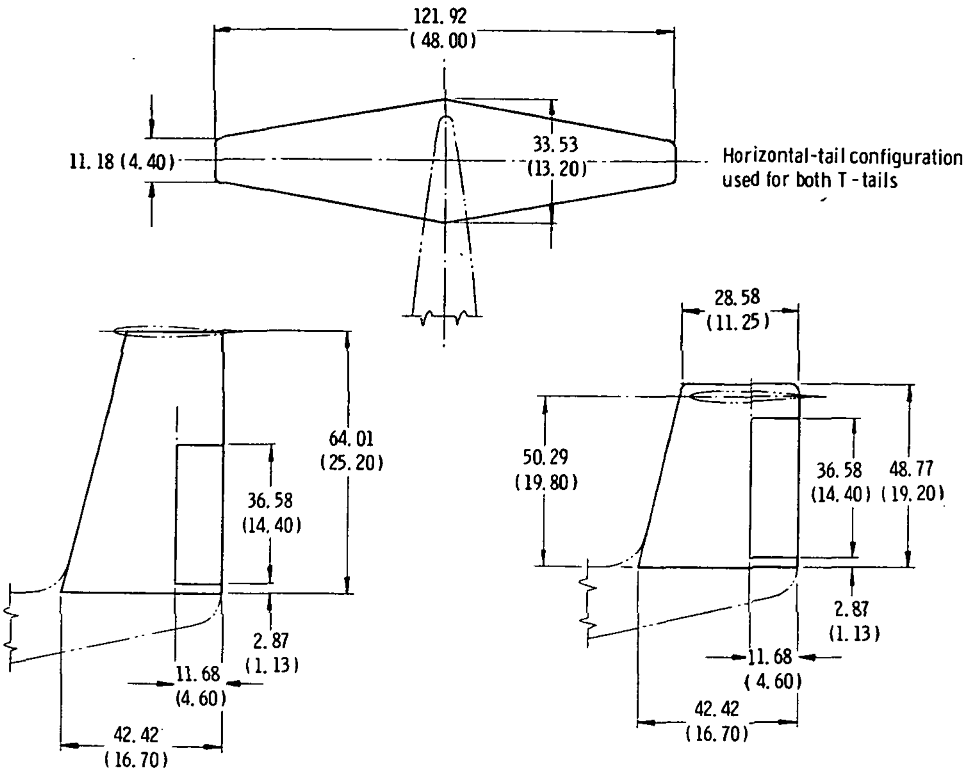

High T-tail

T-tail

(a) T-tail configuration.

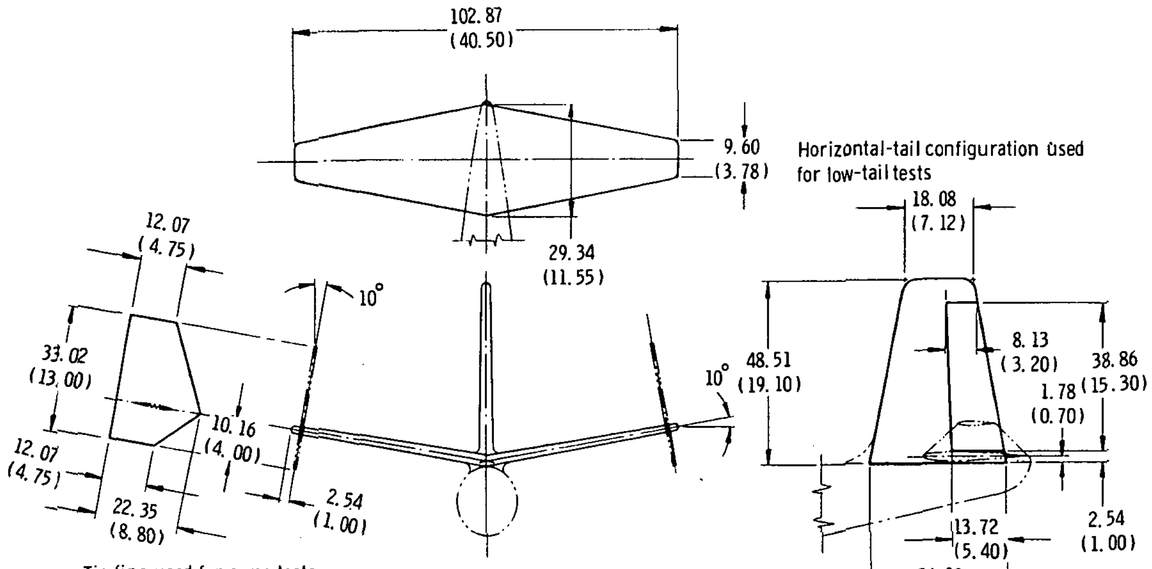

Tip fins used for some tests
(center fin removed when tip fins used)

Low-tail tip fins

Low tail

(b) Low-tail configuration.

Figure 4.- Horizontal-tail and vertical-tail configurations tested. All linear dimensions are in centimeters (inches).

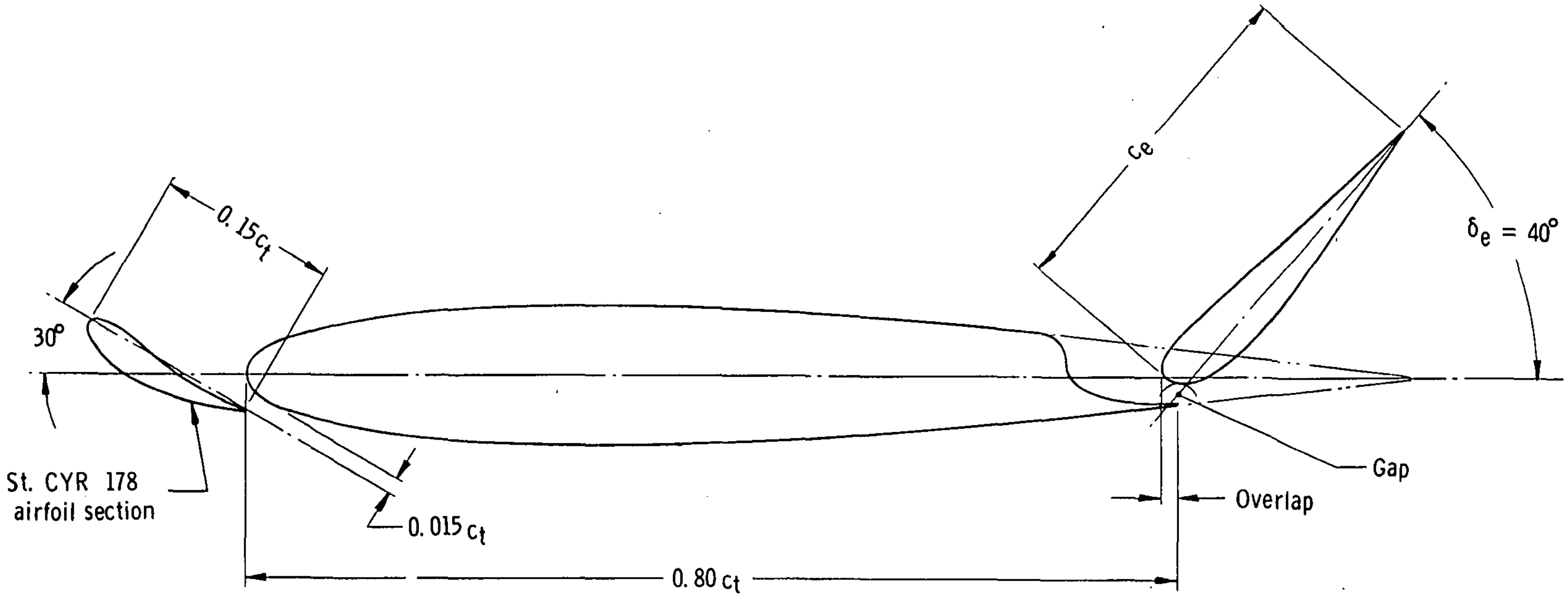

	Low tail	High tail
δ_e	40°	40°
c_e	0.45 c_t	0.30 c_t
Gap	0.015 c_t	0.015 c_t
Overlap	0.015 c_t	0.015 c_t

Figure 5.- Horizontal-tail high-lift devices.

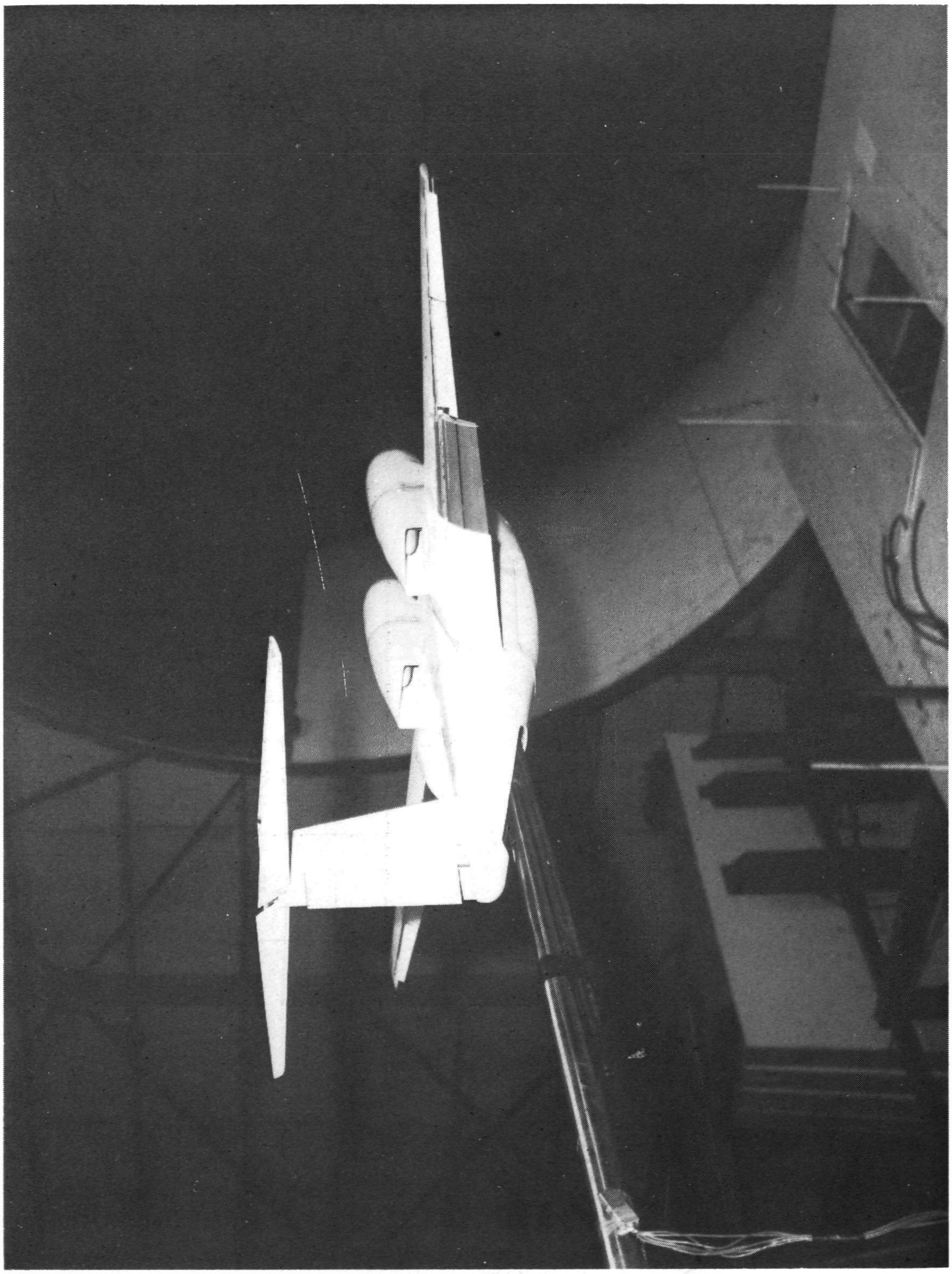

L-73-8829

Figure 6.- Model installed in the Langley full-scale tunnel.

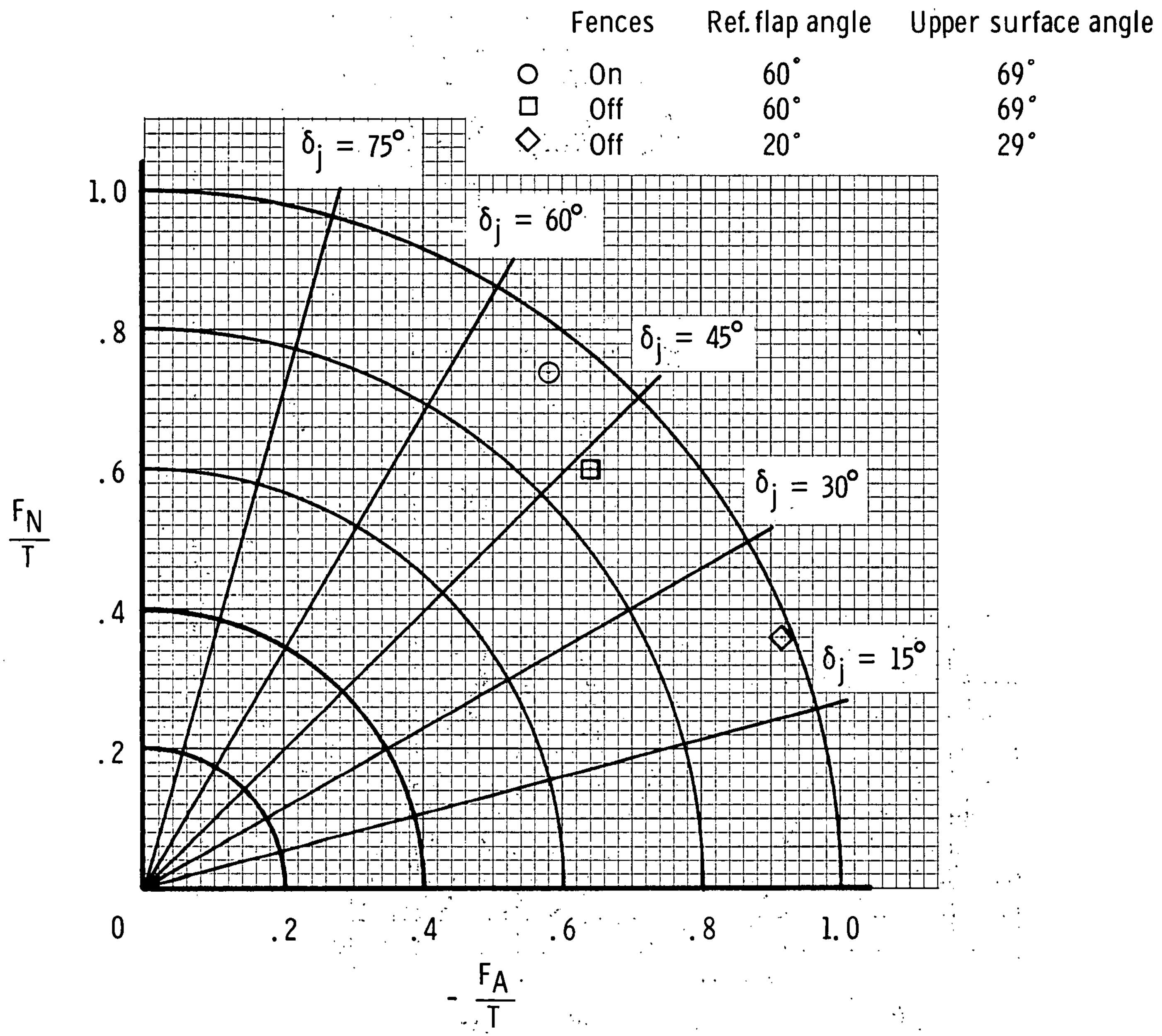

Figure 7.- Summary of flap turning efficiency and turning angle; full power.

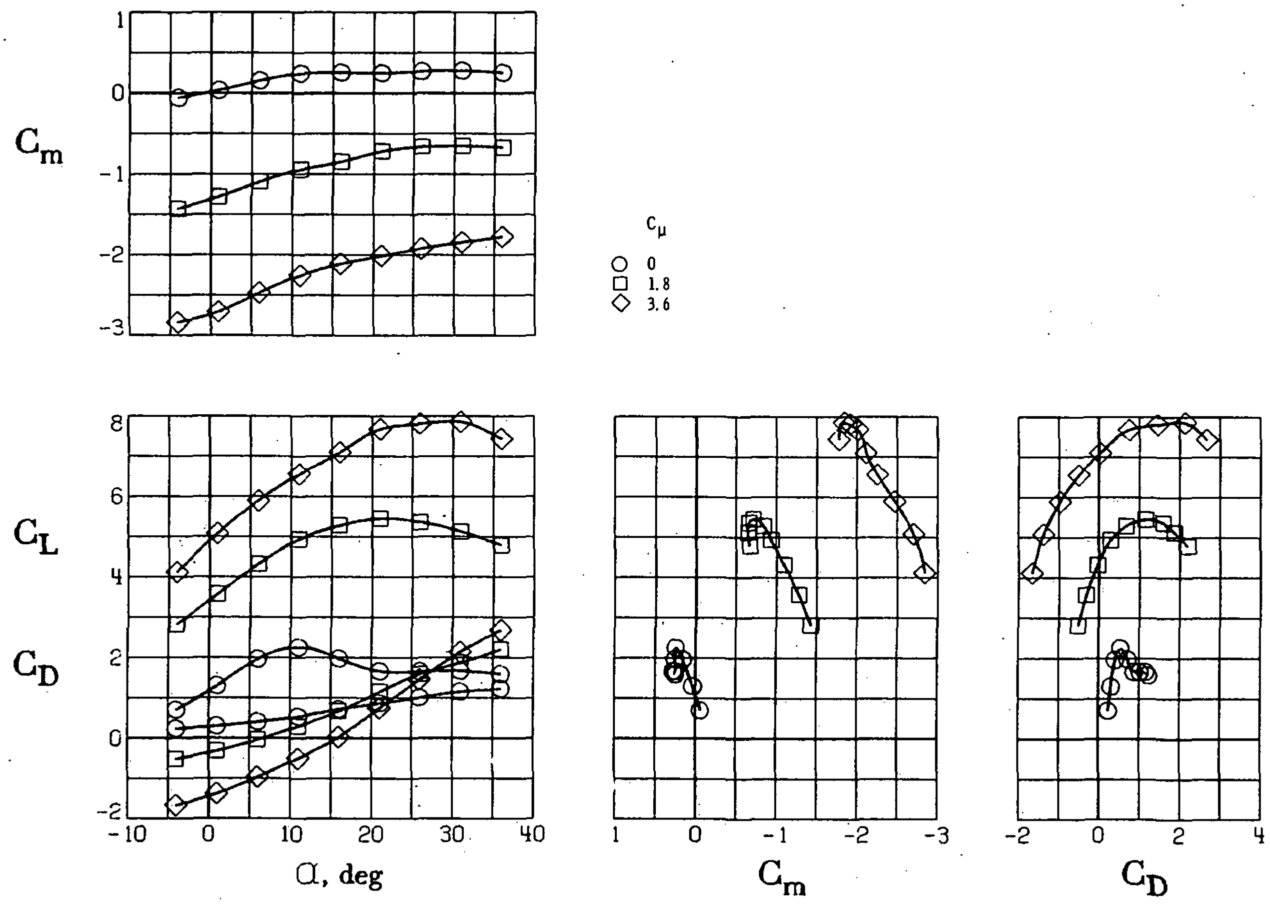

(a) BLC off.

Figure 8.- Longitudinal aerodynamic characteristics of the model with tail off for $\delta_f = 60^\circ$.

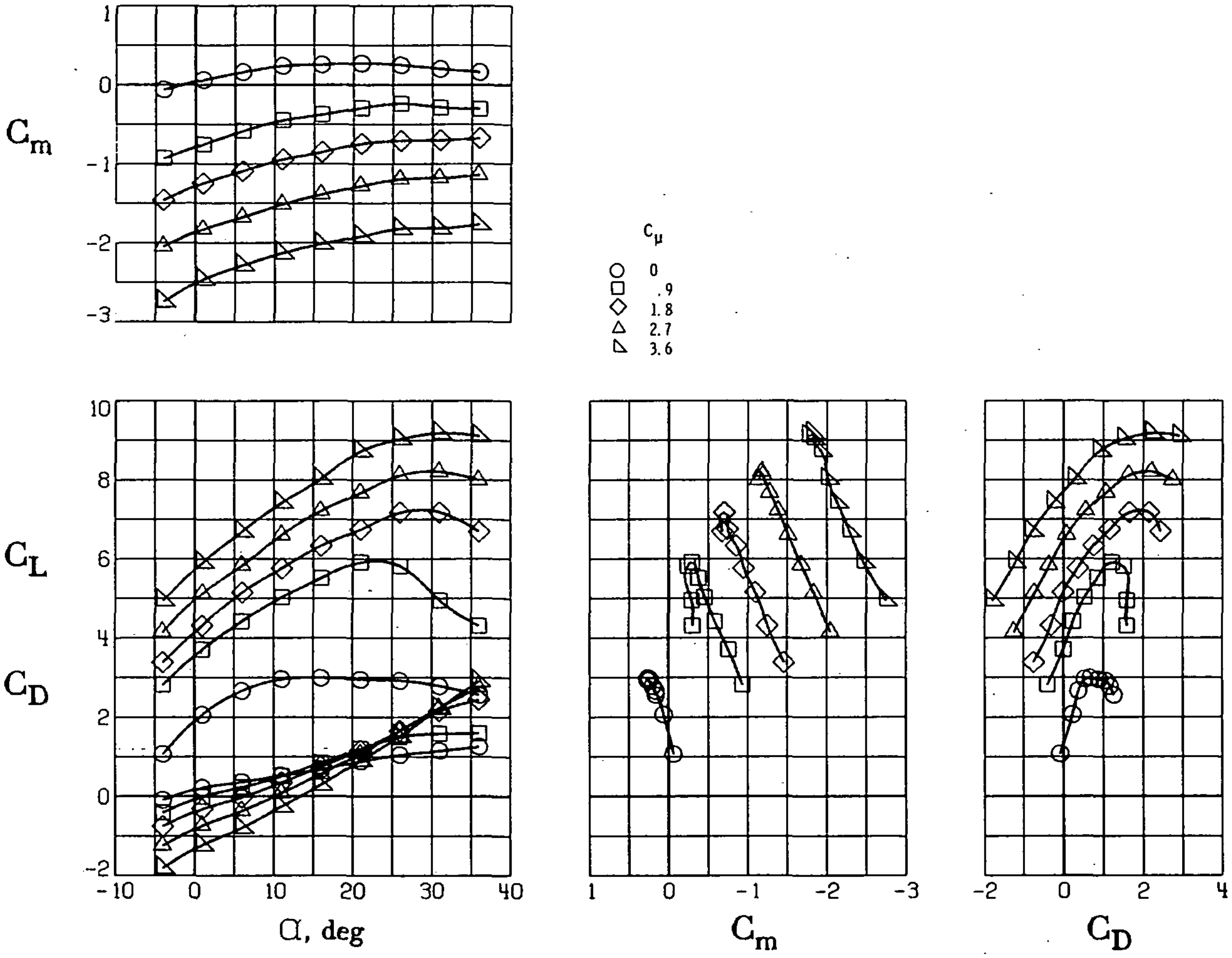

(b) $C_{\mu,le} = 0.035$; $C_{\mu,a} = 0.035$.

Figure 8.- Concluded.

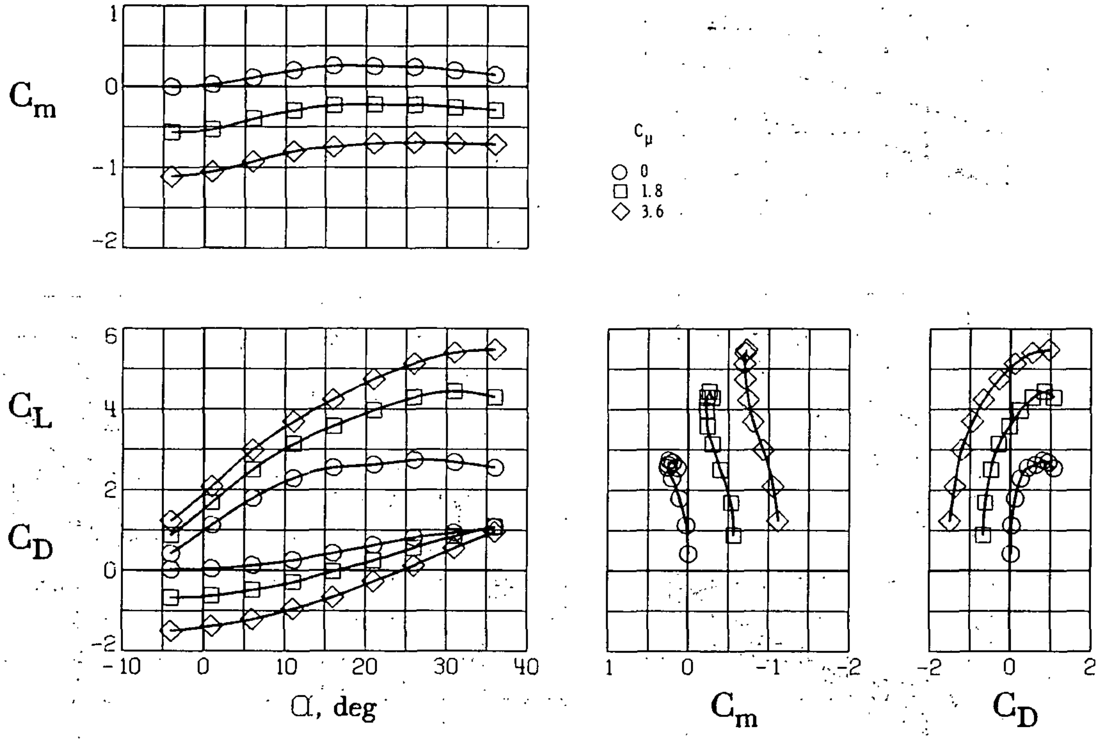

Figure 9.- Longitudinal aerodynamic characteristics of the model with tail off for $\delta_f = 20^{o}$. $C_{\mu,le} = 0.035$; $C_{\mu,a} = 0.035$.

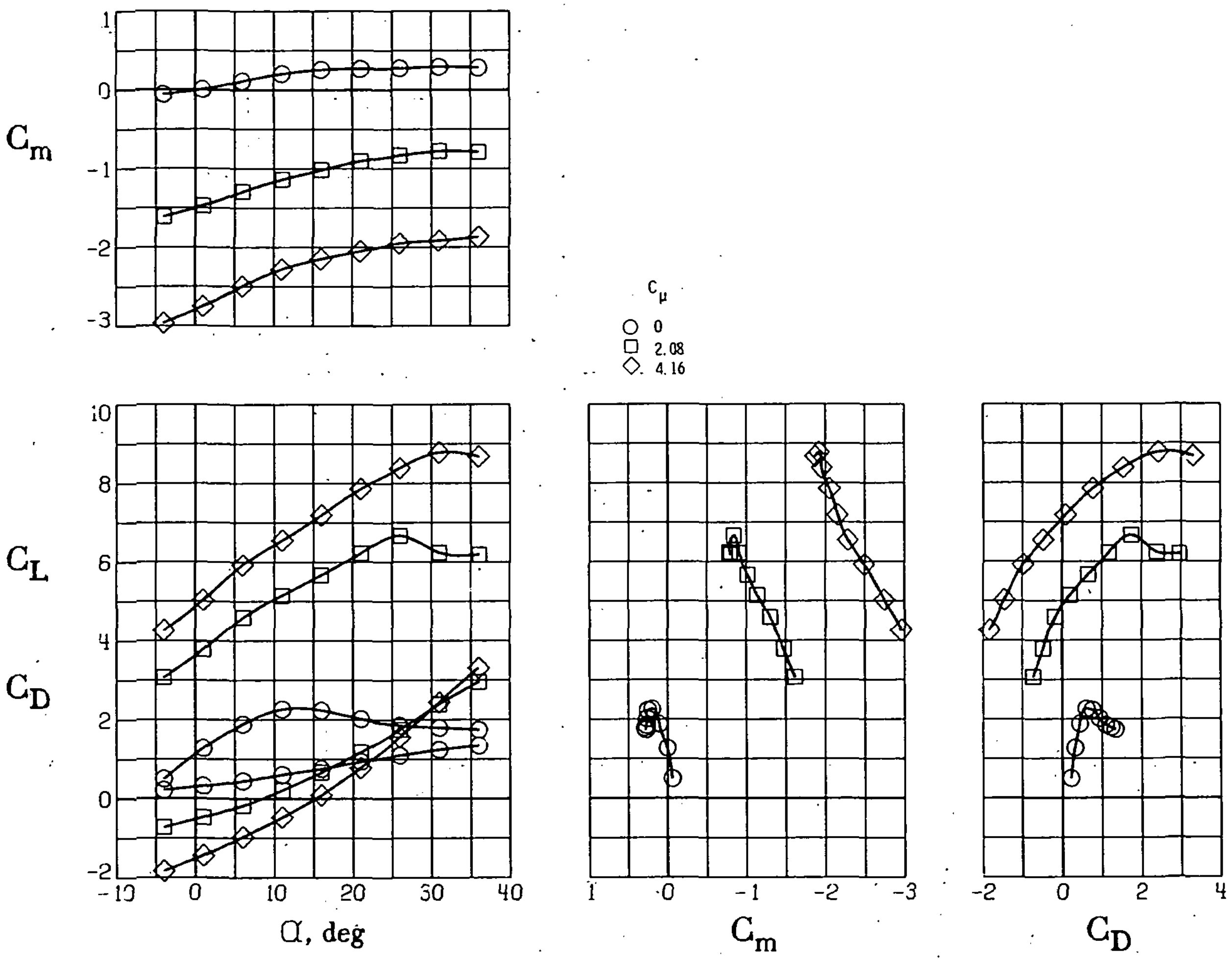

(a) BLC off.

Figure 10.- Longitudinal aerodynamic characteristics of the model with aspect-ratio-6.0 wing. Tail off; $\delta_f = 60^\circ$. Coefficients are based on short-wing geometry.

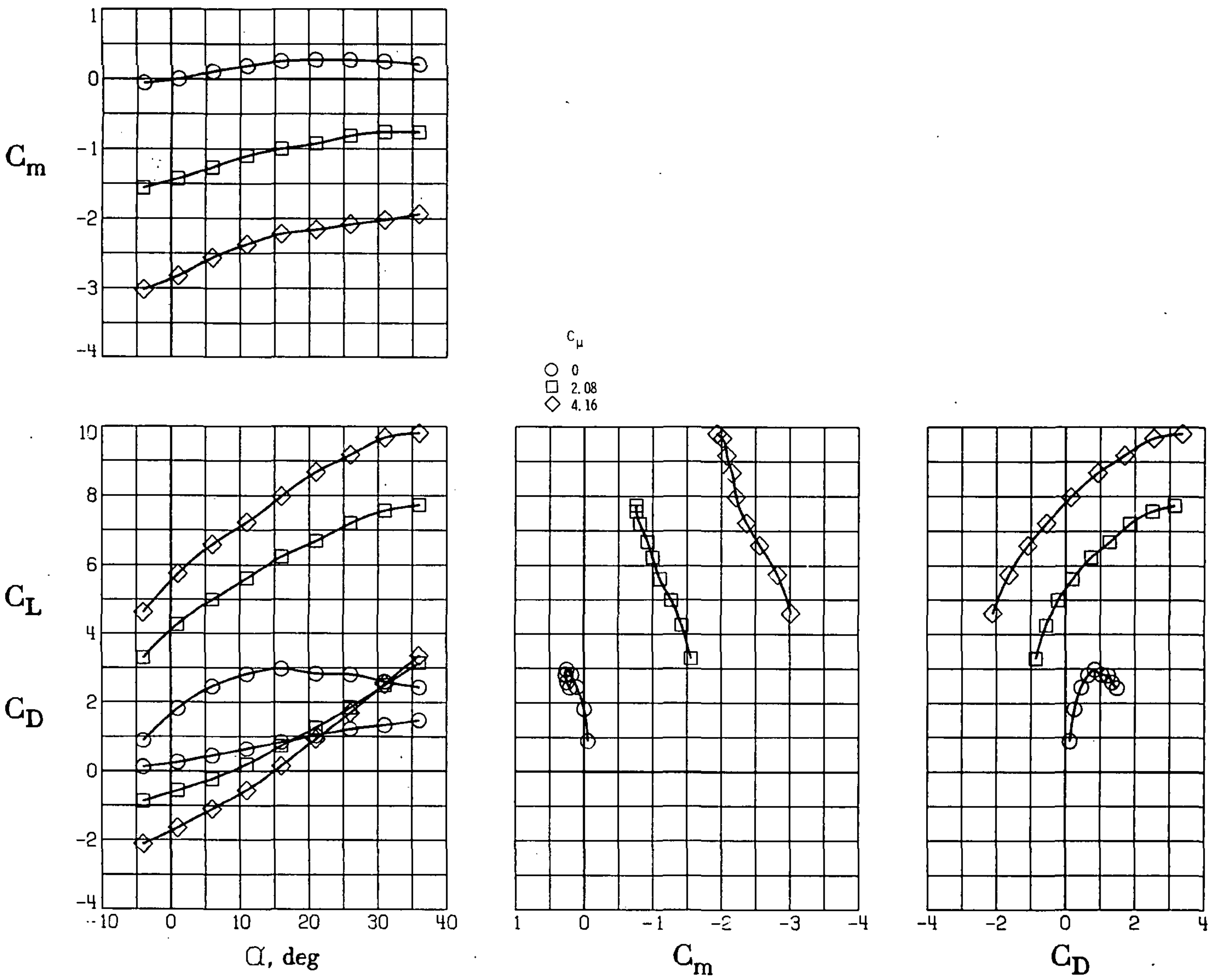

(b) $C_{\mu,le} = 0.025$; $C_{\mu,a} = 0.018$.

Figure 10.- Concluded.

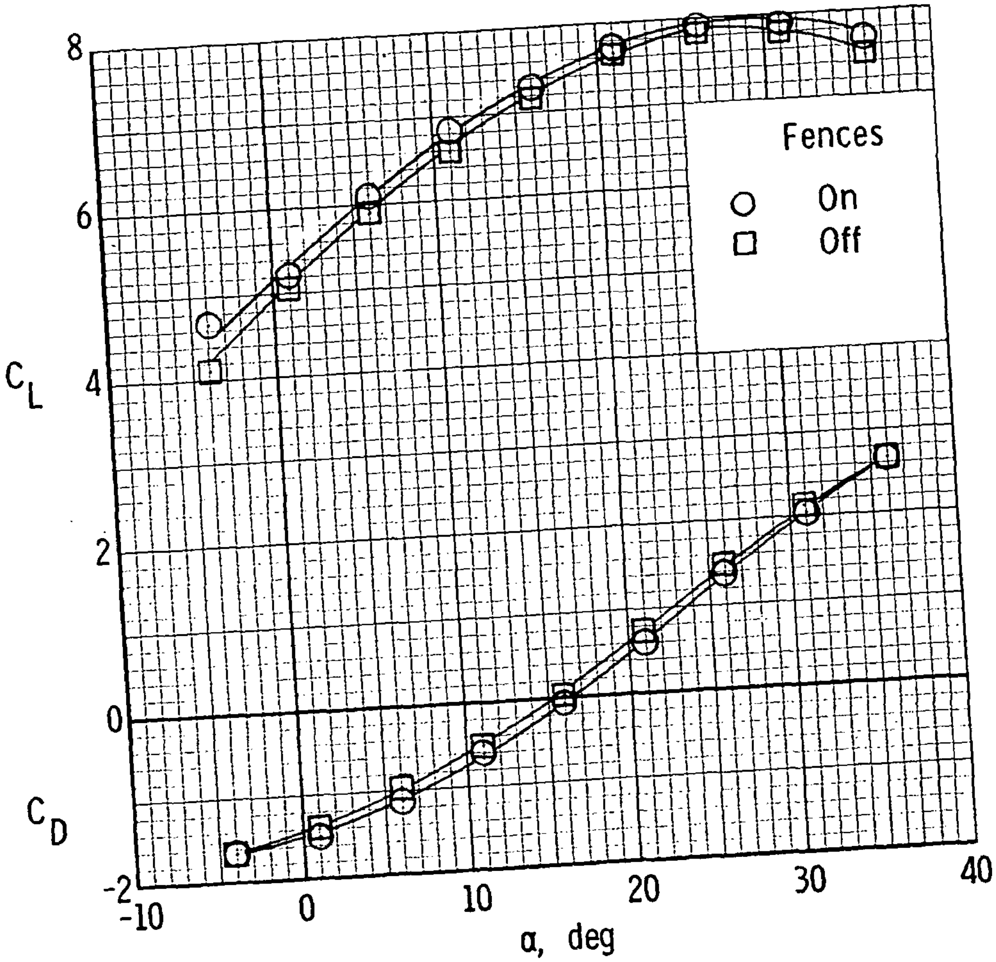

Figure 11.- Effect of fences on inboard side of nacelle. $C_\mu = 3.6$; tail off; BLC off; $\delta_f = 60^o$.

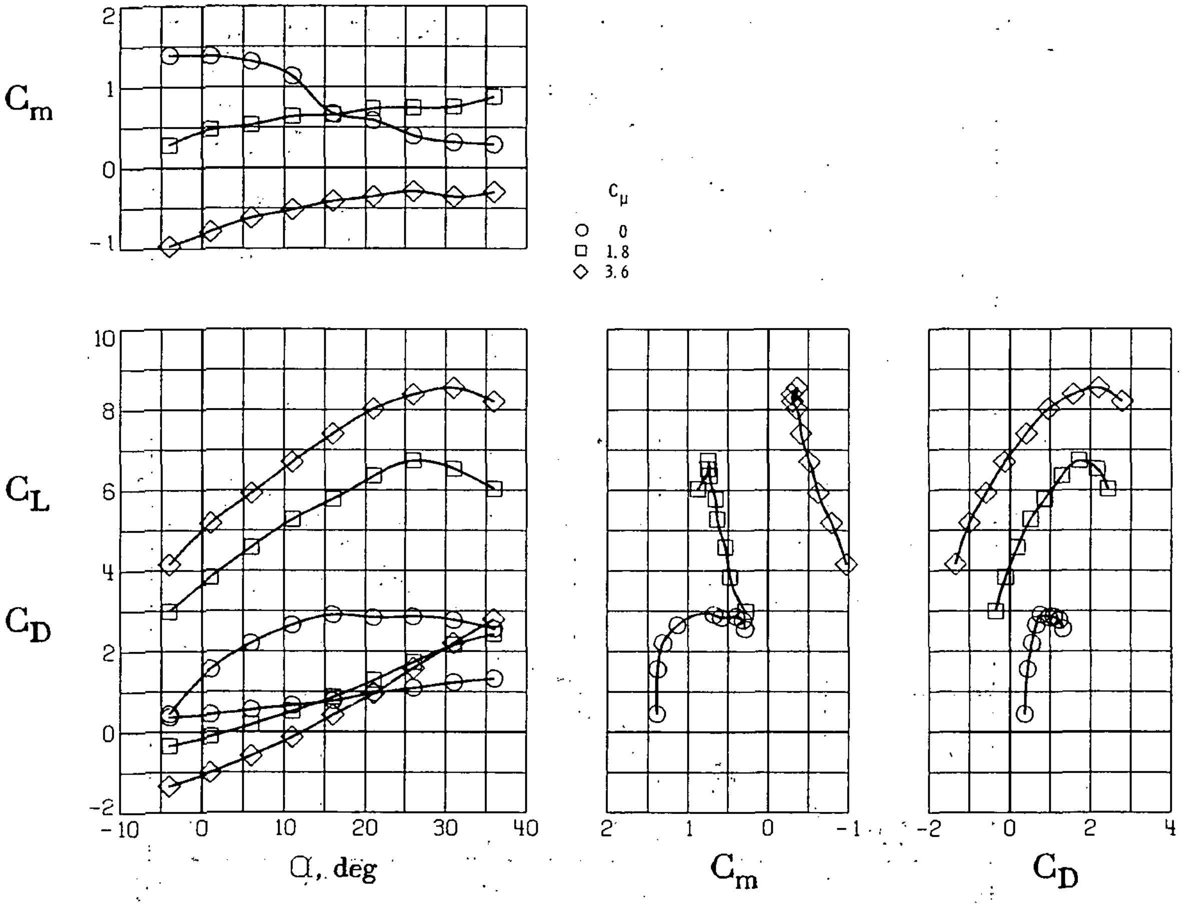

(a) $i_t = 0^\circ$.

Figure 12.- Longitudinal aerodynamic characteristics of the model with T-tail. $\delta_f = 60^\circ$; $C_{\mu,le} = 0.035$; $C_{\mu,a} = 0.035$.

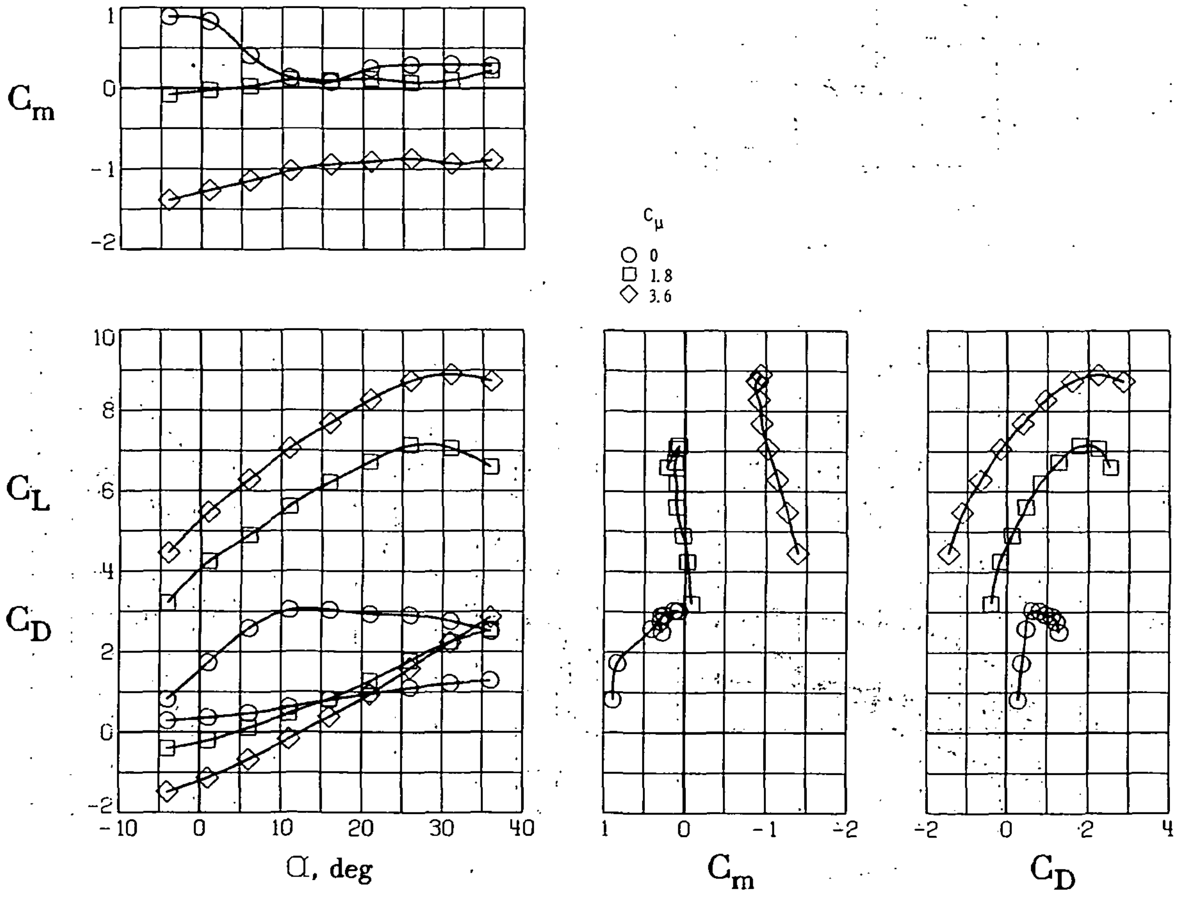

(b) $i_t = 5^o$.

Figure 12.- Continued.

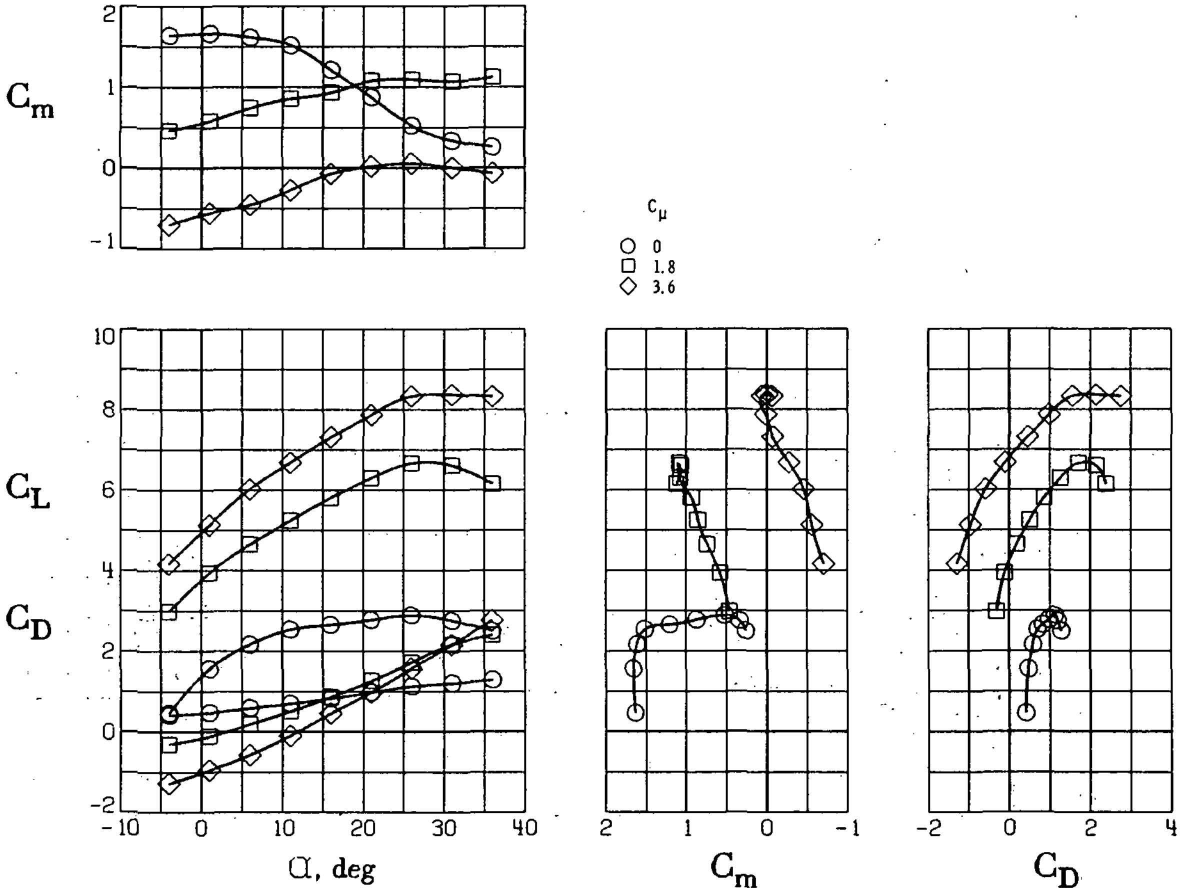

(c) $i_t = -5^{\circ}$.

Figure 12.- Concluded.

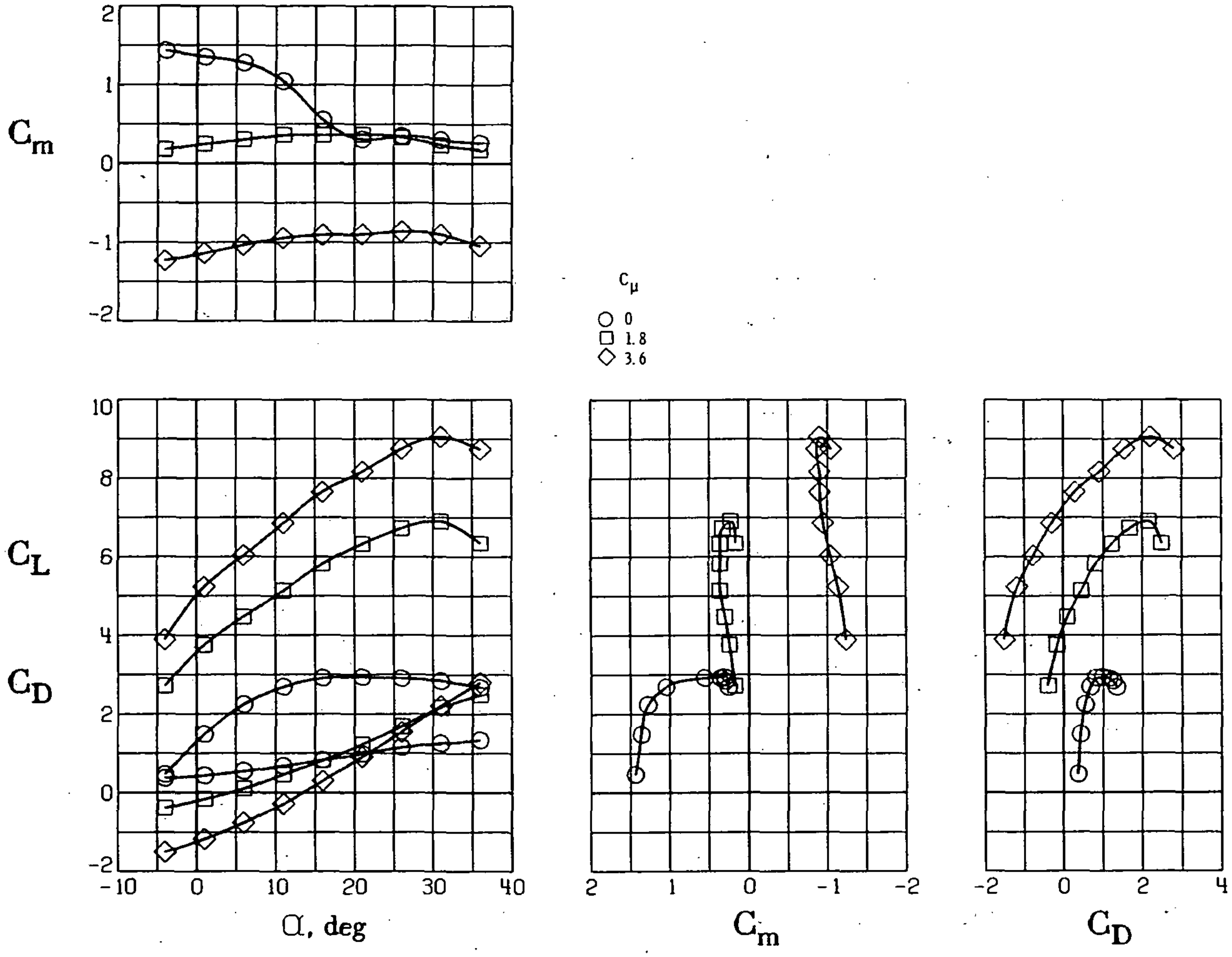

Figure 13.- Longitudinal aerodynamic characteristics of the model with high T-tail. $i_t = 0^\circ$; $\delta_f = 60^\circ$; $C_{\mu,le} = 0.035$; $C_{\mu,a} = 0.035$.

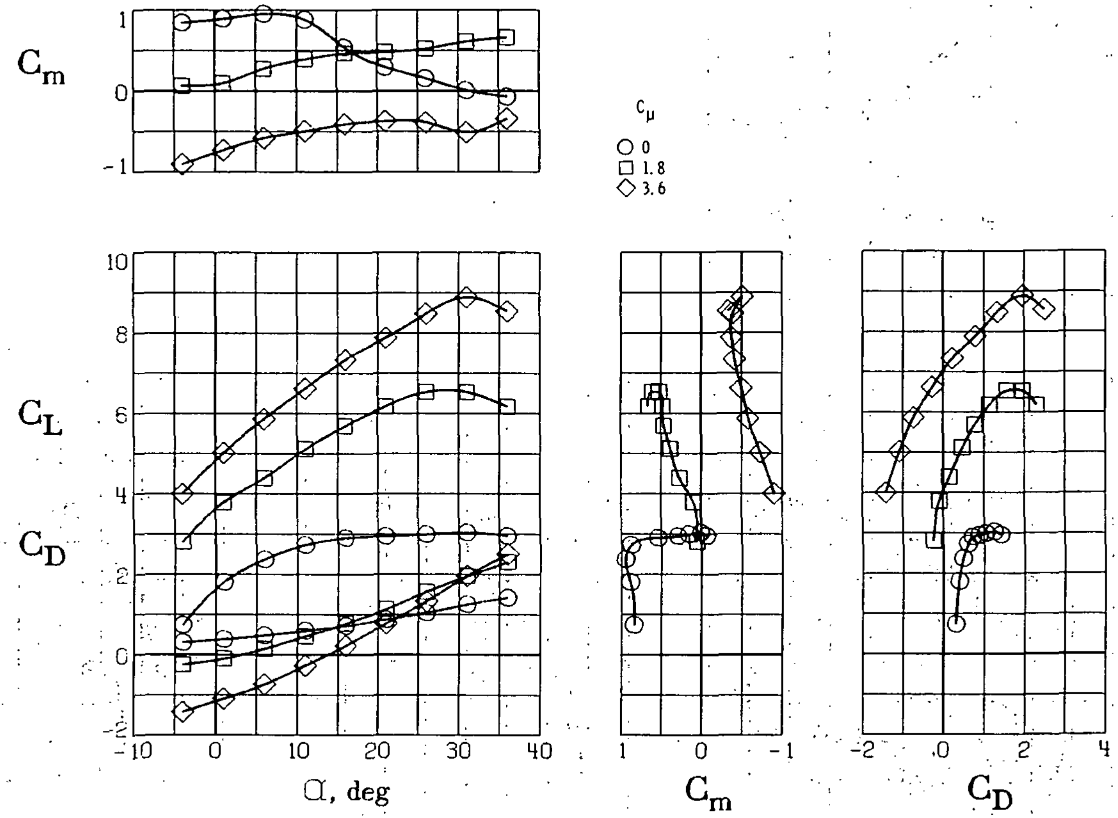

(a) $i_t = 0^\circ$.

Figure 14.- Longitudinal aerodynamic characteristics of the model with low tail. $\delta_f = 60^\circ$; $C_{\mu,le} = 0.035$; $C_{\mu,a} = 0.035$.

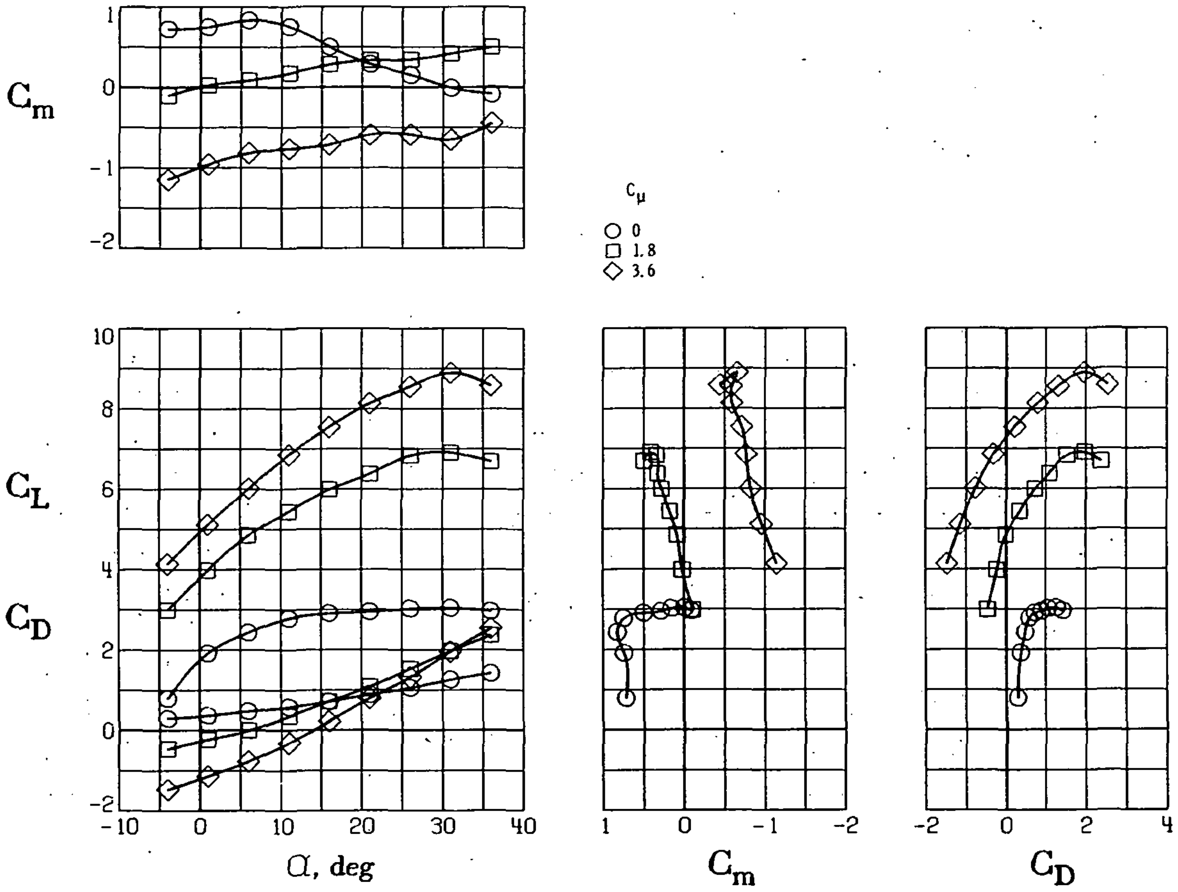

(b) $i_t = 5^{\circ}$.

Figure 14.- Continued.

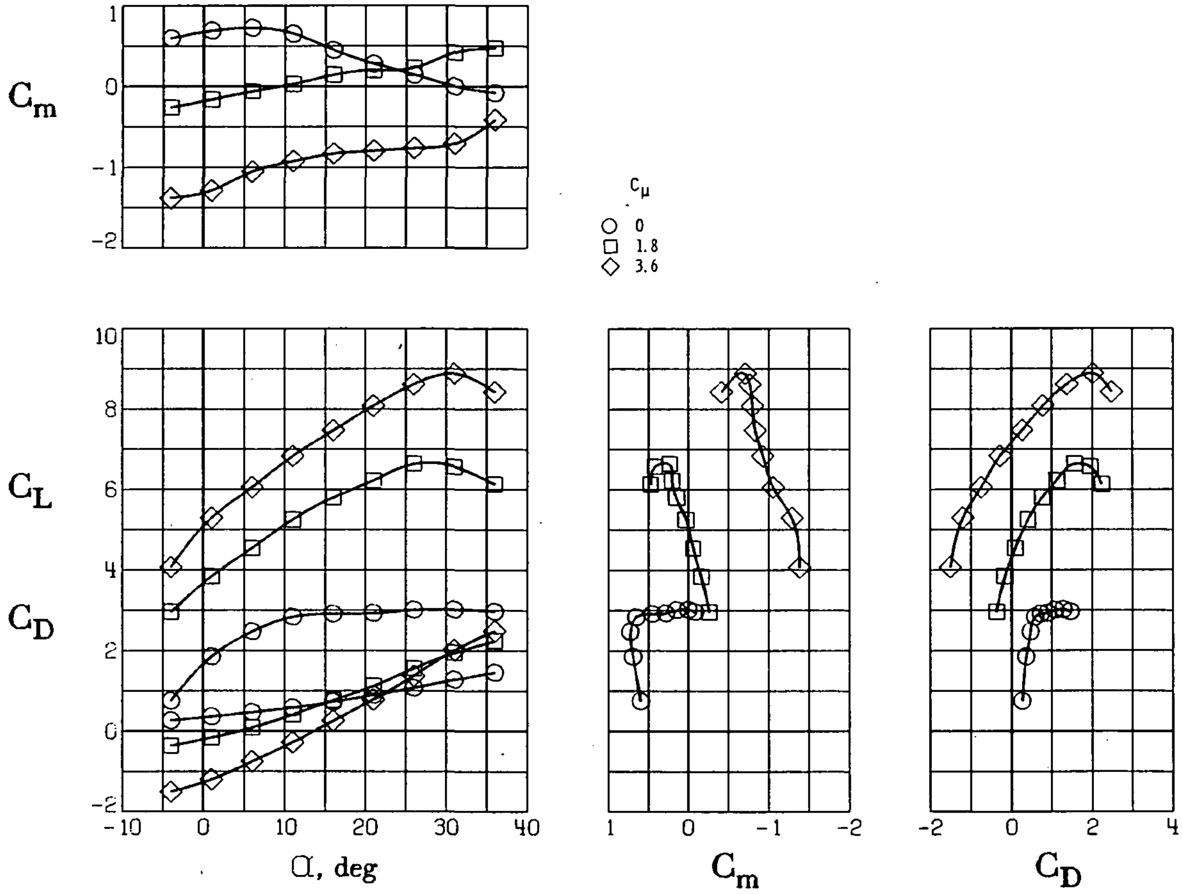

(c) $i_t = 10^{\circ}$.

Figure 14.- Concluded.

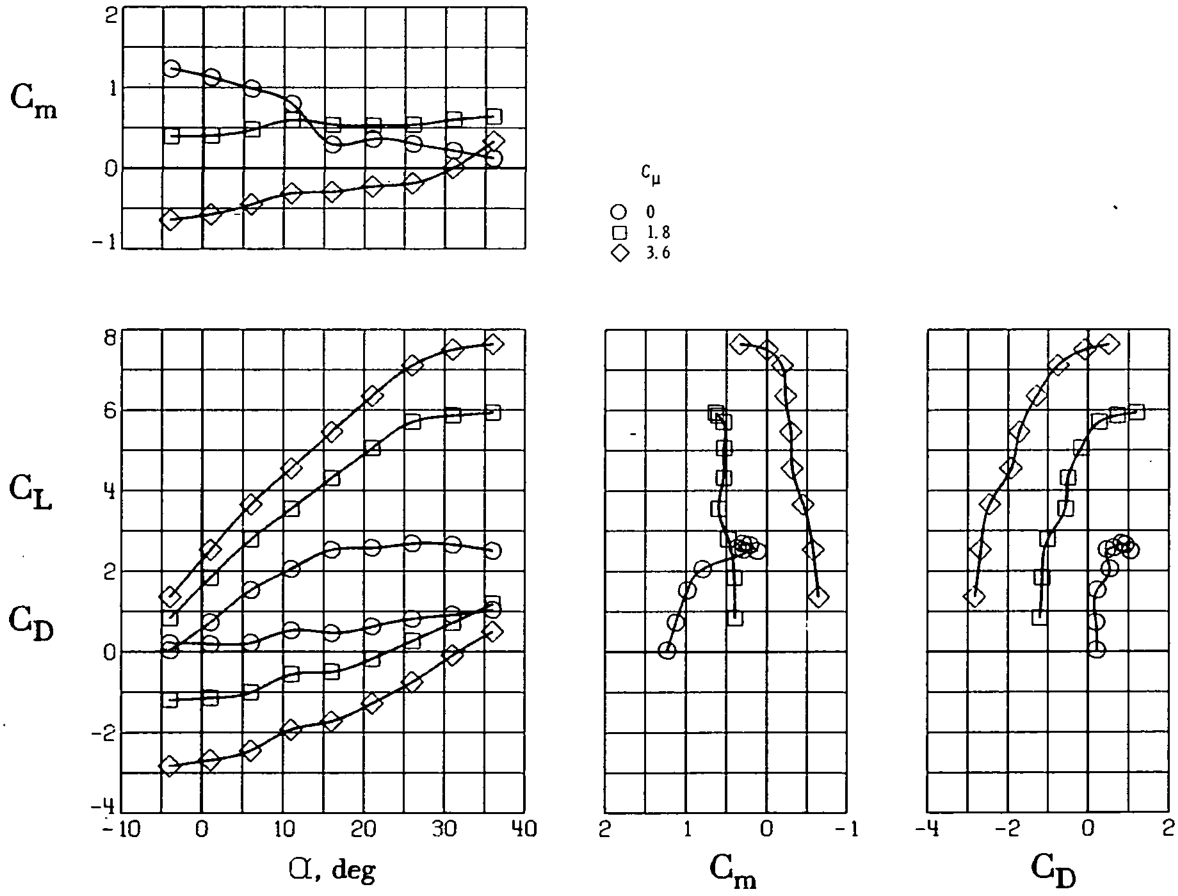

(a) $i_t = 0^\circ$.

Figure 15.- Longitudinal aerodynamic characteristics of the model with T-tail. $\delta_f = 20^\circ$; $C_{\mu,le} = 0.035$; $C_{\mu,a} = 0.035$.

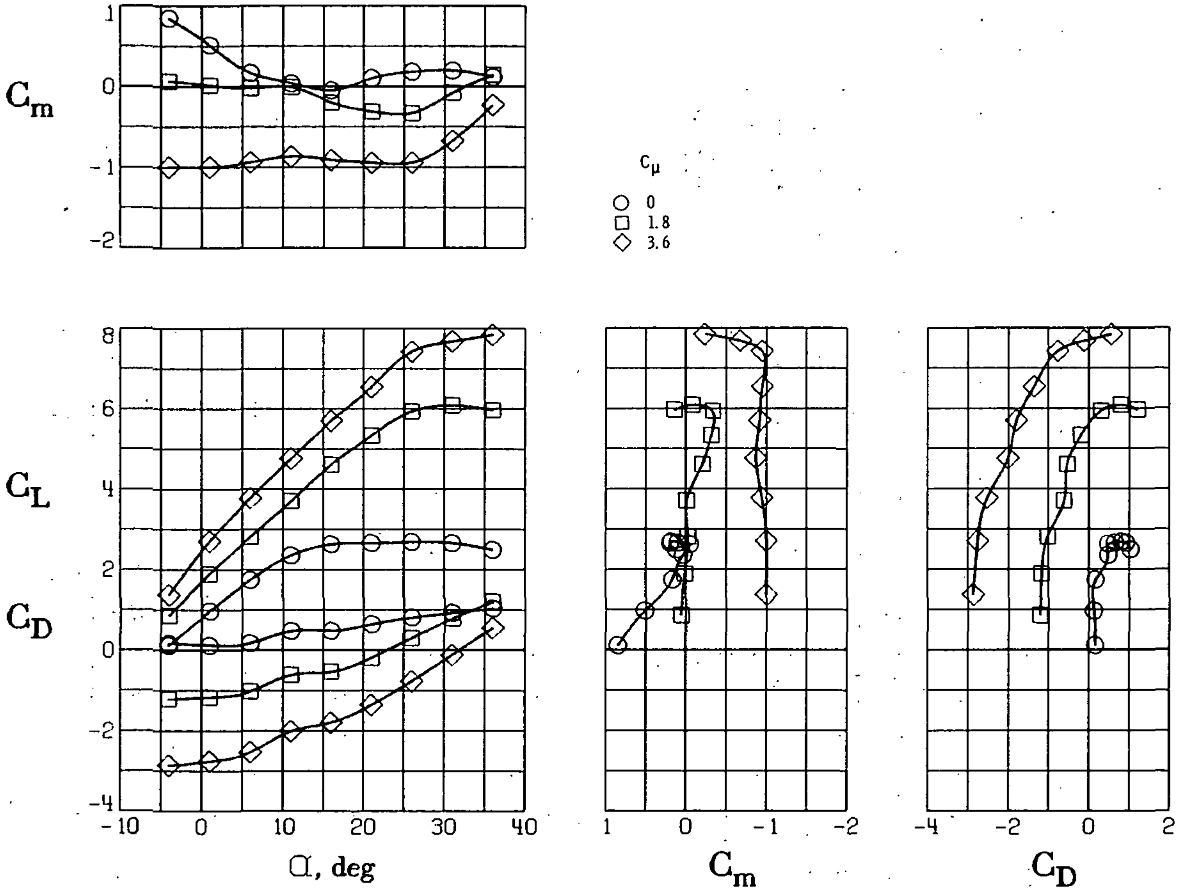

(b) $i_t = -5^{\circ}$.

Figure 15.- Continued.

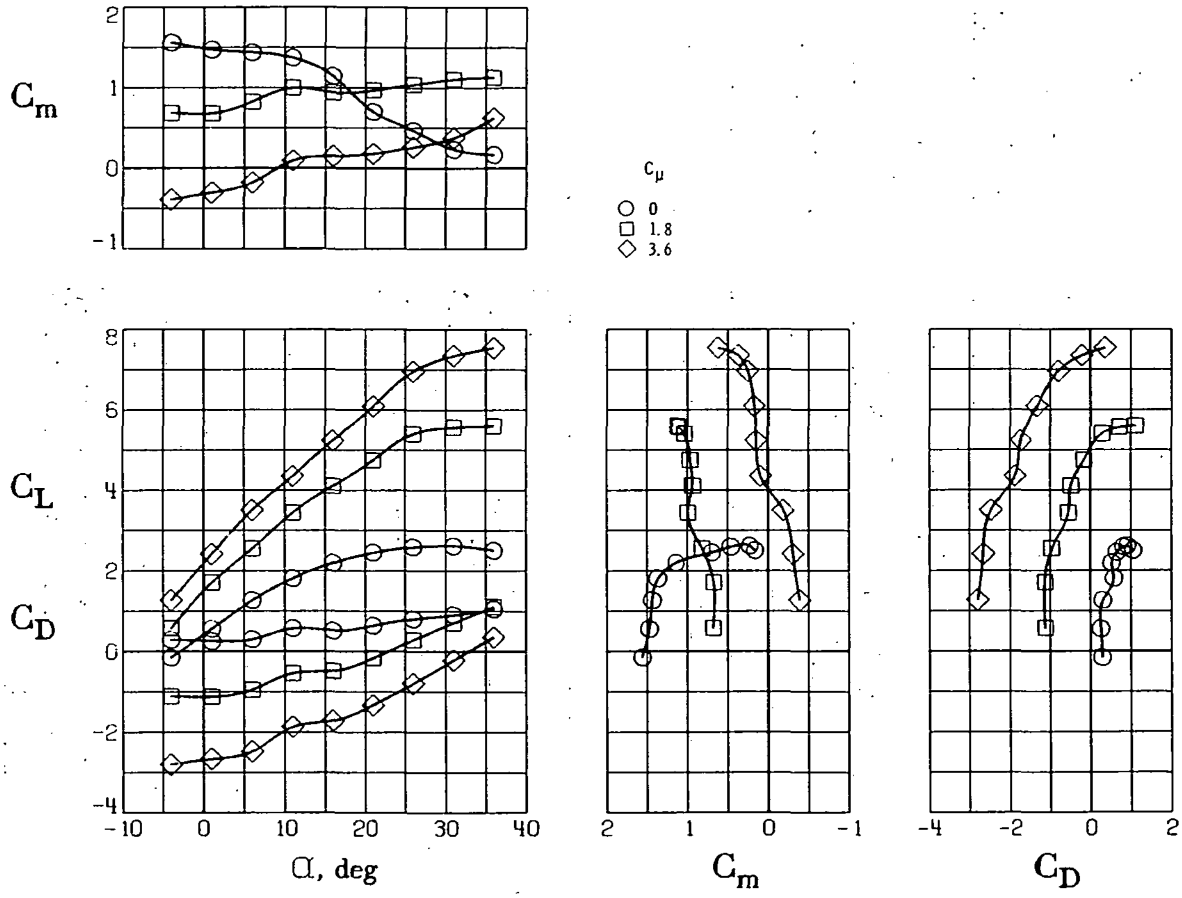

(c) $i_t = 5^\circ$.

Figure 15.- Continued.

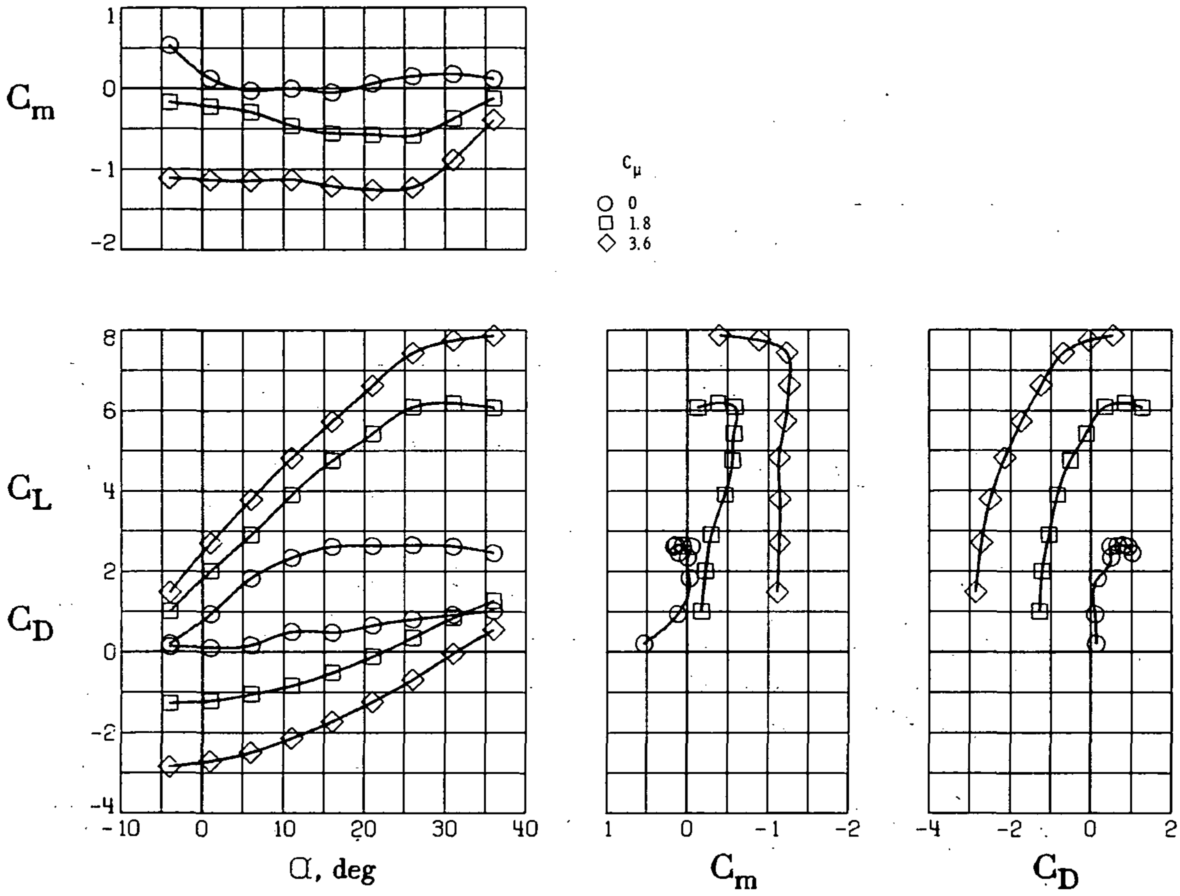

(d) $i_t = 7.5^\circ$.

Figure 15.- Concluded.

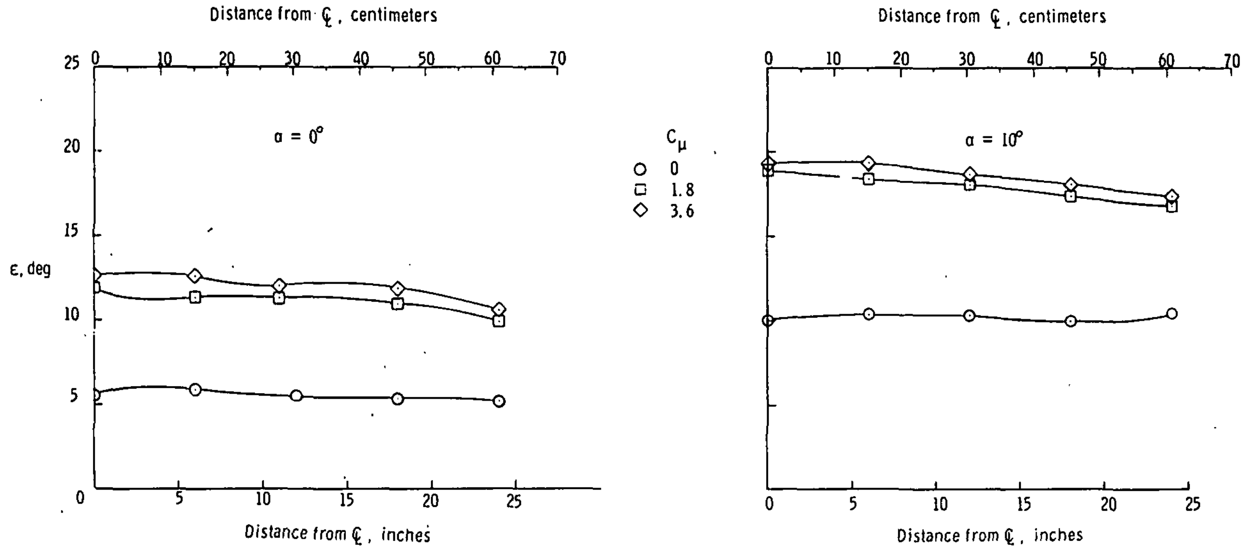

(a) T-tail.

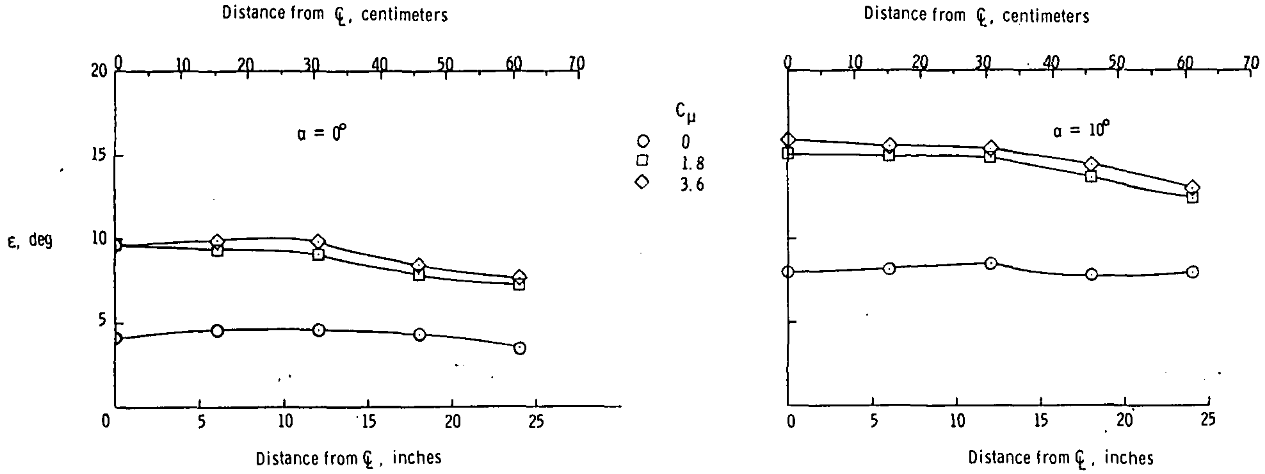

(b) High T-tail.

Figure 16.- Downwash variation across span of horizontal tail. $\delta_f = 60^{\circ}$; $C_{\mu,le} = 0.035$; $C_{\mu,a} = 0.035$.

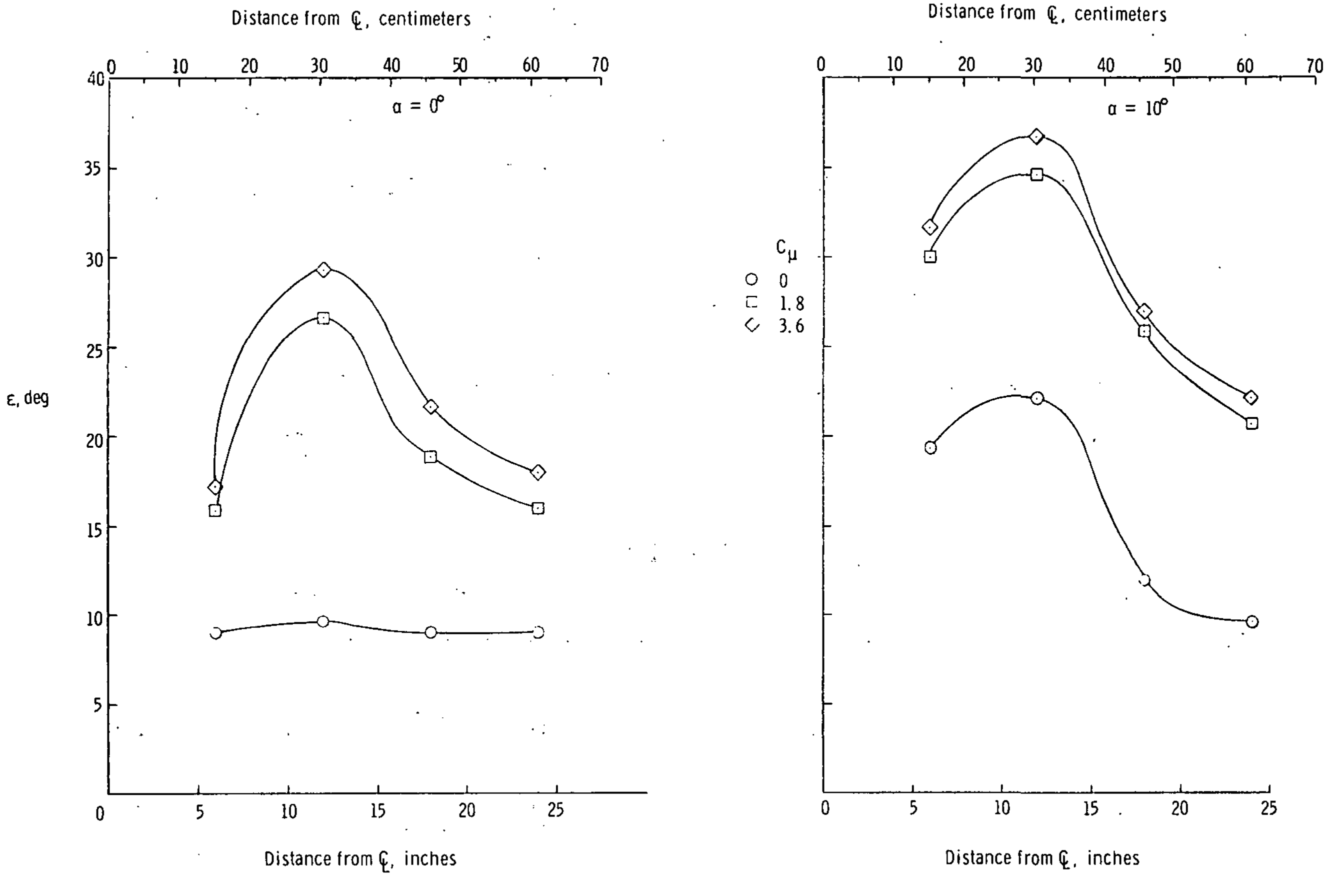

(c) Low tail.

Figure 16.- Concluded.

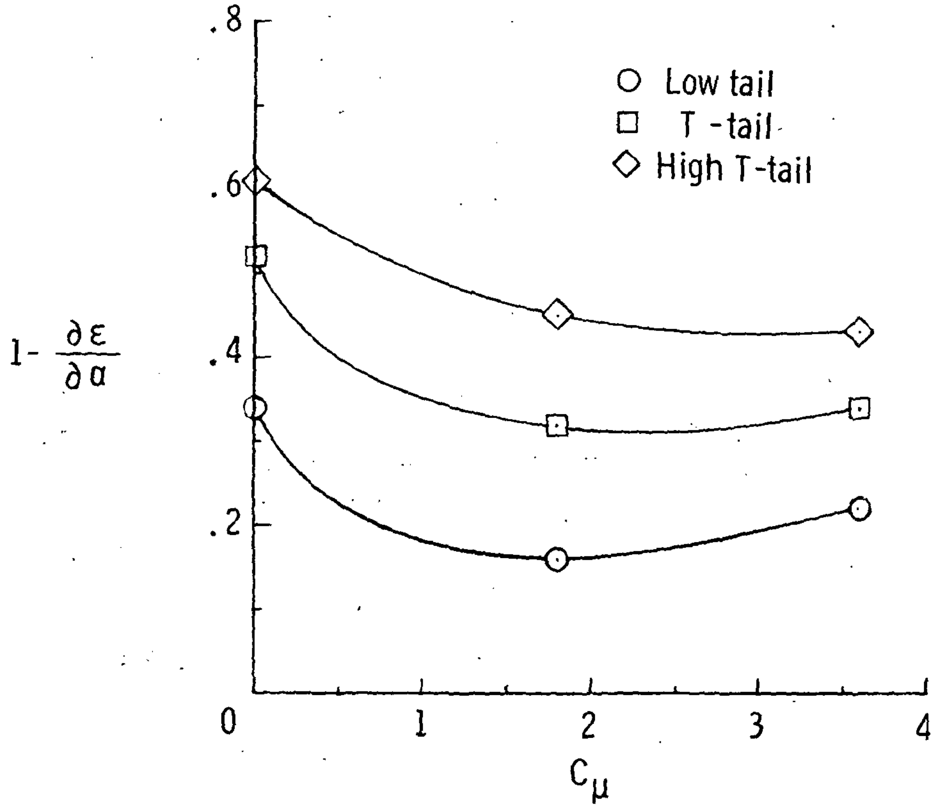

Figure 17.- Variation of downwash factor with thrust coefficient. $\delta_f = 60^o$; $C_{\mu,le} = 0.035$; $C_{\mu,a} = 0.035$.

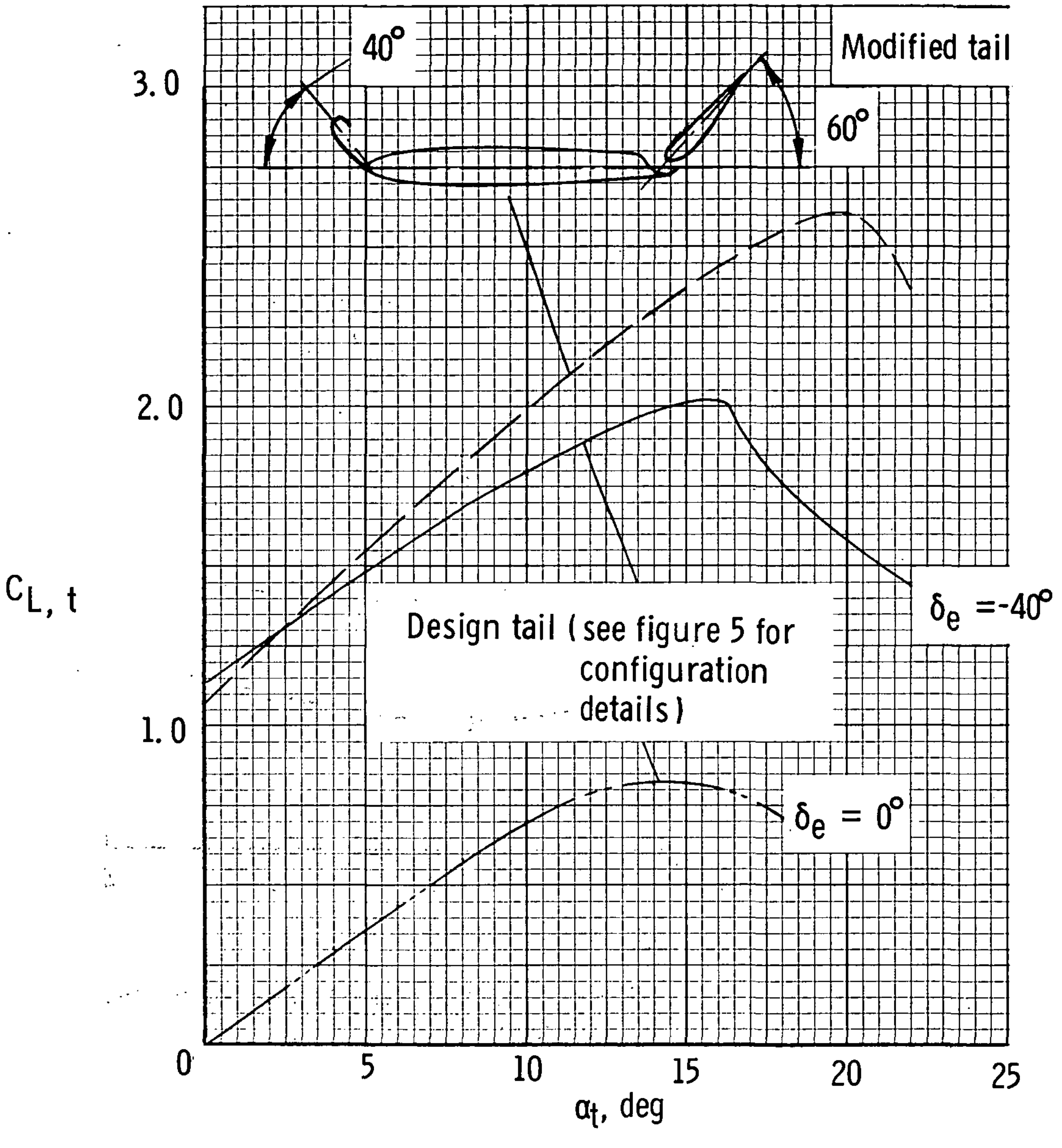

Figure 18.- Effect of various high-lift devices on lift performance of T-tail horizontal tail.

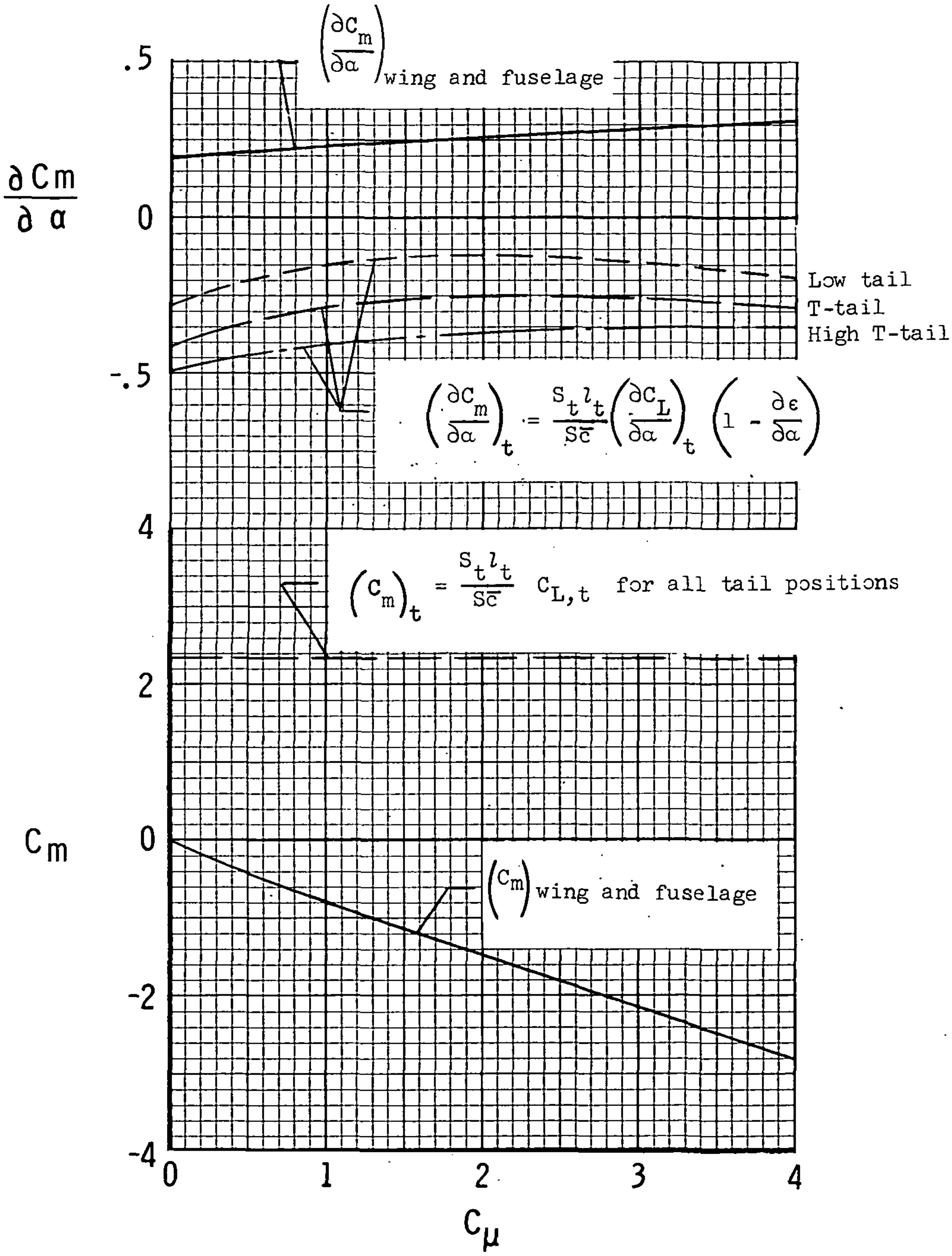

Figure 19.- Horizontal-tail characteristics required for longitudinal stability and trim. Modified horizontal tail; $\delta_f = 60^o$; $C_{\mu,le} = 0.035$; $C_{\mu,a} = 0.035$.

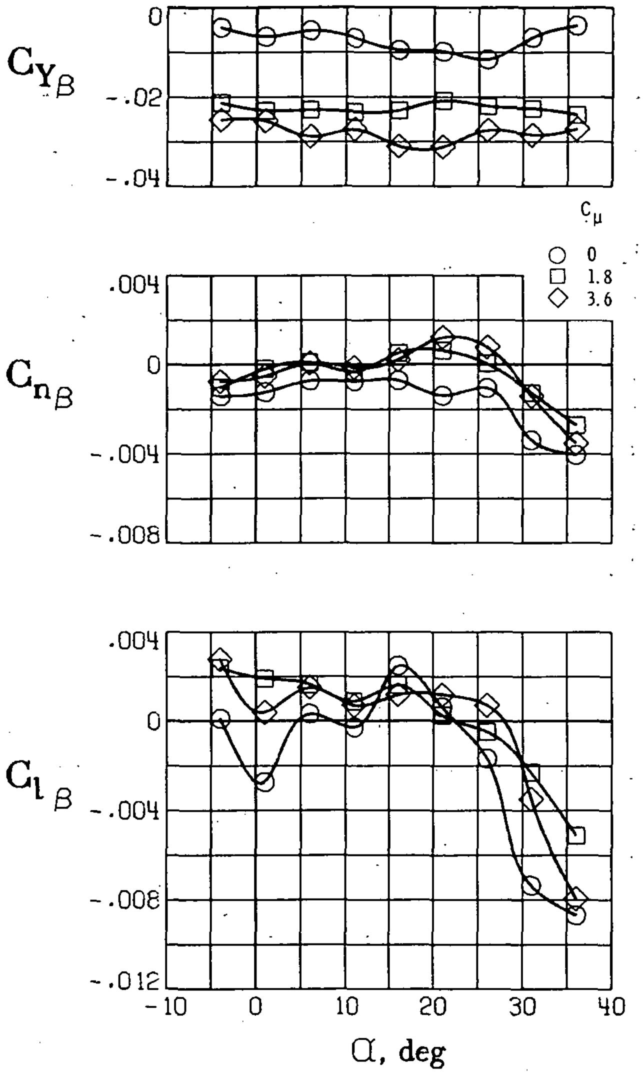

(a) T-tail off.

Figure 20.- Lateral stability characteristics of the model. $\delta_f = 60^o$; $C_{\mu,le} = 0.035$; $C_{\mu,a} = 0.035$.

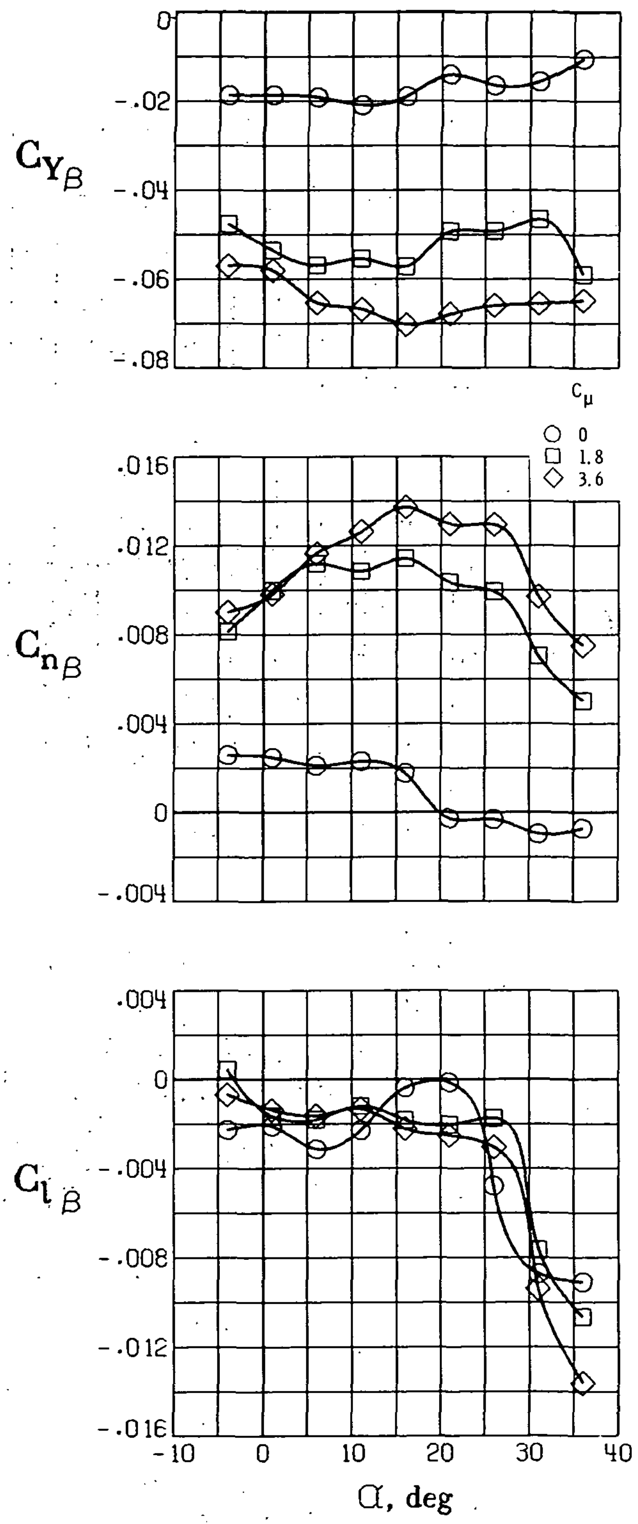

(b) T-tail on.

Figure 20.- Concluded.

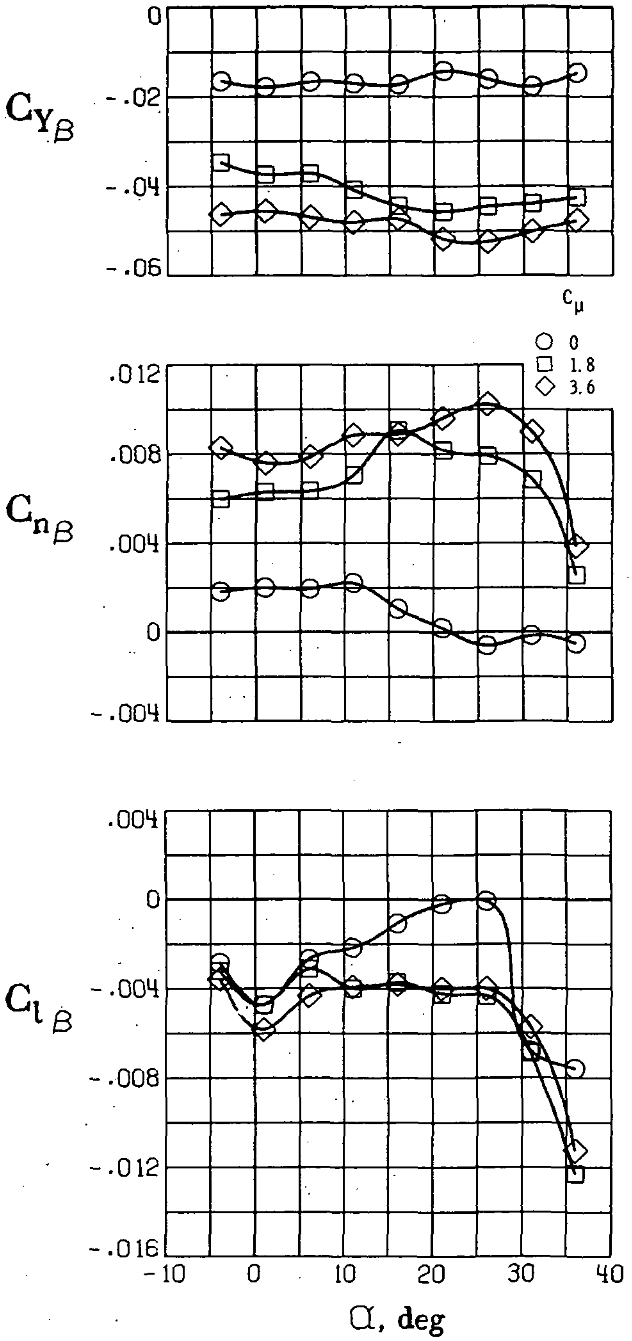

Figure 21.- Lateral stability characteristics of the model with T-tail. $\delta_f = 20^\circ$; $C_{\mu,le} = 0.035$; $C_{\mu,a} = 0.035$.

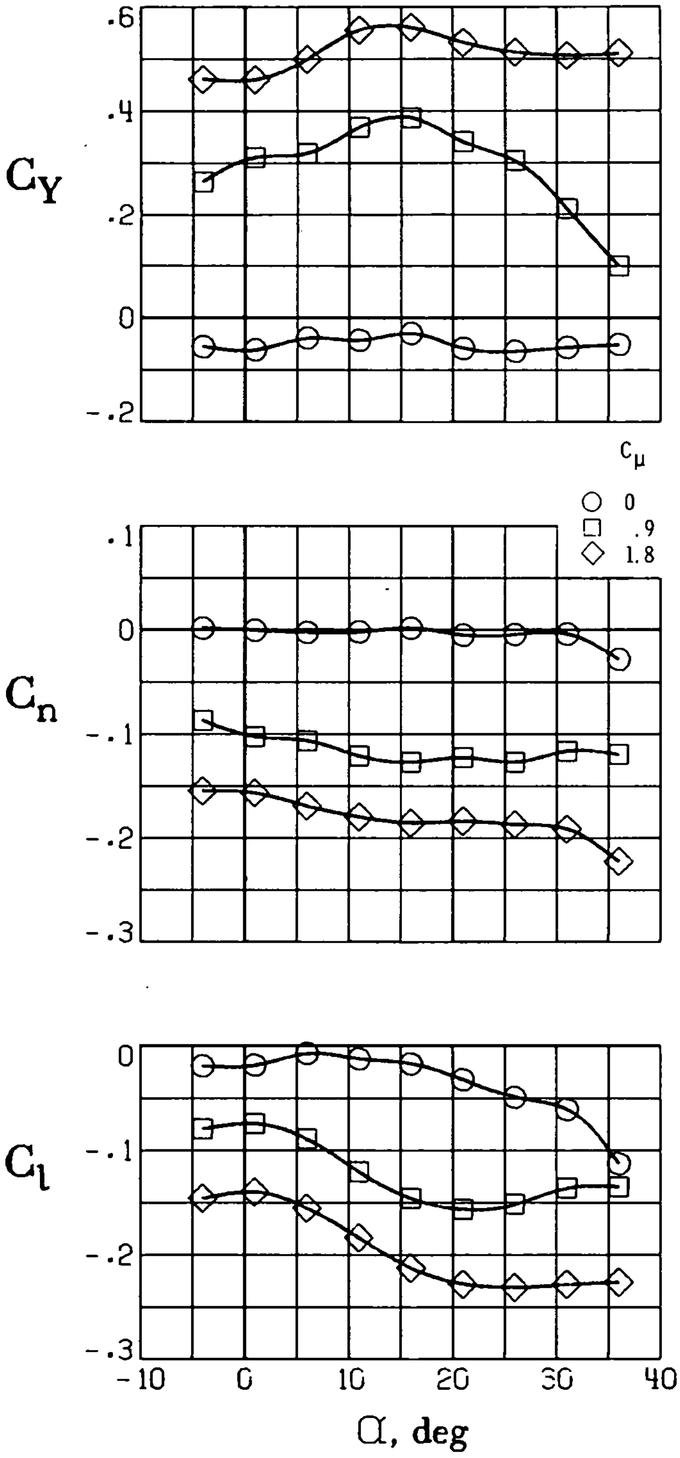

(a) Lateral characteristics.

Figure 22.- Lateral and longitudinal aerodynamic characteristics of the model with T-tail and the left engine inoperative. $\delta_f = 60^o$; $C_{\mu,le} = 0.035$; $C_{\mu,a} = 0.035$.

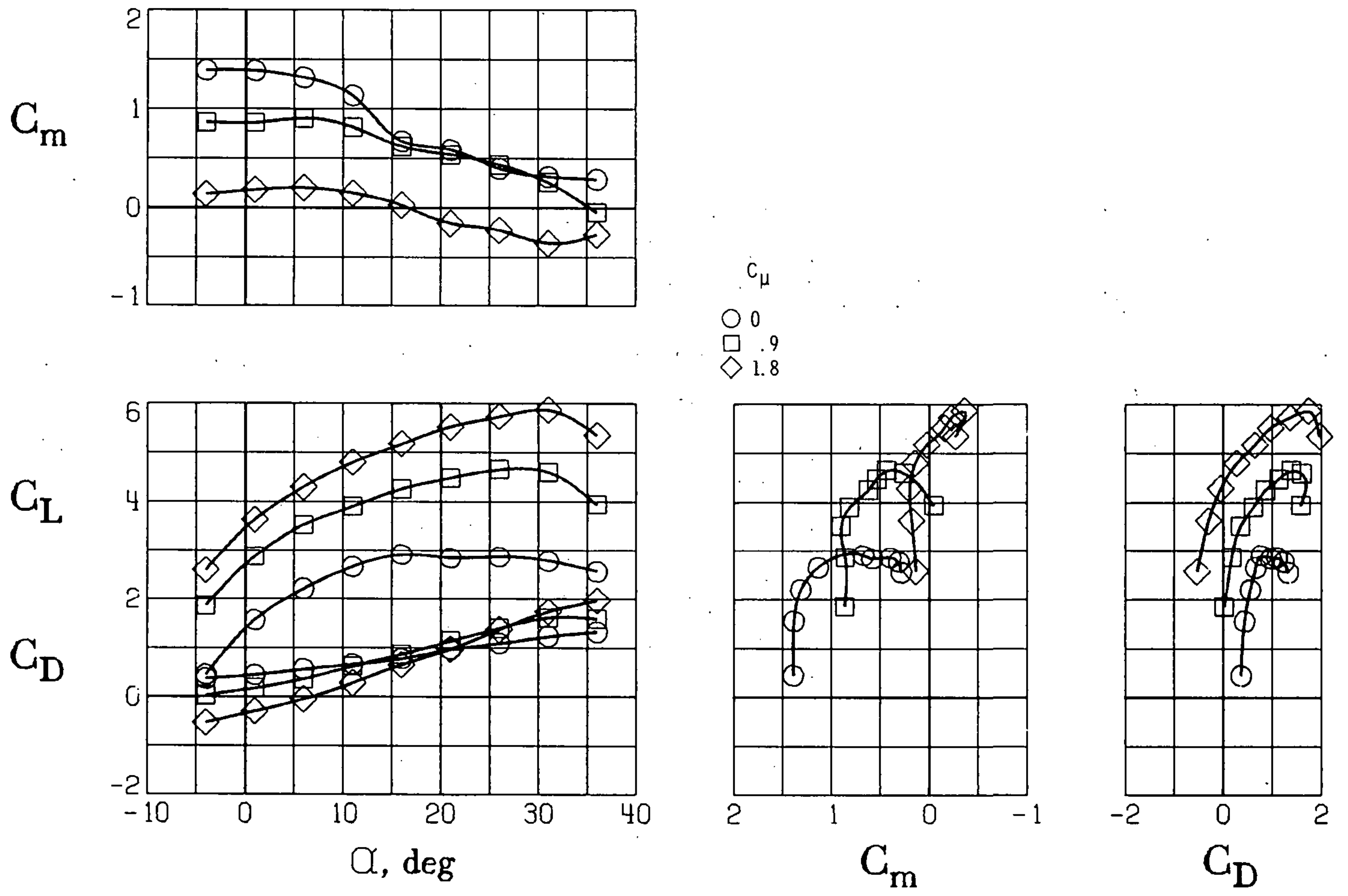

(b) Longitudinal characteristics.

Figure 22.- Concluded.

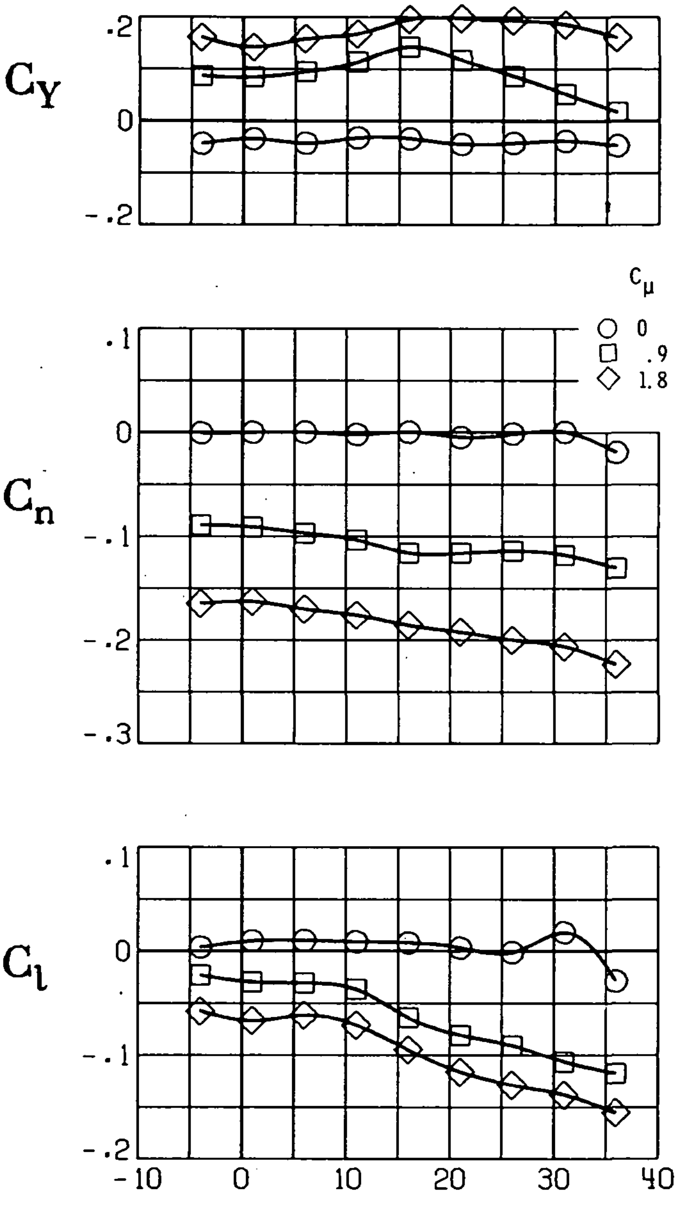

(a) Lateral characteristics.

Figure 23.- Lateral and longitudinal aerodynamic characteristics of the model with T-tail and the left engine inoperative. $\delta_f = 20^\circ$; $C_{\mu,le} = 0.035$; $C_{\mu,a} = 0.035$.

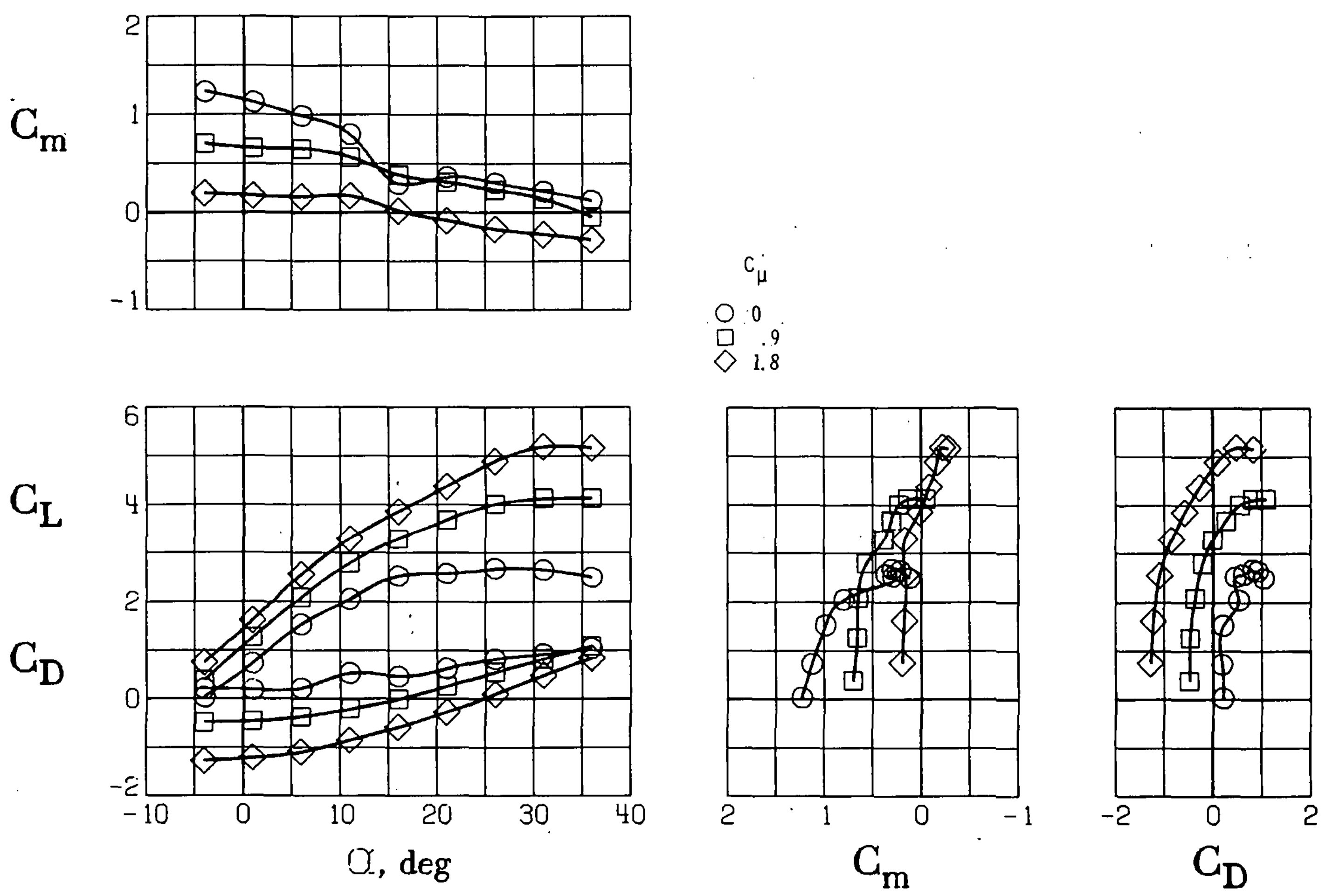

(b) Longitudinal characteristics.

Figure 23.- Concluded.

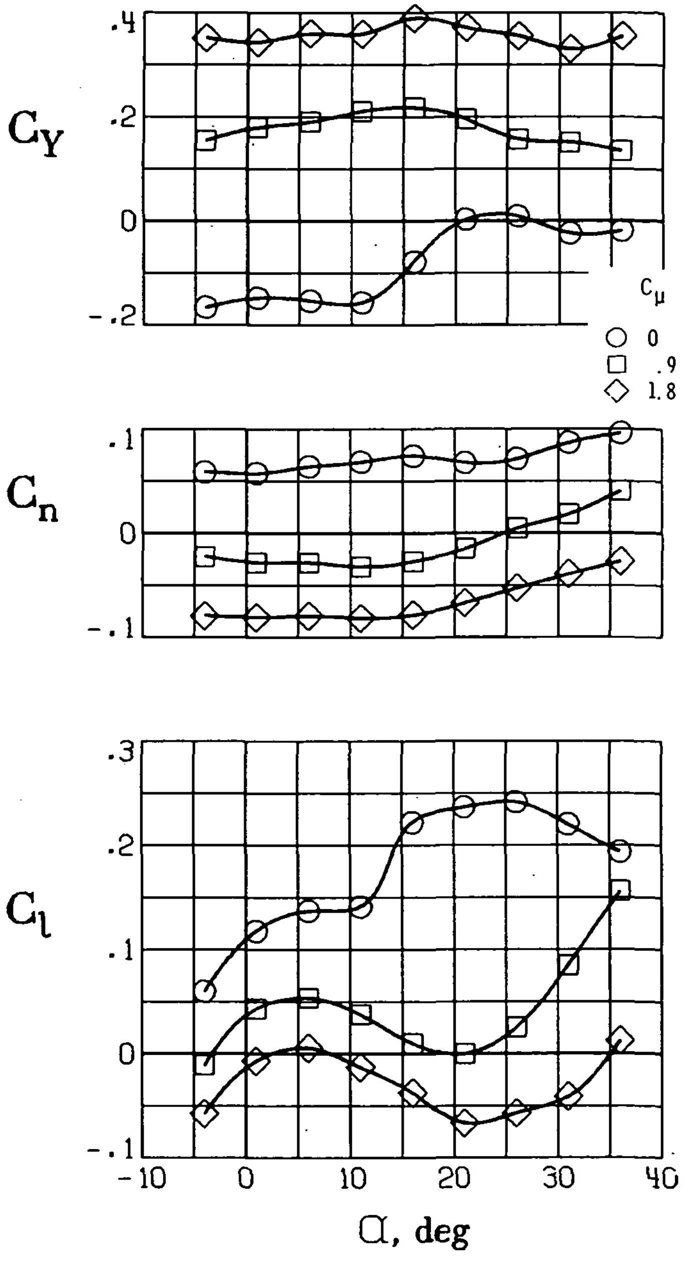

(a) Lateral characteristics.

Figure 24.- Lateral and longitudinal aerodynamic characteristics of the model with T-tail and the left engine inoperative. $\delta_f = 60^\circ$; $C_{\mu,le,L} = 0.040$; $C_{\mu,le,R} = 0$; $C_{\mu,a,L} = 0.035$; $C_{\mu,a,R} = 0$; $\delta_r = -30^\circ$.

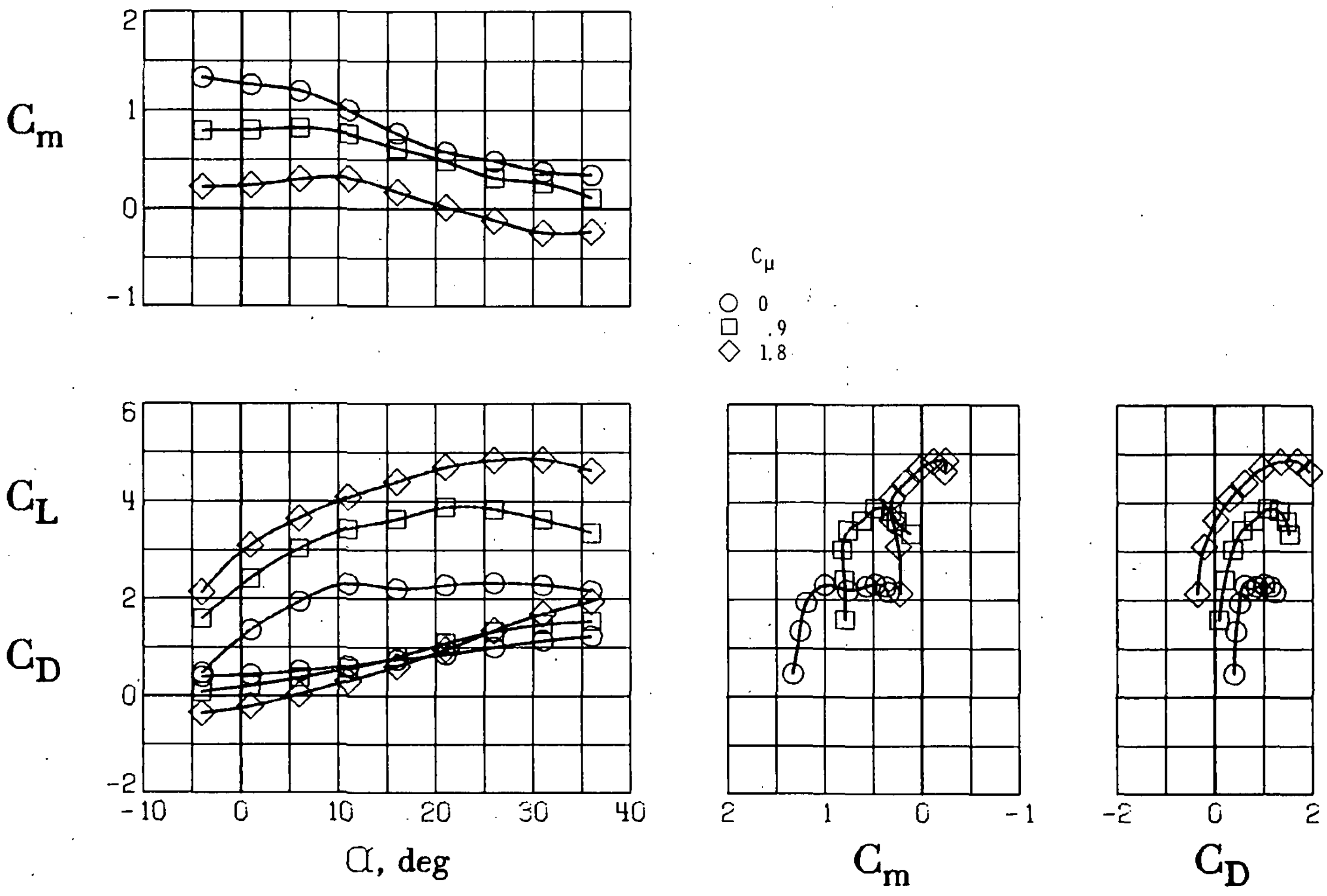

(b) Longitudinal characteristics.

Figure 24.- Concluded.

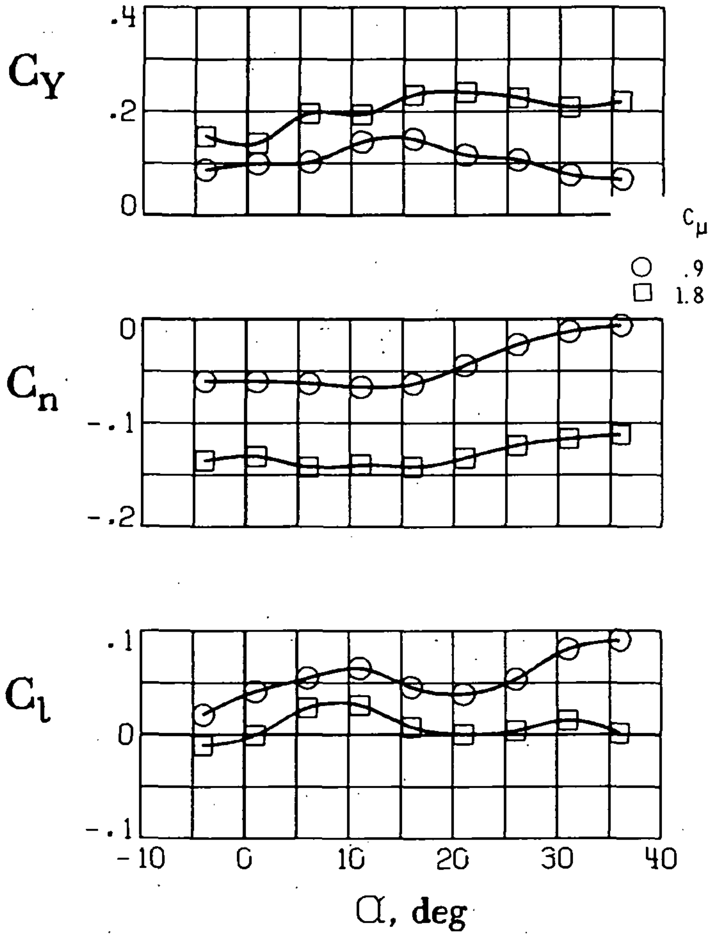

(a) Lateral characteristics.

Figure 25.- Lateral and longitudinal aerodynamic characteristics of the model with T-tail and the left engine inoperative. $\delta_f = 20^\circ$; $C_{\mu,le,L} = 0.035$; $C_{\mu,le,R} = 0$; $C_{\mu,a,L} = 0.050$; $C_{\mu,a,R} = 0$; $\delta_r = -30^\circ$.

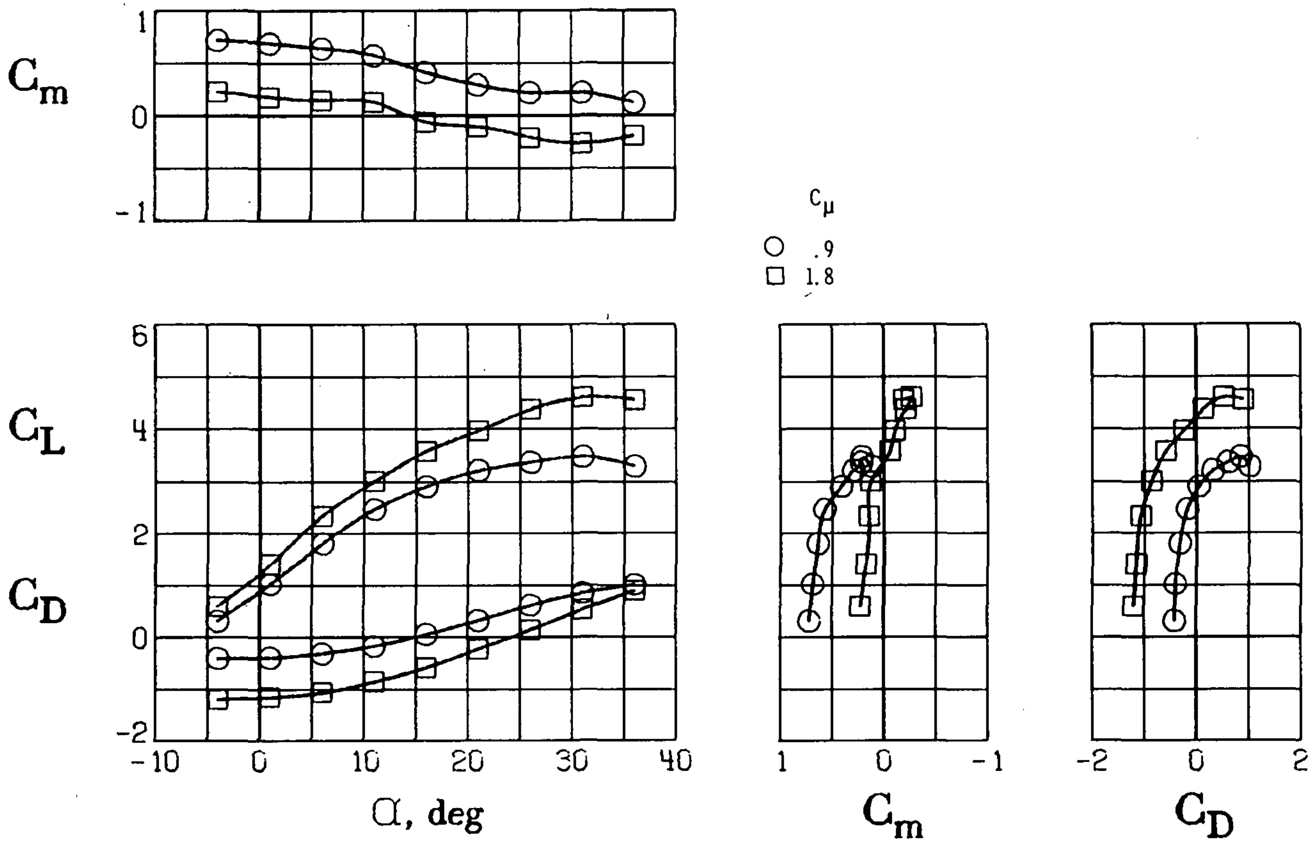

(b) Longitudinal characteristics.

Figure 25.- Concluded.

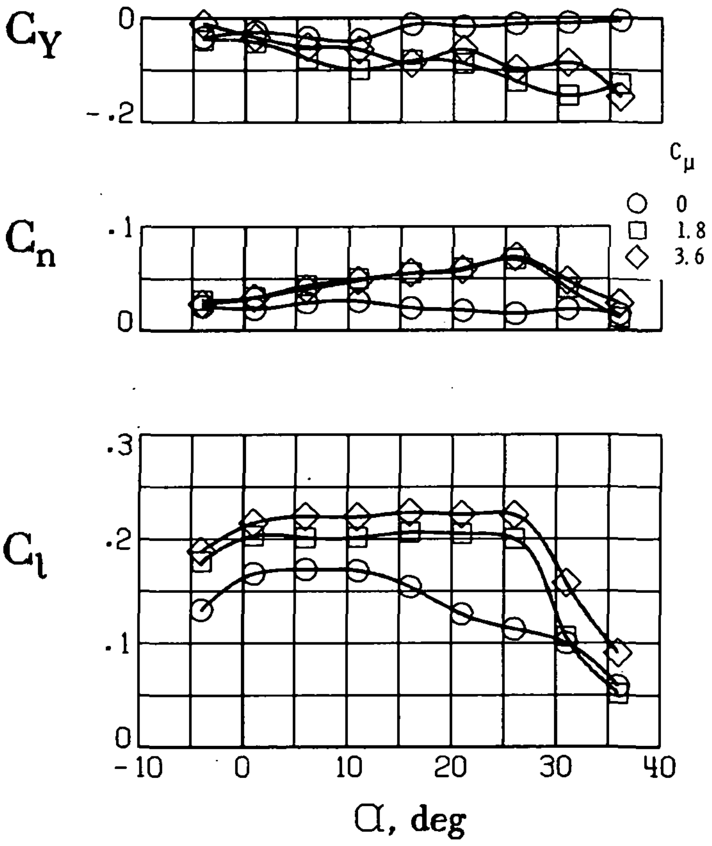

(a) Lateral characteristics.

Figure 26.- Effect of spoilers on lateral and longitudinal characteristics of the model with T-tail. $\delta_f = 60^o$; $C_{\mu,le} = 0.035$; $C_{\mu,a} = 0.035$; $\delta_{s,L} = 0^o$; $\delta_{s,R} = 45^o$.

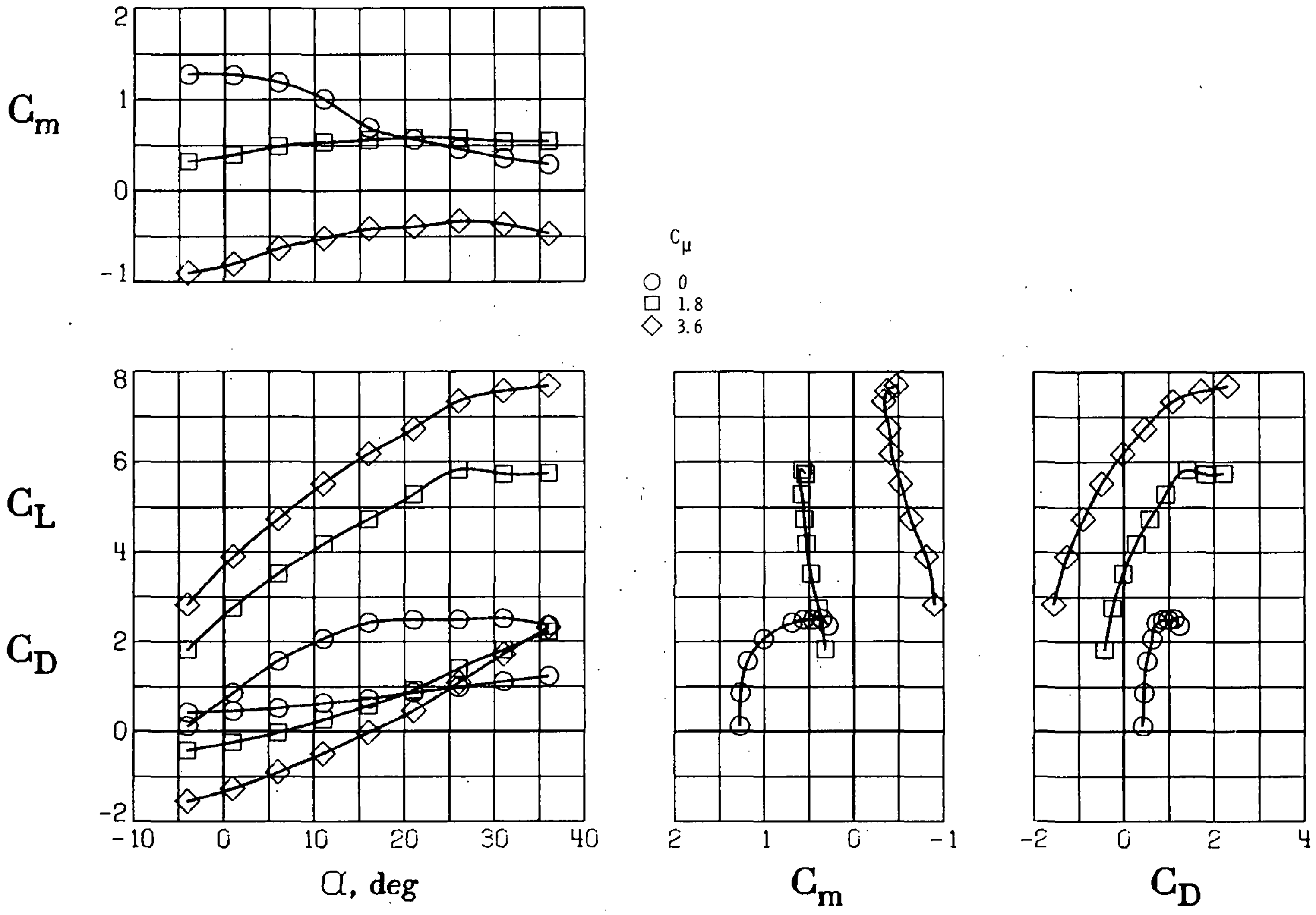

(b) Longitudinal characteristics.

Figure 26.- Concluded.

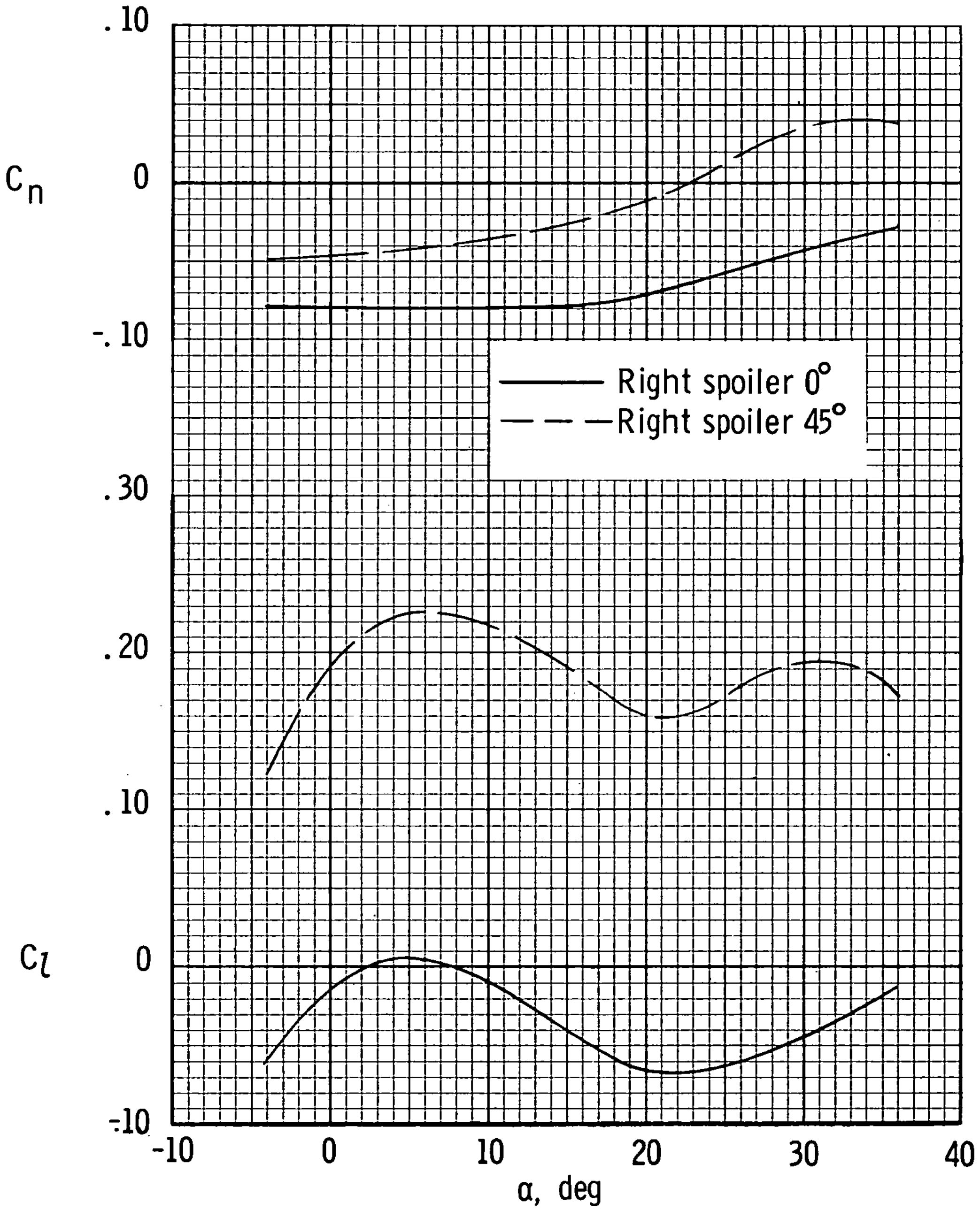

Figure 27.- Rolling-moment and yawing-moment characteristics with the left engine inoperative. $\delta_f = 60^\circ$; $C_\mu = 1.8$; $C_{\mu,le,L} = 0.040$; $C_{\mu,le,R} = 0$; $C_{\mu,a,L} = 0.035$; $C_{\mu,a,R} = 0$; $\delta_r = -30^\circ$.

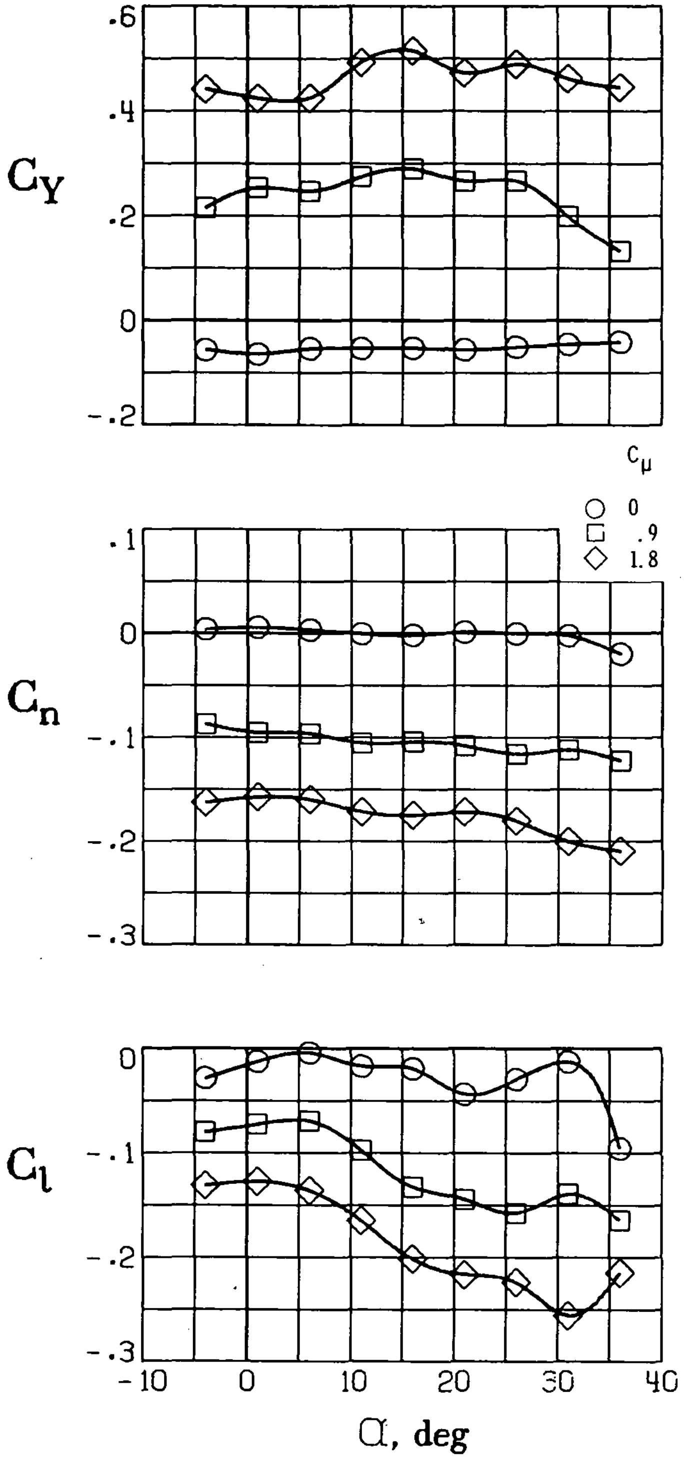

(a) Lateral characteristics.

Figure 28.- Lateral and longitudinal characteristics of the model with T-tail, left engine inoperative, and flap slots open behind left engine. $\delta_f = 60^\circ$; $C_{\mu,le} = 0.035$; $C_{\mu,a} = 0.035$.

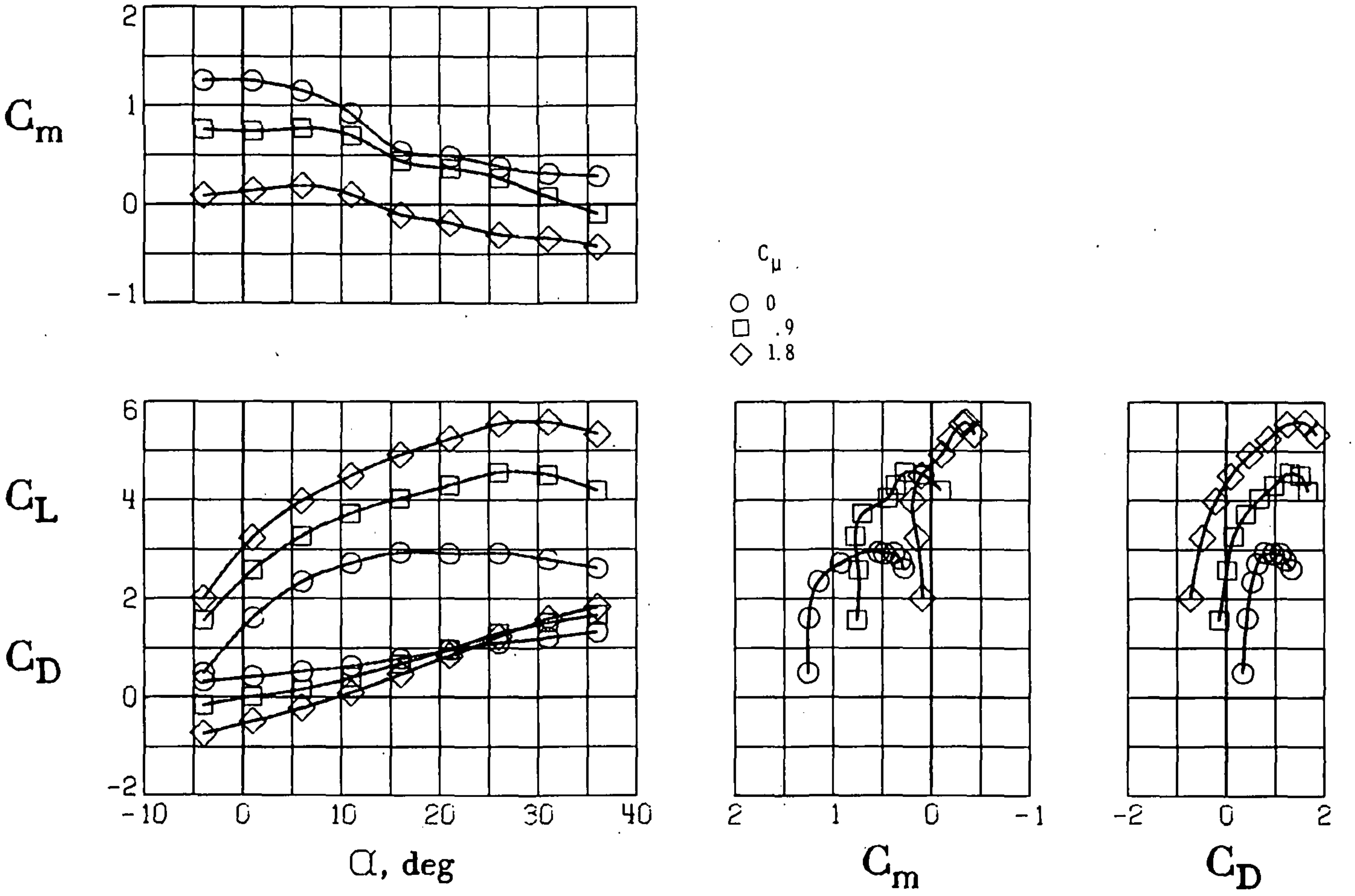

(b) Longitudinal characteristics.

Figure 28.- Concluded.

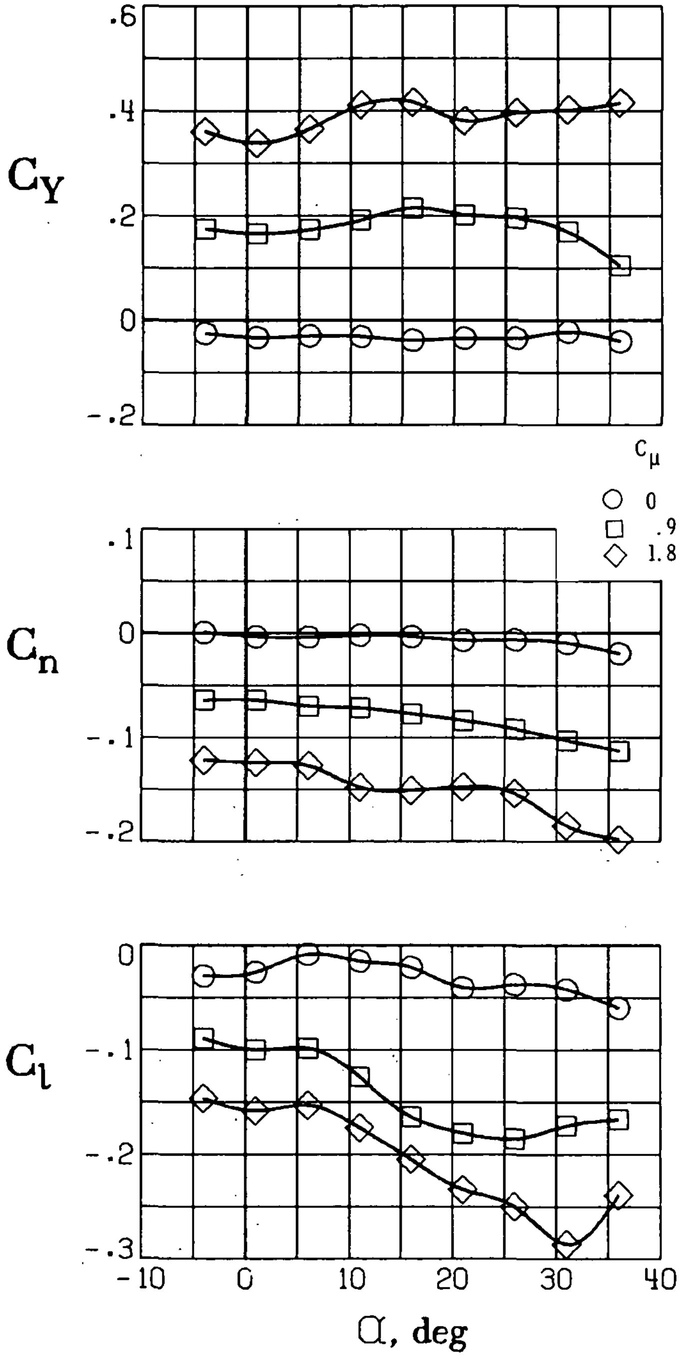

(a) Lateral characteristics.

Figure 29.- Lateral and longitudinal characteristics of the model with tail off, left engine inoperative, and flap slots open behind left engine. $\delta_f = 60^o$; $C_{\mu,le} = 0.035$; $C_{\mu,a} = 0.035$.

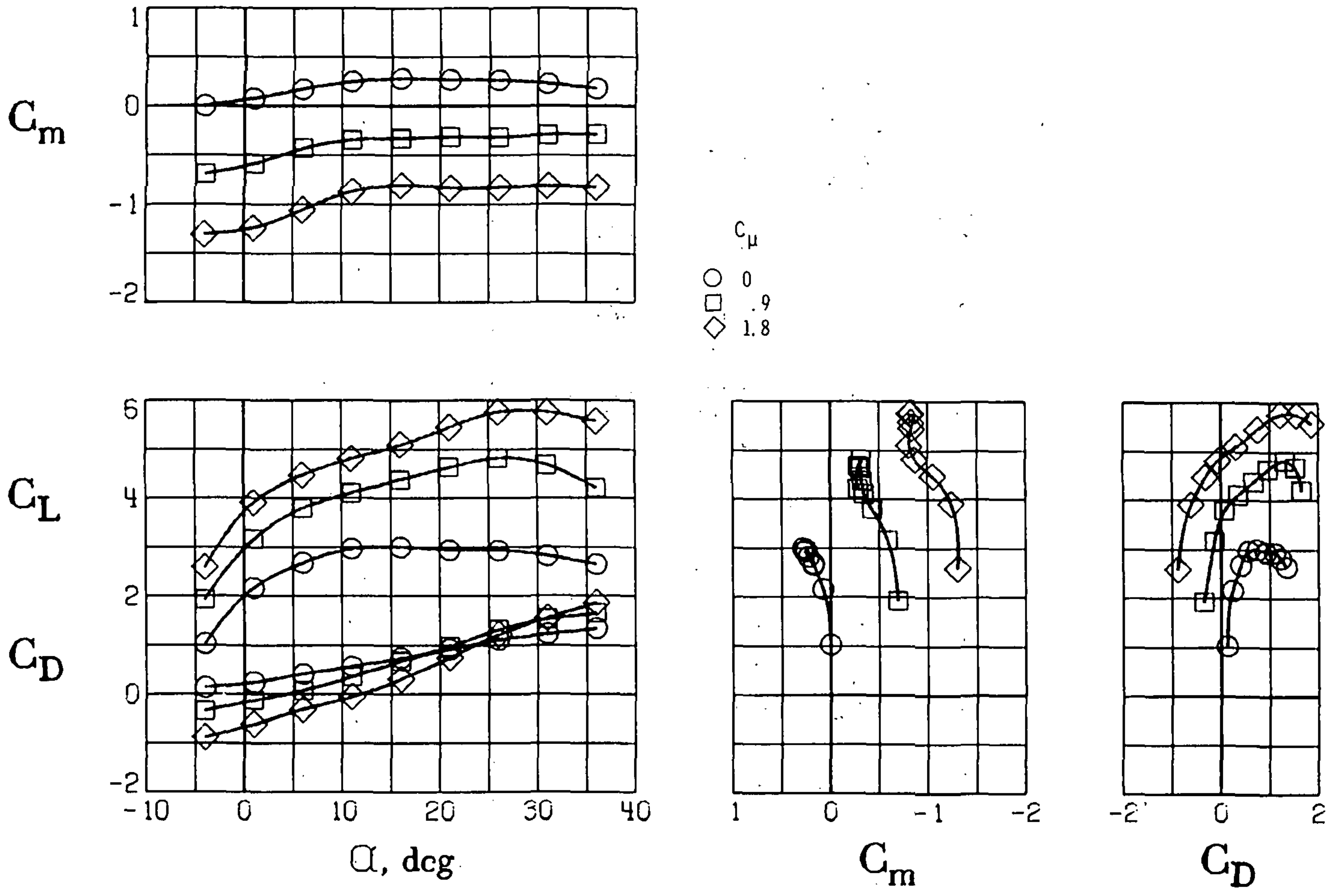

(b) Longitudinal characteristics.

Figure 29.- Concluded.

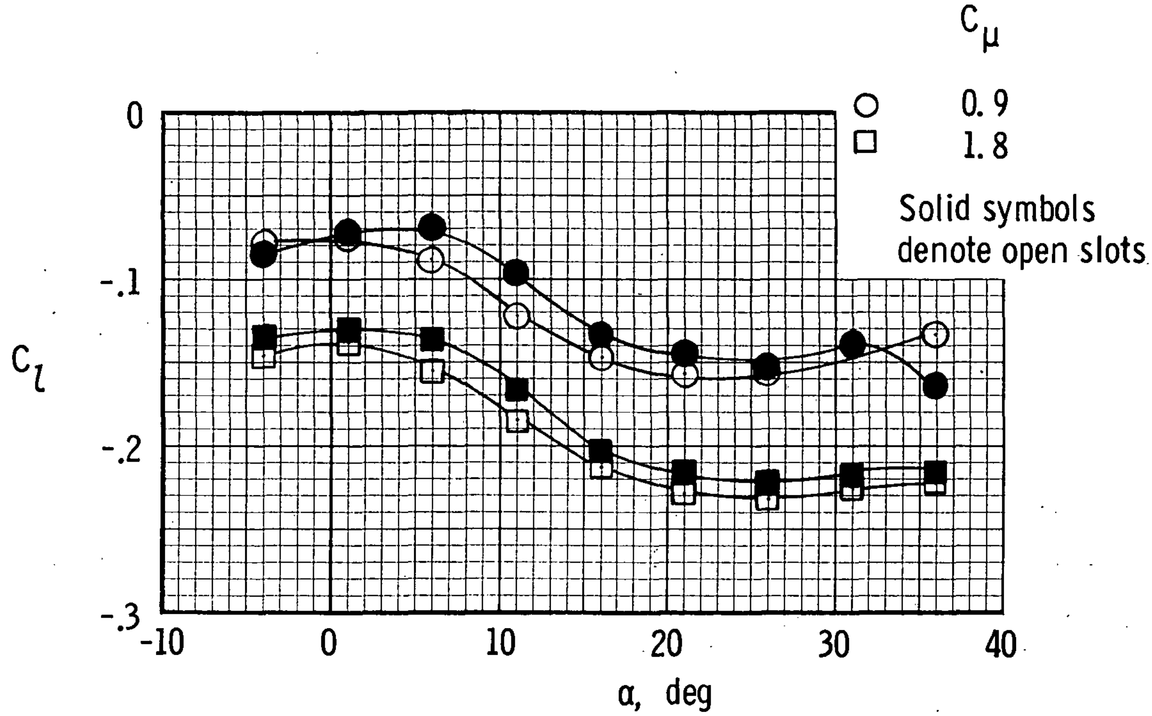

Figure 30.- Effect of opening flap slots behind inoperative engine. $C_{\mu,le} = 0.035$; $C_{\mu,a} = 0.035$; tail on; $\delta_f = 60^\circ$.

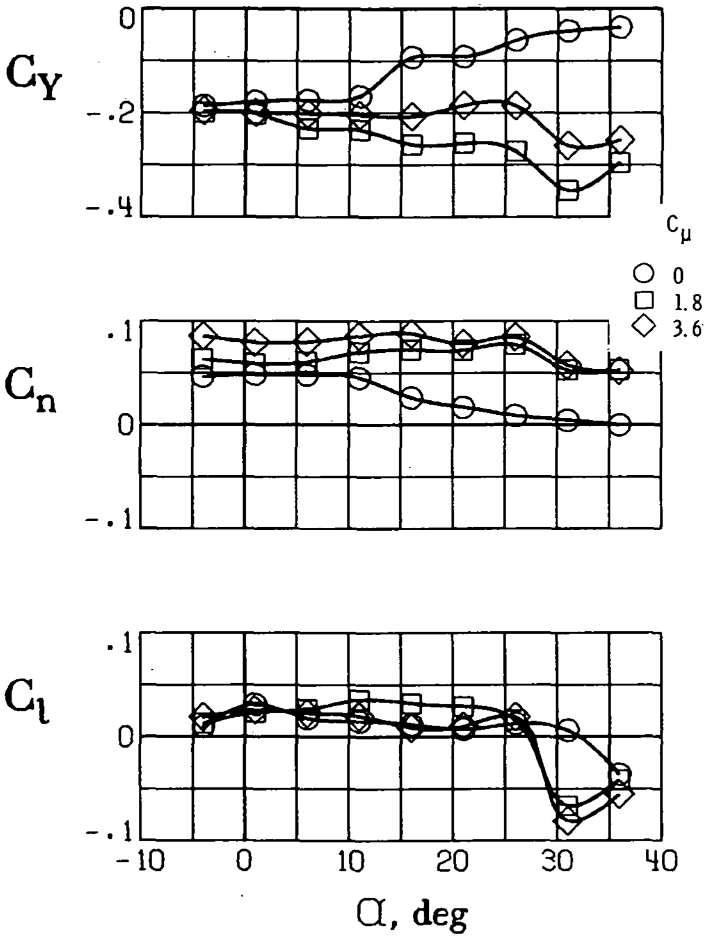

(a) Lateral characteristics.

Figure 31.- Effect of rudder on lateral and longitudinal characteristics of the model with T-tail. $\delta_f = 60^o$; $C_{\mu,le} = 0.035$; $C_{\mu,a} = 0.035$; $\delta_r = -30^o$.

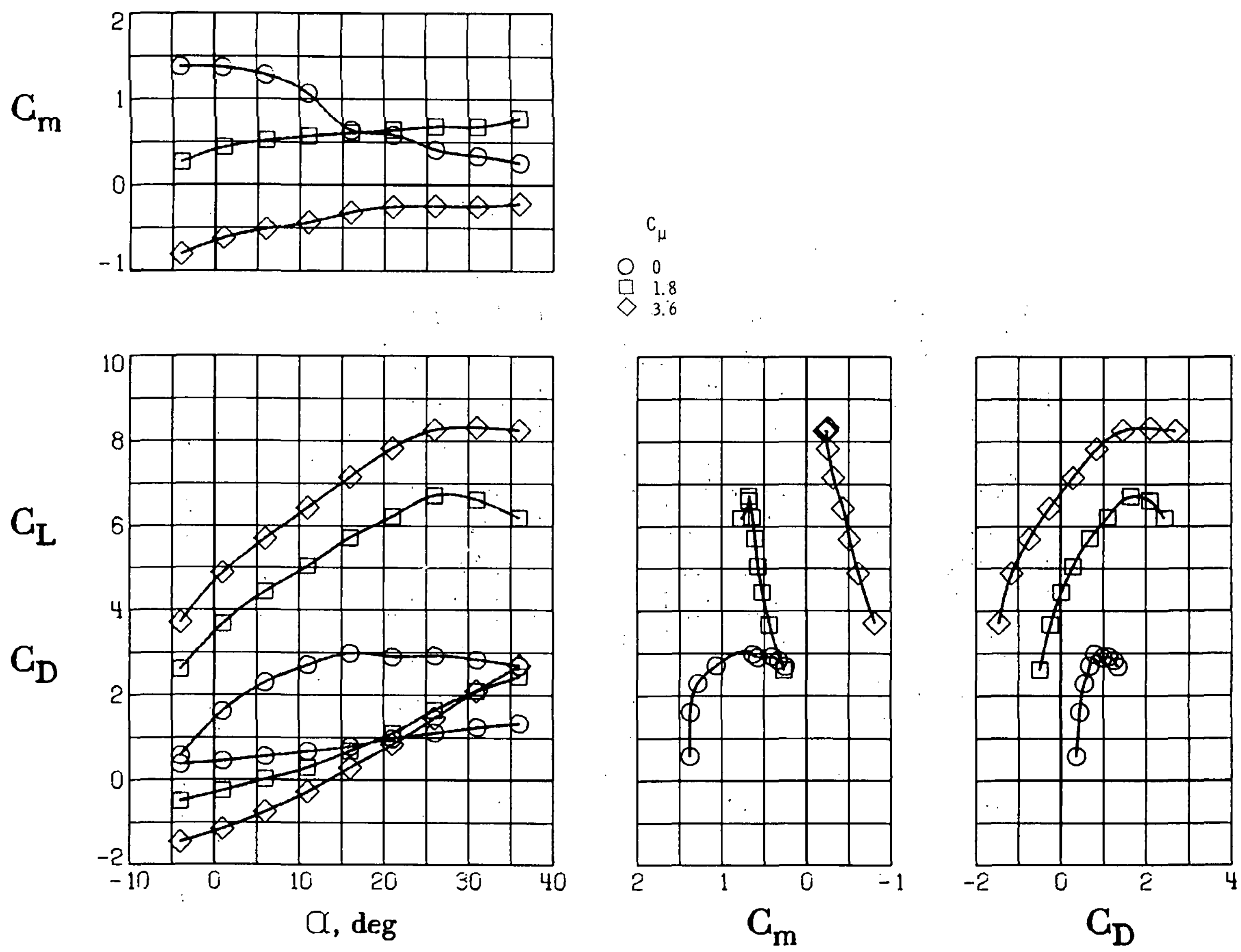

(b) Longitudinal characteristics.

Figure 31.- Concluded.

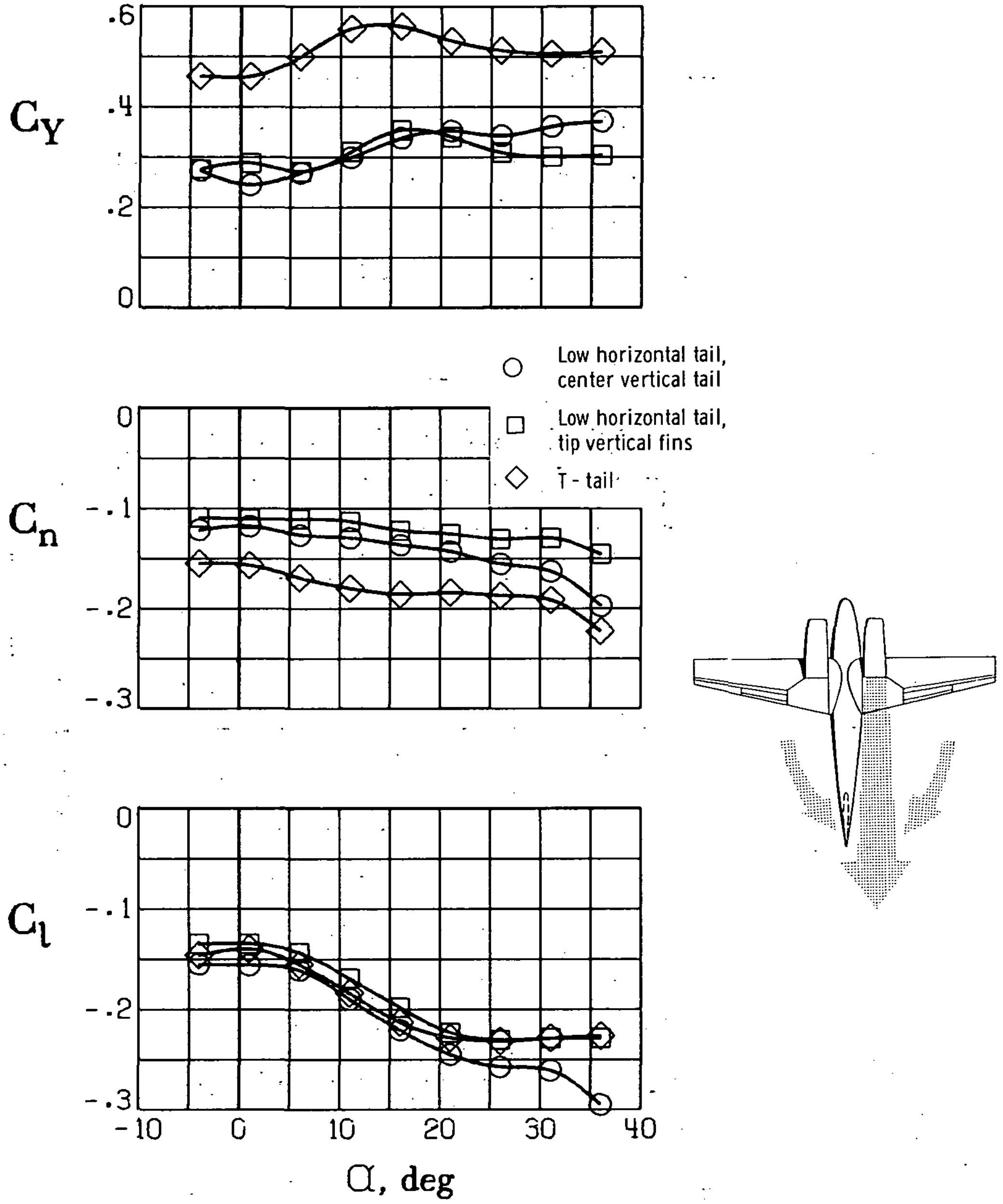

(a) Lateral characteristics.

Figure 32.- Effect of tail configuration on the lateral and longitudinal characteristics of the model with the left engine inoperative. $\delta_f = 60^o$; $C_\mu = 1.8$; $C_{\mu,le} = 0.035$; $C_{\mu,a} = 0.035$.

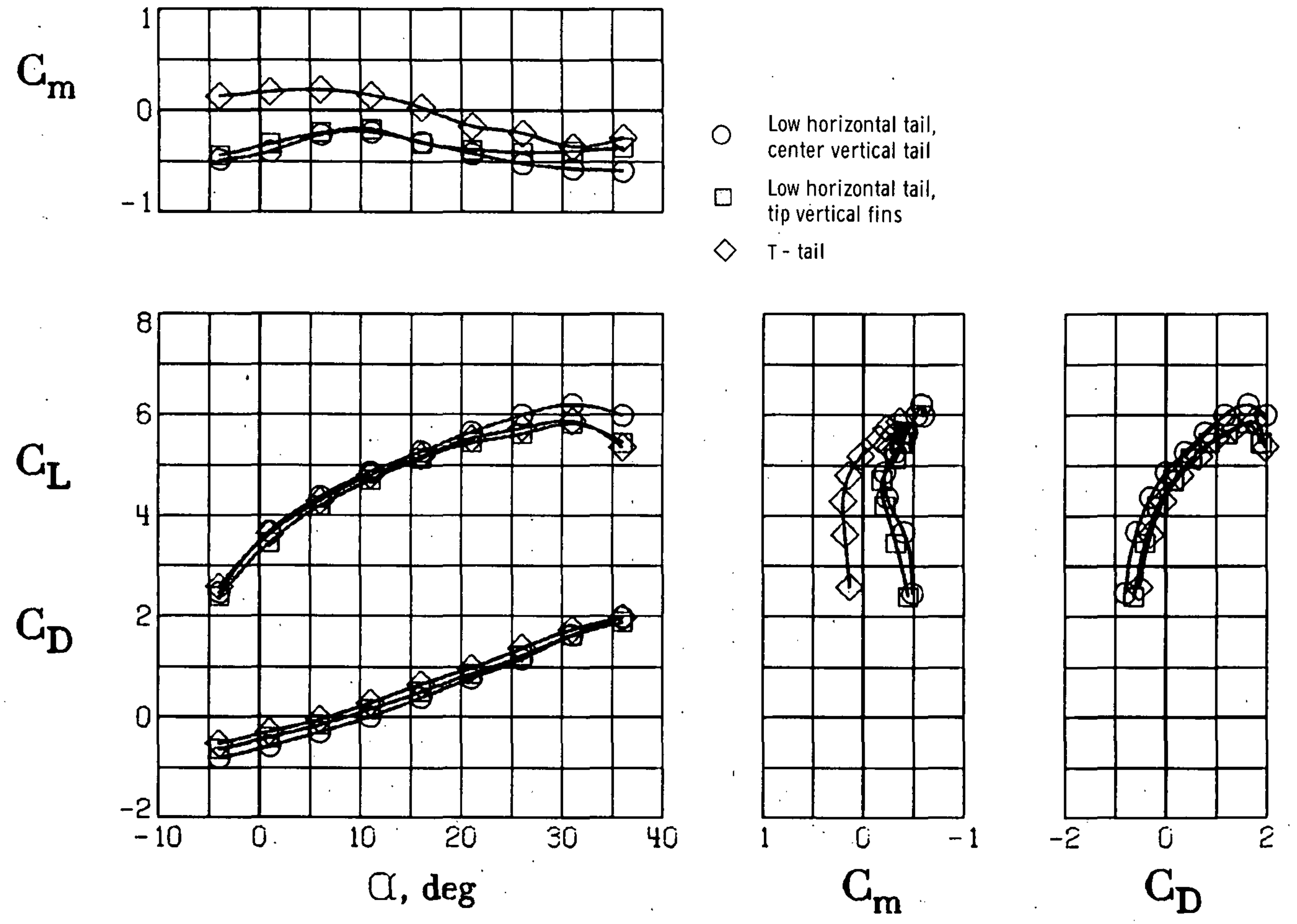

(b) Longitudinal characteristics.

Figure 32.- Concluded.

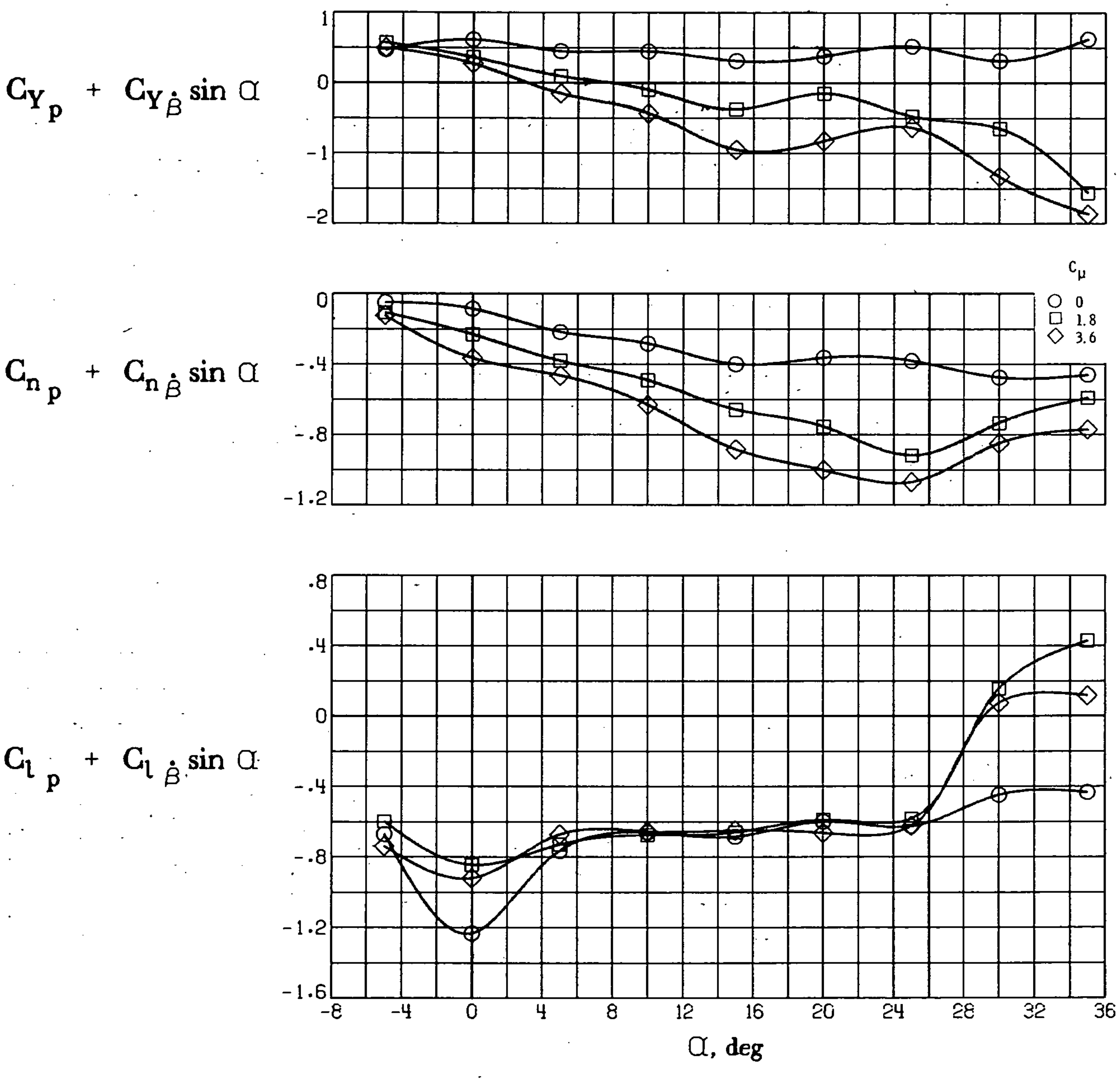

(a) k = 0.32.

Figure 33.- Dynamic stability derivatives due to rolling for model with T-tail. $\delta_f = 60^o$; $C_{\mu,le} = 0.035$; $C_{\mu,a} = 0.035$.

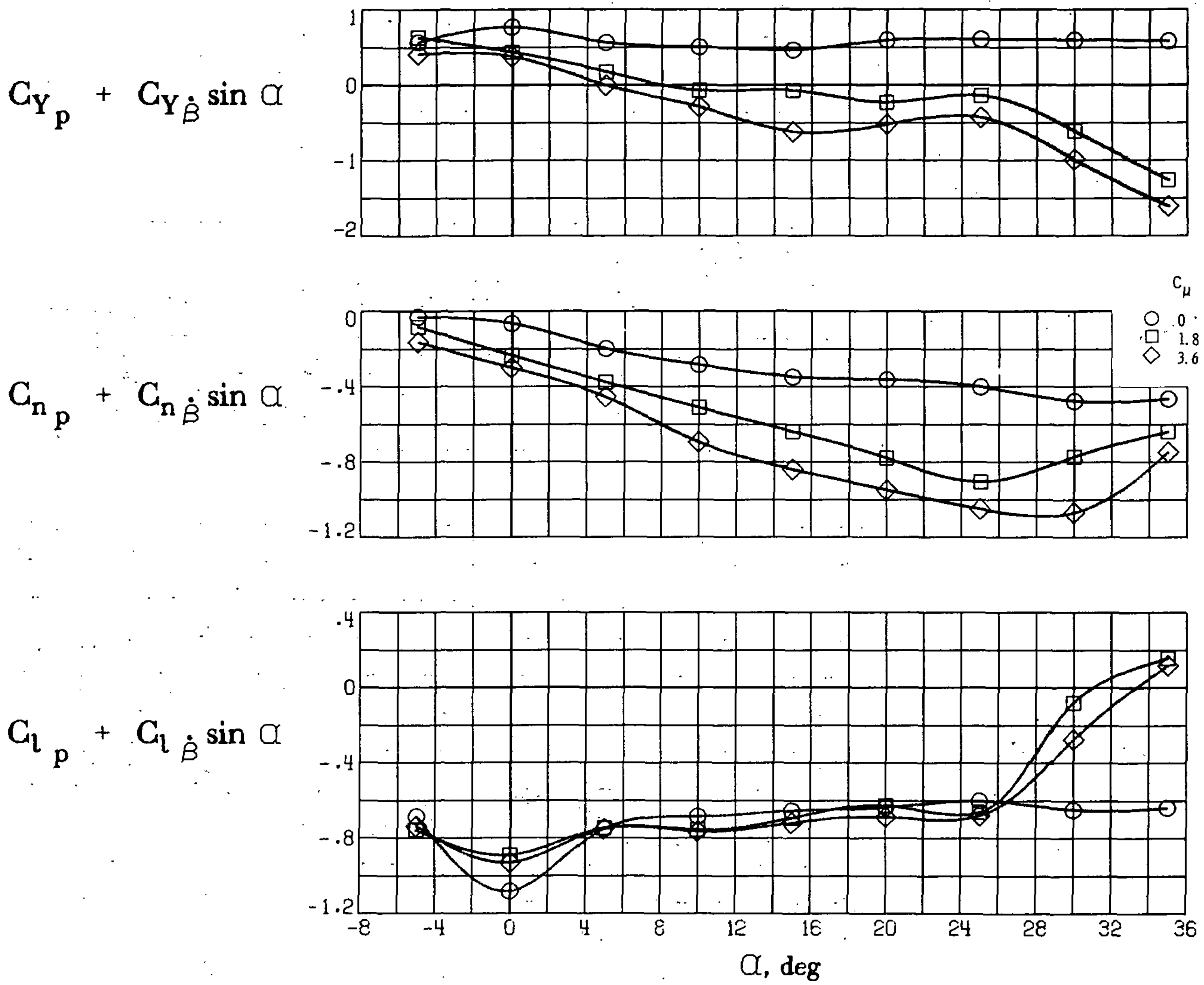

(b) k = 0.64.

Figure 33.- Concluded.

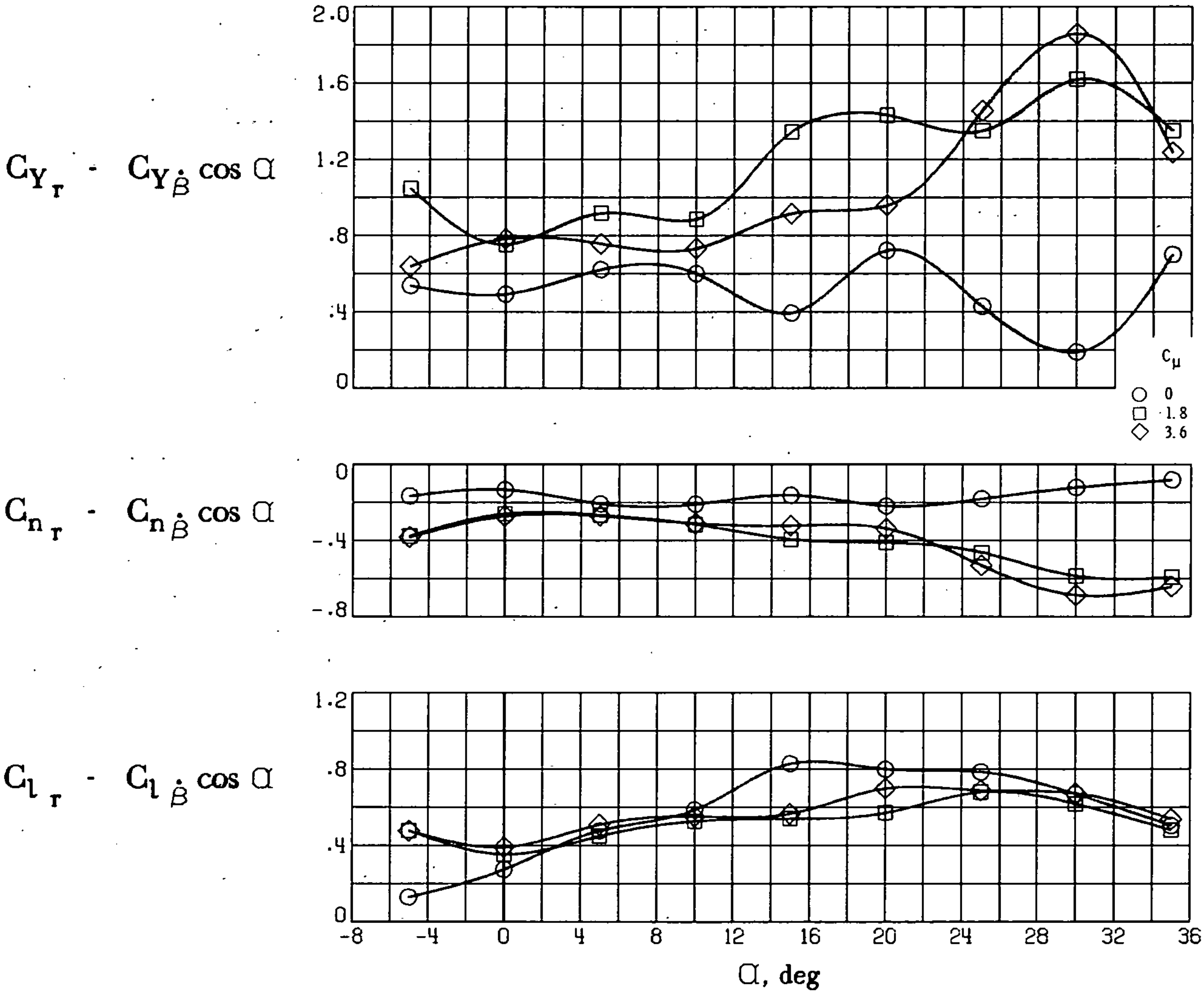

(a) k = 0.32.

Figure 34.- Dynamic stability derivatives due to yawing for model with T-tail. $\delta_f = 60^o$; $C_{\mu,le} = 0.035$; $C_{\mu,a} = 0.035$.

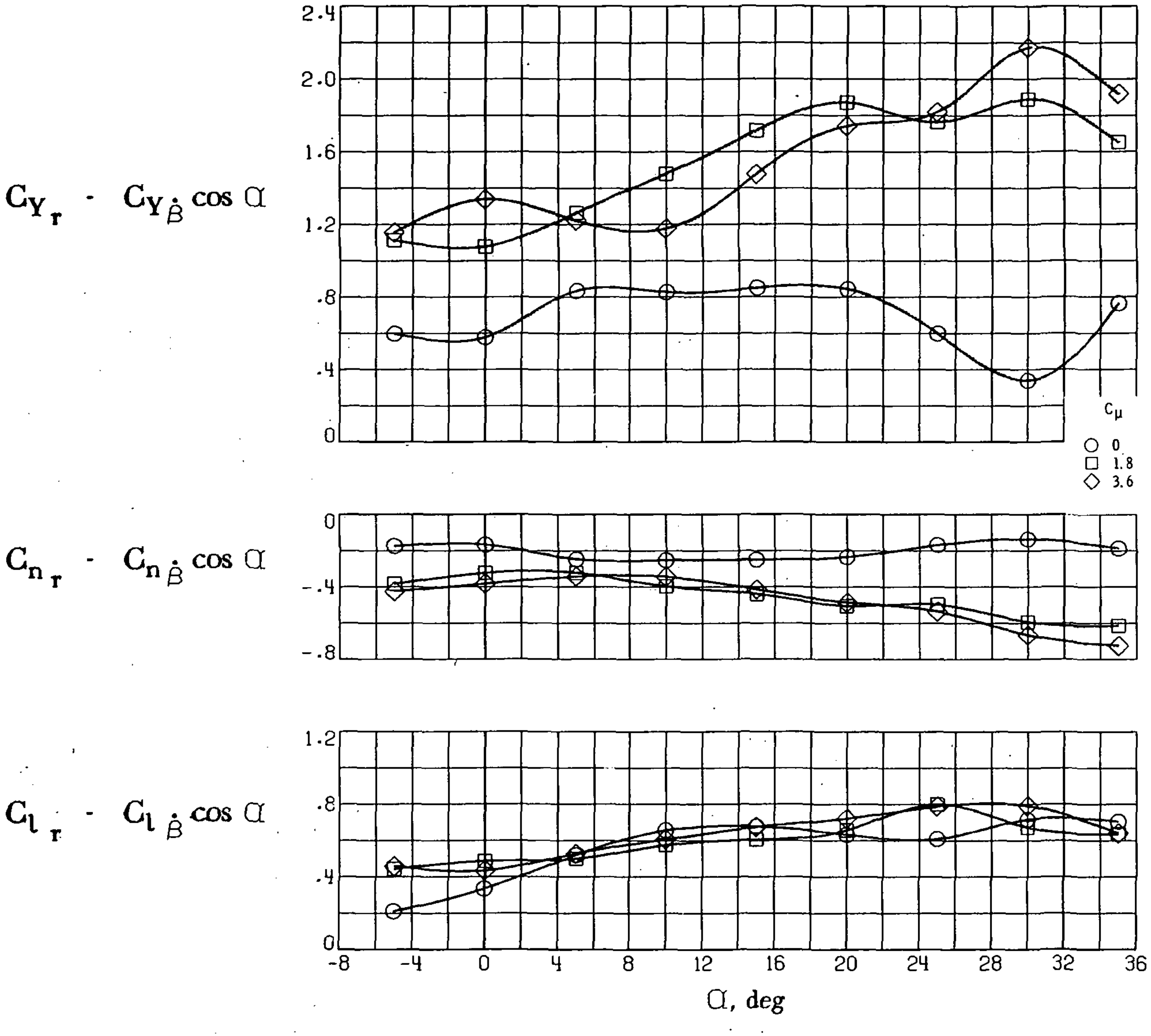

(b) k = 0.64.

Figure 34.- Concluded.

NASA-Langley, 1975 L-9758

NATIONAL AERONAUTICS AND SPACE ADMINISTRATION
WASHINGTON, D.C. 20546

OFFICIAL BUSINESS
PENALTY FOR PRIVATE USE $300

SPECIAL FOURTH-CLASS RATE
BOOK

POSTAGE AND FEES PAID
NATIONAL AERONAUTICS AND
SPACE ADMINISTRATION
451

057 001 C1 U 01 741213 S00120ES
PHILCO FORD CORP
AERONUTRONIC DIV
AEROSPACE & COMMUNICATIONS OPERATIONS
ATTN: TECHNICAL INFO SERVICES
JAMBOREE & FORD ROADS
NEWPORT BEACH CA 92663

POSTMASTER: If Undeliverable (Section 158 Postal Manual) Do Not Return

---

> *"The aeronautical and space activities of the United States shall be conducted so as to contribute . . . to the expansion of human knowledge of phenomena in the atmosphere and space. The Administration shall provide for the widest practicable and appropriate dissemination of information concerning its activities and the results thereof."*
>
> —NATIONAL AERONAUTICS AND SPACE ACT OF 1958

NASA SCIENTIFIC AND TECHNICAL PUBLICATIONS

TECHNICAL REPORTS: Scientific and technical information considered important, complete, and a lasting contribution to existing knowledge.

TECHNICAL NOTES: Information less broad in scope but nevertheless of importance as a contribution to existing knowledge.

TECHNICAL MEMORANDUMS: Information receiving limited distribution because of preliminary data, security classification, or other reasons. Also includes conference proceedings with either limited or unlimited distribution.

CONTRACTOR REPORTS: Scientific and technical information generated under a NASA contract or grant and considered an important contribution to existing knowledge.

TECHNICAL TRANSLATIONS: Information published in a foreign language considered to merit NASA distribution in English.

SPECIAL PUBLICATIONS: Information derived from or of value to NASA activities. Publications include final reports of major projects, monographs, data compilations, handbooks, sourcebooks, and special bibliographies.

TECHNOLOGY UTILIZATION PUBLICATIONS: Information on technology used by NASA that may be of particular interest in commercial and other non-aerospace applications. Publications include Tech Briefs, Technology Utilization Reports and Technology Surveys.

Details on the availability of these publications may be obtained from:

SCIENTIFIC AND TECHNICAL INFORMATION OFFICE
NATIONAL AERONAUTICS AND SPACE ADMINISTRATION
Washington, D.C. 20546